HHS Public Access

Author manuscript

Brain Behav Immun. Author manuscript; available in PMC 2024 July 01.

Published in final edited form as:

Brain Behav Immun. 2024 July ; 119: 665–680. doi:10.1016/j.bbi.2024.03.028.

Stress-induced mucin 13 reductions drive intestinal microbiome shifts and despair behaviors

Courtney R. Rivet-Noor[a,b,c,d,*], **Andrea R. Merchak**[a,b,c], **Caroline Render**[e], **Naudia M. Gay**[a,b,c], **Rebecca M. Beiter**[a,b,c], **Ryan M. Brown**[a,b,c], **Austin Keeler**[f], **G. Brett Moreau**[g], **Sihan Li**[b], **Deniz G. Olgun**[h,i], **Alexandra D. Steigmeyer**[j], **Rachel Ofer**[k], **Tobey Phan**[b], **Kiranmayi Vemuri**[k], **Lei Chen**[l], **Keira E. Mahoney**[j], **Jung-Bum Shin**[b], **Stacy A. Malaker**[j], **Chris Deppmann**[f], **Michael P. Verzi**[k], **Alban Gaultier**[a,b,*]

[a]Center for Brain Immunology and Glia, University of Virginia School of Medicine, Charlottesville, VA 22908, USA

[b]Department of Neuroscience, University of Virginia School of Medicine, Charlottesville, VA 22908, USA

[c]Graduate Program in Neuroscience, University of Virginia School of Medicine, Charlottesville, VA 22908, USA

[d]Department of Molecular Genetics and Microbiology, Duke University, Durham, NC 27710, USA

[e]Undergraduate Department of Global Studies, University of Virginia College of Arts and Sciences, Charlottesville, VA 22904, USA

[f]Department of Biology, University of Virginia College of Arts and Sciences, Charlottesville, VA 22904, USA

[g]Division of Infectious Diseases and International Health, Department of Medicine, University of Virginia School of Medicine, Charlottesville, VA, USA

[*]Corresponding authors at: Department of Molecular Genetics and Microbiology, Duke University, 323A CARL Building Box 3580, 213 Research Drive, Durham, NC 27710, USA (C.R.R.-N.); Department of Neuroscience, University of Virginia, 409 Lane Road, MR4 Rm 5126, Charlottesville, VA 22908, USA (A.G.). courtney.rivetnoor@duke.edu (C.R. Rivet-Noor), ag7h@virginia.edu (A. Gaultier).

Credit authorship contribution statement

Courtney R. Rivet-Noor: Writing – review & editing, Writing – original draft, Visualization, Validation, Methodology, Formal analysis, Data curation, Conceptualization. **Andrea R. Merchak:** Investigation. **Caroline Render:** Investigation. **Naudia M. Gay:** Investigation. **Rebecca M. Beiter:** Investigation. **Ryan M. Brown:** Investigation. **Austin Keeler:** Investigation. **G. Brett Moreau:** Formal analysis. **Sihan Li:** Formal analysis. **Deniz G. Olgun:** Formal analysis. **Alexandra D. Steigmeyer:** Investigation. **Rachel Ofer:** Investigation. **Tobey Phan:** Formal analysis. **Kiranmayi Vemuri:** Investigation. **Lei Chen:** Investigation. **Keira E. Mahoney:** Investigation. **Jung-Bum Shin:** Supervision. **Stacy A. Malaker:** Supervision. **Chris Deppmann:** Supervision. **Michael P. Verzi:** Supervision. **Alban Gaultier:** Writing – review & editing, Writing – original draft, Supervision, Project administration, Investigation, Funding acquisition, Data curation, Conceptualization.

Declaration of competing interest

The authors declare the following financial interests/personal relationships which may be considered as potential competing interests: S. A.M. is an inventor on a Stanford patent related to the use of mucinases as research tools; she is also a consultant for InterVenn Biosciences. A.G. is a consultant for Novoron Bioscience.

Appendix A. supplementary material

Supplementary data to this article can be found online at https://doi.org/10.1016/j.bbi.2024.03.028.

[h]Undergraduate Department of Computer Science, University of Virginia School of Engineering and Applied Science, Charlottesville, VA 22904, USA

[i]Undergraduate Department of Neuroscience Studies, University of Virginia College of Arts and Sciences, Charlottesville, VA 22904, USA

[j]Department of Chemistry, Yale University, New Haven, CT 06511, USA

[k]Department of Genetics, Human Genetics Institute of New Jersey, Rutgers Cancer Institute of New Jersey, Rutgers Center for Lipid Research, Division of Environmental & Population Health Biosciences, EOHSI, New Brunswick, NJ 08901, USA

[l]School of Life Science and Technology, Key Laboratory of Developmental Genes and Human Disease, Southeast University, Nanjing, China

Abstract

Depression is a prevalent psychological condition with limited treatment options. While its etiology is multifactorial, both chronic stress and changes in microbiome composition are associated with disease pathology. Stress is known to induce microbiome dysbiosis, defined here as a change in microbial composition associated with a pathological condition. This state of dysbiosis is known to feedback on depressive symptoms. While studies have demonstrated that targeted restoration of the microbiome can alleviate depressive-like symptoms in mice, translating these findings to human patients has proven challenging due to the complexity of the human microbiome. As such, there is an urgent need to identify factors upstream of microbial dysbiosis. Here we investigate the role of mucin 13 as an upstream mediator of microbiome composition changes in the context of stress. Using a model of chronic stress, we show that the glycocalyx protein, mucin 13, is selectively reduced after psychological stress exposure. We further demonstrate that the reduction of *Muc13* is mediated by the *Hnf4* transcription factor family. Finally, we determine that deleting *Muc13* is sufficient to drive microbiome shifts and despair behaviors. These findings shed light on the mechanisms behind stress-induced microbial changes and reveal a novel regulator of mucin 13 expression.

Keywords

Mucins; Mucin 13; Depression; Microbiome; Despair behavior; Chronic stress

1. Introduction

Depression and anxiety impact millions of people worldwide (Santomauro et al., 2021). Although many treatments for these disorders exist, high rates of treatment-resistant cases remain. With up to 60% of patients unable to find satisfactory symptom resolution, the need for further investigation into novel therapeutic treatments is high (Fava, 2003). While the etiology of depression remains complex, one of the largest known contributing factors is stress (Heim and Binder, 2012; McGonagle and Kessler, 1990). Stress and depression are both associated with changes in the gut microbiome, and alterations in gut microbiome composition are present in depressed patients and conserved in animal models of depression (Lach et al., 2018; Foster and McVey Neufeld, 2013). Due to this, the microbiome has been

extensively targeted as a potential treatment for mental health disorders: modification of the microbiome has been shown to reduce depression symptoms in humans and depressive-like behaviors in mice (Marin et al., 2017; Tian et al., 2022; Berding and Cryan, 2022; Valles-Colomer et al., 2019). While promising, efforts to broadly manipulate the human microbiome remain inconsistent due to the microbiome's complexity, unknown microbe-microbe interactions, therapeutic microbes failing to colonize, microbe resource availability, and host heterogeneity (Berding and Cryan, 2022; Park et al., 2022; Zmora et al., 2018). To circumvent current microbiome therapeutic limitations and increase chances of successful microbial alterations in patients, there is a critical need to identify key conserved, targetable regulators of the microbiome.

The mucus layer is critical to maintaining both intestinal homeostasis and overall health. In the absence of mucus proteins, known as mucins, sweeping microbiome changes and spontaneous disease occur (Borisova et al., 2020; Hansson, 2020; Johansson et al., 2011; Van der Sluis et al., 2006; Velcich et al., 2002). Mucins are highly glycosylated proteins that fall into two categories: soluble mucins and transmembrane mucins (Hansson, 2020; Johansson MEVaH, G. C. The Mucins, 2016). While soluble mucins make up the gel-like layer that is commonly associated with mucus, transmembrane mucins remain tethered to the cell membrane (Hansson, 2020; Pelaseyed and Hansson, 2020). In the intestines, mucin 2 is the dominant soluble mucin, while mucin 13 and mucin 17 primarily represent the intestinal transmembrane mucins (collectively known as the glycocalyx) (Hansson, 2020; Pelaseyed and Hansson, 2020). Both soluble and transmembrane mucins have important roles in regulating the intestine and microbiome (Hansson, 2020). The mucus layer provides both a food source and anchor point for intestinal bacteria (Hansson, 2020). Recent works have demonstrated that the mucus layer drives the stability and composition of the microbiome by providing a permissive state for bacterial growth and selecting for specific bacteria along the intestines via varying availability of glycan chains (Van Herreweghen et al., 2020; Duncan et al., 2021; Sicard et al., 2017; Werlang et al., 2019). Supporting this idea, deletion of core 1 O-glycans in mice results in dramatic alterations of the microbiome composition and spontaneous colitis (Sommer et al., 2014; Fu et al., 2011).

Mucin expression is responsive to a variety of signals such as inflammation, infection, microbial products, and stress hormones (Hansson, 2020; Wheeler et al., 2019. Epub 2019/10/16.; Cairns et al., 2017; van Putten and Strijbis, 2017; Sheng et al., 2013; Gao et al., 2018; Silva et al., 2014). Specifically, stress hormones have been shown to alter the glycosylation patterns of mucins (Sommer et al., 2014; Silva et al., 2014; Biol-N'garagba et al., 2003). As changes in glycosylation have also been shown to change microbiome composition, these reports support the concept that stress may induce alterations in the mucus layer in a way that changes the microbial niche (Werlang et al., 2019; Kudelka et al., 2020; Bergstrom et al., 2020; Gamage et al., 2020). However, to date, no studies have attempted to understand the relationship between stress, mucin expression, and microbiome changes.

Given the strong evidence supporting the role of the mucus layer in microbiome homeostasis and regulation, as well as the known ways in which stress can alter mucin glycosylation, we hypothesized that exposure to chronic stress alters the mucus layer to initiate microbiome

changes. Here, we demonstrate that a model of chronic stress, in addition to altering the microbiome, selectively alters the expression of transmembrane mucin, mucin 13. This change is not observed after microbiome transfer from "stressed" mice into antibiotic treated or germ-free animals. This suggests that mucin 13 expression is not reduced by changes in the microbiome, but rather another mechanism regulates its expression. In addition, we demonstrate the transcription factor hepatocyte nuclear factor 4 (HNF4) regulates *Muc13* expression by binding the *Muc13* promoter. Supporting this, deletion of *Hnf4* dramatically reduced *Muc13* expression. Finally, we demonstrate that deletion of *Muc13* induces baseline despair behaviors, renders animals more susceptible to anxiety-like behaviors, and alters microbial signatures in a way that mimics the composition of microbes after stress exposure. Together, these findings suggest that Mucin 13 and HNF4 are mechanistic upstream regulators of stress-induced microbiome shifts.

2. Materials and methods

2.1. Mice

C57BL/6J and BALB/cJ mice were purchased from Jackson Laboratories (strain #000664 and #000651, respectively). Mice were bred in-house and kept on a 12-h light/dark schedule. All mice were group housed up to 5 mice per cage unless separated for fighting, the only male pup in a litter, or designated to a stressed group, where they were singly housed. All behavioral interventions were performed between 8 am and 3 pm and animals were sacrificed between 7 am and 1 pm. For stress experiment euthanization, all mice were removed from the overnight stressor at 7am. Euthanization began immediately upon removal from the overnight stressor and continued until all animals were sacrificed. Experimental and control animals were sacrificed in alternating patterns to ensure proper controls for circadian consideration. *Villin-Cre*^{ERT2}; *Hnf4a*$^{F/F}$; *Hnf4g*$^{Crispr/Crispr}$ animals (*Hnf4* DKO) were generated at Rutgers University under the care of the Verzi lab. Inducible knockouts for sequencing were given 1 injection of tamoxifen (50 mg/kg) for 2–3 days (2–3 total doses) to catch early changes in the intestines. HNF4 DKO mice used for qPCR were given 1 injection of tamoxifen (50 mg/kg) for 4 days (4 total doses). Animals were harvested on the 5th day. All control animals were given saline.

Mucin 13 knockout lines were generated using the iGONAD technique as described, using a BTX ECM 830 Electroporation System (Harvard Apparatus) (Gurumurthy et al., 2019; Ohtsuka et al., 2018). Briefly, the *Muc13* sequence was taken from the UCSC genome browser, mouse assembly Dec. 2011 (GRCm38/mm10), Genomic Sequence (chr16:33,794,037–33,819,927) (Kent et al., 2002). Exons 1 and 2 including the intervening intron where analyzed with CRISPOR (http://crispor.tefor.net/; Concordet and Haeussler, 2018). Exon 2, containing the protein start sequence, was targeted for excision at two target sequences + PAM sites: Exon2_protein_start_sequence GCAA-GAGCAGCTACCATGAA (AGG) and Exon2_end_of_exon AGTCTCCTTTTGGTGACCGT (GGG). Alt-R S.p. HiFi Cas9 Nuclease, tracrRNA, and crRNA XT for the two target sequences were purchased (IDT). Prior to surgery, the Alt-R CRISPR/Cas9 reagents were prepared according to IDT guidelines: crRNA-XT and tracrRNA were annealed to form the gRNA, complexed to the

S.p HiFi Cas9 nuclease, and then diluted with sterile Opti-MEM with Fast Green FCF to aid visualization.

Plugged females were anesthetized and maintained with isoflurane ~16 h after copulation was assumed to have occurred (estimated copulation around midnight, surgeries were done at 4 pm). Anesthesia was confirmed by toe pinch and eyes were lubricated with Puralube ointment. The lower dorsal skin of the mouse was soaked in betadine followed by two washes with isopropanol. A dorsal incision was made to expose the ovaries, oviduct, and uterine horn. Using a pulled micropipette, ~1.5 μL of the CRISPR/Cas9 solution was drawn up and then injected between the infundibulum and ampulla, intraoviductally dispensing the solution slowly to avoid backflow. The oviduct was covered in a wetted, sterile kimwipe and immediately electroporated using 3-mm platinum tweezer rode electrodes (BTX) delivering 50 V for 5 ms with 1 s interval for 8 square-wave pulses using a BTX ECM 830 Electroporation System (Harvard Apparatus). The oviduct was returned to the abdominal cavity and the procedure was repeated on the opposite side oviduct. Once both oviducts were injected and electroporated, the incision was sutured, and the stitches secured with liquid bandage before receiving a postop subcutaneous injection of ketoprofen (5 mg/kg of mouse body weight) with subsequent injections for up to five days as needed. All procedures were approved by the University of Virginia ACUC (protocol #3918). All experiments were conducted and reported according to ARRIVE guidelines.

2.2. Stress experiments and behavioral tests

Unpredictable Chronic Mild Restraint Stress (UCMRS) experiments and behavioral experiments (the forced swim, tail suspension, sucrose preference, open field, elevated plus maze, and nestlet shred tests) were performed as previously described. (Rivet-Noor et al., 2022).

Stress protocol: For UCMRS, all animals were single housed. Mice were exposed to 2 h of restraint stress and one overnight stressor per day. Restraint stress was performed by putting mice into ventilated 50 mL conical tubes for 2 h. Overnight stressors included one of the following: 45-degree cage tilt, wet bedding, or 2x cage change. Wet bedding was performed by wetting standard cage bedding with ~200 mL of murine drinking water. 2x cage change included replacing cage bases 2x within 24 hr. 45-degree cage tilt included propping cages up to ~45-degrees overnight.

Behavioral tests: All testing (with exception of the nestlet shred and sucrose preference tests) was recorded on a Hero Session 5 or 8 GoPro and analyzed with Noldus behavioral software.

Nestlet shred: Mice were moved into fresh individual cages and allowed to habituate for 1 h. After 1 h, a weighed nestlet was placed in the center of the cage. Mice were allowed to interact with the nestlet for 30 min. After 30 min, nestlets were removed and weighed. Before weighing, excess nestlet was stripped from the main piece of nestlet by lightly dragging fingers across each area of the nestlet starting from the center (center up, center left, center right, center down). Once completed, nestlet was flipped and the process was

repeated for the corners (center to upper right, center to upper left, center to lower right, center to lower left). Equal pressure was applied to each nestlet. Change in amount shredded and percent shredded were calculated from the weighed nestlet values.

Sucrose preference test: Mice were housed individually and given 2 water bottles/cage. One water bottle contained normal drinking water, the other contained 1% sucrose water. Mice had access to the bottles for 3 days. On Day 0, bottles were primed, weighed, and put in cages. Day 1: 24 h later, water bottles were removed from cages and weighed. Once weighed, bottles were replaced, but with swapped positions (i.e.- if sucrose was on the left on Day 0, it was on the right on Day 1). The first night of sucrose preference is considered habituation and the values are not included in analysis. Day 2: 24 h after replacing water bottles, bottles were weighed and replaced as on day 1. Day 3: 24 h after replacing water bottles, bottles were removed and weighed for a final time. Sucrose preference was calculated by determining the percentage of each bottle drunk on day 2 and 3 and averaging those values.

Elevated plus maze: Mice were placed on an elevated plus maze apparatus and allowed to explore for 5 min. The elevated plus maze was cleaned with 70% ethanol between each run and recorded on a GoPro Hero Session 5 or 8. Files were analyzed with Noldus behavior software.

Open field/DeepLabCut: Animals were placed into a 14in × 14in box with opaque walls and a raised clear bottom (18in). Animals were allowed to explore freely for 10 min. Hero session 8 cameras were placed ~18in below the box to record animal movements from below. Noldus behavioral software was used to determine if animals were in the perimeter or center of the box. Videos were also used for DeepLabCut analysis. Analysis is described below.

2.3. Metabolite mass spectrometry

25 μL of serum was extracted using 500 μL of cold acetonitrile followed by vortexing and 10 min of centrifugation at 14K rpm. 450 μL of the resulting supernatant was transferred to a clean Eppendorf and dried completely by Speedvac. Each sample was reconstituted with 25 μL of 50% methanol in 0.1% formic acid/water, vortexed and transferred to autosampler vials for analysis by mass spectrometry. Eleven metabolites were quantitated by PRM (parallel reaction monitoring) using a Thermo Orbitrap ID-X mass spectrometer coupled to a Waters BEH C18 column (15 cm × 2.1 mm). Metabolites were eluted with a Vanquish UHPLC system over a 15 min gradient (10 μL injection, 200 μL/min, buffer A – 0.1% formic acid in water, buffer B – 0.1% formic acid in methanol). The mass resolution was set to 120K for detection using the transitions outlines in Extended Data Table 6.

Raw data files for samples, blanks, and calibration curves were imported into Skyline (https://skyline.ms/project/home/begin.view). Calibration curves were generated with a linear regression. Peak areas for analytes in samples were used for quantification based in the generated calibration curves. Raw files can be downloaded for analysis at https://www.metabolomicsworkbench.org under study ID: ST002345.

2.4. Intestinal tissue mass spectrometry

Frozen intestinal tissue sections were homogenized use the Cryo-Cup Grinder (BioSpec Products, Cat. No. 206) according to manufacturer's instructions. Pulverized tissue was transferred into ice-cold 150 μL dialyzable lysis buffer, consisting of 1% N-octylglucoside (Research Products International, N02007), 1% CHAPS (Research Products International, C41010), 50 mM Tris (American Bio, AB14044), 100 mM NaCl (Research Products International, S23025), 2 mM $MgCl_2$ (American Bio, AB09006), benzonase (Sigma Aldrich, E1014), and protease inhibitor (Roche, 11836170001). Samples were rotated at 4 °C for 2 h, followed by centrifugation for 30 min at 15,000 rcf and passed through a 0.7 μm filter. $StcE^{E447D}$ was expressed and purified as previously described (Malaker et al., 2019; Malaker et al., 2022). 500 μg of NHS-Activated Agarose Slurry (Thermo Fisher Scientific, 26200) was activated with 1 mM HCl and PBS. $StcE^{E447D}$ (1 mL of 1.45 mg/mL) was added to the slurry and rotated at 4 °C for 3 h. Beads were rinsed with 100 mM Tris and the reaction quenched with 100 mM acetate buffer. Beads were washed with 20 mM Tris. Beads were then washed and stored in 20 mM Tris 150 mM NaCl. Filtered supernatants were rotated overnight at 4 °C with 100 μL $StcE^{E447D}$-NHS bead slurry and 0.01 M EDTA. All reactions were brought up to 1 mL with 20 mM Tris 150 mM NaCl. Beads were then rinsed with 10 mM Tris 1 M NaCl, 10 mM Tris 150 mM NaCl, 10 mM NaCl and MS grade water (Thermo Scientific, 51140). Protein was eluted with 1% sodium deoxycholate (Research Products International, D91500–25.0) in 50 mM Ammonium bicarbonate (AmBic) (Honeywell Fluka, 40867), at 95 °C for 5 min. Dithiothreitol (DTT) (Sigma Aldrich, D0632) was added to 20% of the eluent to a final concentration of 2 mM and allowed to react at 65 °C for 25 min. Alkylation in 5 mM iodoacetamide (IAA) (Sigma Aldrich, I1149) was performed for 15 min in the dark at room temperature. 0.05μg of sequencing-grade trypsin (Promega, V5111) was added to each 20% aliquot and allowed to react for 3 h at 37 °C. Reactions were quenched by adding 1 μL formic acid. All reactions were diluted to a volume of 100 μL prior to desalting. Desalting was performed using 10 mg Strata-X 33 μm polymeric reversed phase SPE columns (Phenomenex, 8B-S100-AAK). Each column was activated using 1 mL acetonitrile (ACN) (Honeywell, LC015) followed by of 1 mL 0.1% formic acid, 1 mL 0.1% formic acid in 50% ACN, and equilibration with addition of 1 mL 0.1% formic acid. After equilibration, the samples were added to the column and rinsed with 200 μL 0.1% formic acid. The columns were transferred to a 1.5 mL tube for elution by two additions of 150 μL 0.1% formic acid in 50% ACN. The eluent was then dried using a vacuum concentrator (LabConco) prior to reconstitution in 10 μL of 0.1% formic acid.

Samples were analyzed by online nanoflow liquid chromatography-tandem mass spectrometry using an Orbitrap Eclipse Tribrid mass spectrometer (Thermo Fisher Scientific) coupled to a Dionex UltiMate 3000 HPLC (Thermo Fisher Scientific). For each analysis, 5 μL was injected onto an Acclaim PepMap 100 column packed with 2 cm of 5 μm C18 material (Thermo Fisher, 164564) using 0.1% formic acid in water (solvent A). Peptides were then separated on a 15 cm PepMap RSLC EASY-Spray C18 Column packed with 2 μm C18 material (Thermo Fisher, ES904) using a gradient from 0 to 35% solvent B. (0.1% formic acid with 80% CAN) in 60 min.

Full scan MS1 spectra were collected at a resolution of 60,000, an automatic gain control of 1E5, and a mass range from 400 to 1500 *m*/*z*. Dynamic exclusion was enabled with a repeat count of 2 and repeat and duration of 8 s. Only charge states 2 to 6 were selected for fragmentation. MS2s were generated at top speed for 3 s. Higher-energy collisional dissociation (HCD) was performed on all selected precursor masses with the following parameters: isolation window of 2 *m*/*z*, stepped collision energies of 25%, 30%, 40%, orbitrap detection (resolution of 7500), maximum inject time of 75 ms, and a standard AGC target.

Label-free quantification was performed using the minimal workflow for MaxQuant according to the established protocol for standard data sets (Tyanova et al., 2016). Files were searched with fully specific cleavage C-terminal to an Arg or Lys residue, with 2 allowed missed cleavages. Carbamidomethyl Cys was set as a fixed modification. Raw data generated from each intestinal section was included and analyzed using Perseus, according to the recommended protocol for label-free interaction data (Fold change > 5 as the cutoff).

2.5. Fecal DNA extraction and 16S rRNA gene sequencing

DNA was isolated from fecal pellets using the phenol/chloroform method as described (Marin et al., 2017). Samples were then processed with QIAquick PCR purification kit (Qiagen #28106). Full protocol is outlined below:

250 μL of 0.1 mm zirconia/silica beads (BioSpec #11079101z) were added to a sterile 2 mL screwtop tube (Celltreat #230830). One 4 mm steel ball was added to each tube (BioSpec #11079132ss). 500 μL of Buffer A (200 mM TrisHCl, pH 8.0, 200 mM NaCl, 20 mM EDTA) and 210 μL of 20% SDS were added to each fecal pellet in a separate 1.7 mL tube. Pellets were vortexed and supernatant transferred to the 2 mL screwtop tube containing beads. 500 μL of Phenol/chloroform/IAA were added to each screwtop tube. Tubes were allowed to beadbeat on high for 4 min at room temperature. Samples were then centrifuge at 12000 rpm for 5 min at 4 °C. 420 μL of the aqueous layer was transferred to a new 1.7 mL tube. 100 μL of the samples was then processed using the Qiagen PCR Purification Kit.

16S sequencing of 3 week UCMRS experiments: The V4 region of the 16S rRNA gene was amplified from each sample using a dual indexing sequencing strategy (Kozich et al., 2013). Samples were sequenced on the MiSeq platform (Illumina) using the MiSeq Reagent Kit v2 (500 cycles, Illumina #MS102–2003) according to the manufacturer's protocol with modifications found in the Schloss Wet Lab SOP (https://github.com/SchlossLab/MiSeq_WetLab_SOP).

All processing and analysis of 16S rRNA sequencing data was performed in R (version 4.1.2) (Team RC, 2021). Raw sequencing reads were processed for downstream analysis using DADA2 (version 1.22.0) (Callahan et al., 2016). Processing included inspection of raw reads for quality, filtering of low-quality reads, merging of paired reads, and removal of chimeric sequences. Length distribution of non-chimeric sequences was plotted to ensure lengths matched the expected V4 amplicon size. Taxonomy was assigned to amplicon sequence variants (ASVs) by aligning reads with the Silva reference database (version 138.1) (Quast et al., 2013).

Microbiota diversity and community composition were analyzed using the packages phyloseq (version 1.38.0), microbiome (version 1.16.0), and vegan (version 2.5.7) (Jari Oksanen et al., 2020; Leo Lahti; McMurdie and Holmes, 2013). The packages tidyverse (version 1.3.0), and ggplot2 (version 3.3.5) were used for data organization and visualization (Hadley Wickham et al., 2019; Wickham, 2016).

Random forest analysis was performed using the randomForest (version 4.6.14), vegan (version 6.0.90), and pROC (version 1.18.0) packages (Kuhn, 2021; Liaw A, 2002; Robin et al., 2011). Samples were first divided into training (70% of samples, divided equally between Baseline and stress samples) and test (30% of samples) sets. The training set was used to tune the "mtry" parameter of the model, while the test set was used to validate model performance. Feature importance was determined using the Gini index, which measures the total decrease in node impurity averaged across all trees. Custom code and detailed instructions can be found at: https://github.com/gbmoreau/Gautier-manuscript. Raw sequencing reads can be found in the NCBI Sequence Read Archive (SRA) database under PRJNA867333.

2.6. Microbiome transfer experiments

Antibiotic microbiome transfer experiments were performed by treating mice with a cocktail of the following antibiotics: ampicillin (Sigma-Aldrich, A8351), neomycin (Sigma-Aldrich, N6386), metronidazole (Sigma-Aldrich, M1547), and vancomycin (Sigma-Aldrich, V1130). Ampicillin, neomycin, and metronidazole were added to water containing 8 g/L of a zero-calorie sweetener at 1 g/L. Vancomycin was added at 500 mg/L. Mice were allowed to drink ad libitum for two weeks and fresh antibiotic solutions were made once per week. After 2 weeks of antibiotic treatment, mice were given an oral gavage of 100 μL of either naïve or stressed fecal slurry (equal weights of collected fecal pellets homogenized in 4 mL PBS) every 2 days for a total of 4 gavage treatments (Fig. 2, panels E and F). Animals were allowed to habituate to the introduced microbiome for 14 days from the first gavage. Germ-free experiments where animals received stress or naïve fecal pellets were described previously (Merchak et al., 2024). Briefly, equal amounts of dirty bedding from naïve or stressed animals was transferred daily to germ-free animal cages for two weeks. After two weeks of dirty bedding transfer, animals were allowed to habituate to the transferred microbiome without further intervention for another two weeks.

2.7. 16S sequencing of microbiome transfer and 1 week UCMRS experiments

Fecal pellet DNA extraction and 16S sequencing of the V4 region was performed by Zymo according to their protocols. Raw sequencing reads can be found in the NCBI Sequence Read Archive (SRA) database under PRJNA878703 and PRJNA866924, respectively.

2.8. Cell culture

HT-29 cells were purchased from ATCC and were grown in McCoy's 5A media (ATCC 30–2007) as per the ATCC website. Cells were plated at a density of 150,000/well and allowed to adhere to 12 well plates overnight in complete media. Cells were treated with 10 μM of the HNF4 antagonist BI6015 (Sigma-Aldrich, 375240) or DMSO control for 24 h.

After 24 h, media was aspirated, and cells were frozen at −80 °C until RNA extraction was performed.

2.9. RNA and ChIP seq experiments

All ChIP Seq experiments were performed previously on duodenal villus tissue as described (Chen et al., 2021a; Chen et al., 2019). Raw data can be found under GEO accession numbers GSE112946 (RNA-seq and ChIP-seq) and GSE148691 (HiChIP-seq).

2.10. DeepLabCut

DeepLabCut analysis was performed as previously described (Rivet-Noor et al., 2022). Full protocol is outlined below:

Animal pose estimation was performed on videos collected during the open field test by using a deep-learning package called DeepLabCut. The detailed mathematical model and network architecture for DeepLabCut was previously published by the Mathis lab (Mathis et al., 2018). We generated a DeepLabCut convolutional neural network to analyze our open field test videos which were trained in a supervised manner: 16 manually labeled points were selected as references of transfer learning, including: nose, left and right eyes, left and right ears, neck, left and right arm, left and right leg, 3 points on body, and 3 points on tail. In total, 15 randomly selected videos were used for building a training dataset. Once trained, DeepLabCut was applied to the collected sample videos and final pose estimations were made.

Estimated mouse poses from DeepLabCut were further analyzed by using a package called Variational Animal Motion Embedding (VAME), which classifies animal behavior in an unsupervised manner. VAME was developed by the Pavol Bauer group and the package can be downloaded at https://github.com/LINCellularNeuroscience/VAME (Luxem et al., 2020). We trained a unique VAME recursive neural network for each experiment, which classifies each frame of the open field test video into 1 of the 25 behavioral motifs. VAME is then applied to all experimental videos to categorize behaviors into 1 of 25 motifs. All behavior motifs were annotated, labeled, and evaluated by blinded human researchers. With annotated frames, we were able to calculate the percentage of time usage of each motif, which is then used for principal component analysis and Kullback-Leibler divergence analysis. Custom code is available upon request.

2.11. RNA extraction and quantitative PCR

For RNA extraction, cultured cells were pelleted, frozen, and lysed. RNA was extracted using the Bioline Isolate II RNA mini kit as per manufacture's protocol (BIO-52073). RNA was quantified with a Biotek Epoch Microplate Spectrophotometer. Normalized RNA was reverse transcribed to cDNA with either the Bioline SensiFast cDNA Synthesis Kit (BIO-65054) or Applied Sciences High-Capacity cDNA Reverse Transcriptase Kit (43–688-13). cDNA was amplified using the Bioline SensiFast NO-ROX kit (BIO-86020), according to manufacturer's instructions. Results were analyzed with the relative quantity (ΔΔCq) method. Most qPCR was performed with Taqman primers purchased from

ThermoFisher (catalog numbers provided in Extended Data Table 5). For assays where commercial primers were not used, primer sequences are listed in Extended Data Table 5.

2.12. Immunofluorescence staining and imaging

1 cm sections of intestinal samples were harvested and snap frozen in an OCT block (Fisher Scientific #14-373-65). Samples were cut on a cryostat in 15 μM sections and placed on microscope slides. Tissue was fixed directly on the slides in carnoy's solution (60% Ethanol, 30% Chloroform, and 10% Glacial Acetic Acid) for 10 min at room temperature. Tissue was washed in 1x PBS for 5 min 3x at room temperature. Antigen retrieval was performed with Tris-EDTA by bringing solution to a boil (~30sec) in a microwave. Slides were washed in 1x PBS 3x for 5 min at room temperature. After final wash, sections were outlined with a hydrophobic pen (Vector Laboratories #H-4000). Samples were blocked for 1 h at room temperature with 1:200 FC block in TBST (1x TBS + 0.3 % Triton X-100) plus 2 % Normal Donkey Serum (Jackson ImmunoResearch #017-000-121). Supernatant was removed and samples were blocked with Mouse on Mouse IgG for 1 h at room temperature (Vector Laboratories #MKB-2213-1). Supernatant was removed and primary antibodies were added. Samples were stained with 1:1000 Mucin 13 (G-10) (Santa Cruz Biotechnology #sc-390115) and 1:1000 Mucin 2 (GeneTex #GTX100664) overnight at 4 °C in blocking solution (1x PBS, 0.5 g bovine serum albumin, 0.5 % Triton X-100) + 2 % normal donkey serum. Control samples were stained in blocking solution + 2 % normal donkey serum with mouse IgG (Jackson ImmunoResearch #015-000-003) and rabbit IgG (Jackson ImmunoResearch #011-000-003) diluted to match the primary antibody concentrations. The next day samples were washed in TBST for 5 min 3x at room temperature. Samples were then incubated in secondary antibodies for 3 h at room temperature in blocking solution + 2 % normal donkey serum. Secondary antibodies used were Donkey Anti-Mouse 488 (Jackson ImmunoResearch #715-545-150) and Donkey Anti-Rabbit 647 (Jackson ImmunoResearch #711-605-152). Secondaries were added at 2 mg/mL. Samples were then stained with Hoechst (1:700) (Thermo Fisher Scientific #H3570) for 15 min in blocking solution + 2 % normal donkey serum. Samples were washed 2x with TBST for 5 min at room temperature. Samples were washed a final time in TBS for 5 min at room temperature and cover-slipped. Finally, slides imaged on a Leica Stellaris 5 confocal microscope.

2.13. Statistical analysis

All statistical analyses-except those associated with DeepLabCut, Mass Spectrometry, and 16S were performed in GraphPad Prism 9. Analyses comparing two groups were performed using a two-tailed T test. If the variances between groups were significantly different, a Welch's correction was applied. Outliers were excluded based on the ROUT test in GraphPad Prism 9. For all analyses, the threshold for significance was at $p < 0.05$. Repeats for each experiment are specified in the figure legend corresponding to the respective panel and in Extended Data Table 4. Additional statistical detail, including all p-values, can be found in Extended Data Table 4.

3. Results

3.1. Unpredictable chronic mild restraint stress drives despair and anxiety-like behaviors and modifies the gut microbiome composition

To investigate the mechanisms of stress-induced microbiome alterations, we used unpredictable chronic mild restraint stress (UCMRS), a version of chronic stress known to induce anxiety- and depressive-like behaviors and alter gut flora (Fig. 1A) (Marin et al., 2017; Mineur et al., 2006). After three weeks, mice exposed to UCMRS showed a significant increase in anxiety-like behaviors characterized by an increase in nestlet shredding and decrease in time spent in the open arms of the elevated plus maze (Fig. 1B). Despair behaviors were also detected through an increase in time inactive in both the tail suspension and forced swim tests. Furthermore, a reduction in sucrose preference, a measure for anhedonia, was observed in UCMRS exposed mice (Fig. 1B). In addition to behavioral readouts, levels of murine stress- and depression- associated markers were measured from serum by mass spectrometry (Fig. 1C and Supplementary Fig. 1A–G). An increase in murine cortisol, but not corticosterone, was detected in stressed mice, confirming a robust chronic stress response (Fig. 1C, Supplementary Fig. 1A). While murine stress responses are often associated with changes in corticosterone, mice also express cortisol to a lesser extent. (Dodiya et al., 2020; Gong et al., 2015; Luo et al., 2018). In addition, while elevations in corticosterone are abundant in acute models of stress, literature suggests that in chronic stress corticosterone levels return to baseline while higher cortisol levels are sustained (Gong et al., 2015). These works, in addition to our own data (Fig. 1C and Supplementary Fig. 1A), demonstrate that cortisol can be used as a measure for chronic stress response in mice. To further examine the impacts of UCMRS on stress and depressive-like responses in mice, we examined the presence of serotonin and glutamine in the serum of naïve or UCMRS exposed mice. Glutamine has been shown to be depleted in both models of chronic stress and animal models of depression, highlighting its reliability as a biomarker for true stress and depressive-like responses in mice (Baek et al., 2020; He et al., 2023; Pfleiderer et al., 2003; Xu et al., 2020). Serotonin depletion has also long been associated with depression in both humans and animal studies (Israelyan et al., 2019; Moncrieff et al., 2023; Vahid-Ansari and Albert, 2021). Consistent with our behavioral and cortisol data, decreases in both serotonin and glutamine were observed, further suggesting a true stress and depressive-like response after UCMRS exposure. No other molecules tested were changed (Supplementary Fig. 1A–G). These data highlight the validity of our model by demonstrating UCMRS induces changes in behavioral outputs and metabolites in mice that are consistent with human anxiety and depression.

We next evaluated stress-induced microbiome composition changes by performing 16S sequencing on fecal DNA from stressed and naïve animals. Using ASV-level data, we observed no differences in measures of alpha diversity (richness (Fig. 1D) or evenness (Supplementary Fig. 1H)). However, there were significant differences in ASV-level derived beta diversity between naïve and stressed animals (Fig. 1E). These differences were driven by changes in community composition at the ASV level; for clarity, bacterial orders are depicted. Consistent with our previous work, stress was associated with relative reductions in *Clostridiales*, *Lactobacillales*, and an expansion of *Bacteroidales* (Fig. 1F and

Supplementary Fig. 1I) (Marin et al., 2017). Specific genus level changes between groups and the associated statistics can be found in Supplementary Fig. 1J and Extended Data Table 1. Lastly, an ASV based random forest model accurately predicted which bacterial orders were most influential in baseline or stressed groups, strengthening the link between stress and specific microbial shifts (Fig. 1G). The Gini index assesses the importance of a particular bacterial order in defining a group by examining how much of a decrease in purity, or accuracy, occurs when a bacterial order is removed for consideration. For example, the removal of *Clostridiales* from consideration when defining the Baseline group (Fig. 1G) results in a more impure (or less accurate) node in the random forest analysis. Orders that do not decrease node impurity are not expected to contribute to group identity and would not be expected to be different between groups. Taken together, these results demonstrate that unpredictable chronic mild restraint stress (UCMRS) induces despair and anxiety-like behaviors in mice, alters murine stress hormone levels, and induces composition shifts in the murine microbiome.

3.2. Unpredictable chronic mild restraint stress reduces Muc13 expression in vivo

While it is well accepted that stress can alter the microbiome in humans and mice (Fig. 1), the mechanisms behind these microbial shifts remain unknown (Bailey et al., 2011; Bastiaanssen et al., 2020; Berding and Cryan, 2022; Karl et al., 2017; Li et al., 2019). Because the mucus layer, primarily composed of heavily glycosylated mucins, provides both an anchor point and nutrient reservoir for bacteria, we hypothesized that a change in mucin composition could induce microbiome shifts (Hansson, 2020; Johansson, 2016; Pelaseyed and Hansson, 2020). To test this, we first evaluated if mucin expression changed in stressed conditions. Using RNA extracted from individual sections of the intestines of mice exposed to UCMRS and naïve controls (Fig. 2A), we examined mucin expression by qPCR. Of all the mucins examined (all detectable intestinal mucins: *Muc1*, *2*, *4*, *13*, and *17*), we found that *Muc13* was uniquely reduced across intestinal segments (Fig. 2B–C and Supplementary Fig. 2A–C). Additionally, to examine mucin changes across genetic background, we examined *Muc13* and *Muc2* expression in BALB/cJ mice exposed to stress. We found a similar reduction in *Muc13*, while no changes in *Muc2* expression were observed (Supplementary Fig. 2D–E). We then sought to examine mucin 13 changes at the protein level by mass spectrometry and immunofluorescence. However, due to the subtle changes observed in *Muc13* transcript expression and the limitations in sensitivity and availability of mucin protein quantification techniques, we were unable to detect differences at the protein level. As quantifying mucin protein levels, especially subtle changes, remains challenging across the glycobiology field, changes in mucin transcript are well accepted as a readout for mucin changes (Harrop et al., 2012; Kesimer and Sheehan, 2012; Malaker et al., 2019, 2022; Tian et al., 2023). Given these known technical limitations and the consistent changes in mucin 13 transcript expression across experiments and genetic backgrounds, we proceeded to investigate the role of mucin 13 in stress-induced microbiome changes.

3.3. Stress-induced Muc13 transcript reductions are driven independently of transferrable microbial products

The microbiome is a known influencer of the mucus layer. While we hypothesized that stress-induced changes in the mucus layer lead to changes in microbiome composition, we

also considered that stress-induced shifts in the microbiome could instead be modulating *Muc13* expression (Hansson, 2020; Sicard et al., 2017). If this was the case, it would suggest that mucin 13 expression changes occur after microbial shifts in our model. To test this hypothesis, we utilized two different models to examine the impacts of the microbiome on mucin 13 expression. First, after treating mice with antibiotics for two weeks, we transferred the fecal microbiomes from naïve or stressed animals via oral gavage (Fig. 2D). After allowing two weeks post reconstitution for microbiome stabilization, intestinal samples were collected to examine microbiome composition and mucin expression (Suez et al., 2018). 16S sequencing revealed that the donor slurries clustered distinctly from each other (Supplementary Fig. 2F, light blue and dark pink). In addition, recipient mice clustered nearer to their donor sample but separately from each other, demonstrating distinct microbiomes and successful transfer of the expected signatures (Supplementary Fig. 2F–G). We next examined RNA expression of intestinal mucins between groups. No change in mucin 13 expression was detected between animals that received a stressed or naïve microbiome (Fig. 2E). In addition, we saw no change in any other mucins expressed between groups (Fig. 2F and Supplementary Fig. 2H–J). These data demonstrate that microbial signatures from transferred stressed or naïve microbiomes are not sufficient to reduce mucin 13 expression.

To complement this approach, we also examined the impact of stressed microbial signatures on mucin expression in germ-free mice. Our lab has successfully demonstrated that microbial signatures from stressed mice can induce despair and anxiety-like behaviors in germ-free mice (Merchak et al., 2024). Therefore, using intestinal samples collected from germ-free mice which were given fecal pellets from naïve or stress-exposed animals, we again examined changes in mucin expression between groups by qPCR. Our results indicated that, like the antibiotic treated mice, no changes in *Muc13* expression were observed between groups after colonization (Fig. 2G). This suggests that microbes from UCMRS exposed mice are not sufficient to induce mucin 13 expression changes in germ-free animals when compared to germ-free animals given microbes from naïve controls. In addition, while we saw no changes in *Muc1*, *Muc4*, or *Muc17,* we did see an expected increase in *Muc*2 expression with microbiome reconstitution in germ-free mice (Fig. 2H and Supplementary Fig. 2K–M) (Johansson et al., 2015). Taken together, these results demonstrate that microbial signatures from stressed animals, while able to induce behavioral changes, are not sufficient to reduce *Muc13* expression in the intestines. This again suggests that the mucin 13 changes observed in stress are not driven by – and likely precede – microbial changes in the intestines. These results support our hypothesis that stress-induced reductions in mucin 13 are driven independently of transferrable microbial signatures.

3.4. Muc13 reductions are driven by reductions in intestinal HNF4

To understand how stress induces reductions in *Muc13* expression, we explored transcription factors which are known to bind to *Muc13* by examining published small intestine and colon ChIP-seq data sets through the UCSC genome browser (Kent et al., 2002). Results revealed 10 transcription factors able to bind to the promoter region of *Muc13* in both the small and large intestines (*Ascl2*; *Cdx2*, *Hnf4α*, *Hnf4γ*, *Vdr*, *Med1*, *Pou2f3*, *Smad4*, *Ctcf*, and *Foxa1*) (Chahar et al., 2014; Lickwar et al., 2022). Hepatocyte nuclear factor 4 (HNF4), a

member of the nuclear receptor superfamily, plays a critical role in regulating metabolism, epithelial tight junctions, and the differentiation and proliferation of enterocytes in the intestines (Babeu and Boudreau, 2014). In addition to these functions, *Hnf*4 expression has been shown to regulate the brush border, the collection of microvilli along the intestinal tract (Chen et al., 2021b). As the brush border is thought to be modulated by the density of the glycocalyx, and therefore transmembrane mucins, HNF4 is a prime candidate to mediate changes in *Muc13* expression (Shurer et al., 2019). Importantly, stress hormones have also been shown to inhibit *Hnf*4 expression in a model of high fat diet (Lu et al., 2022). Together, these works provide a foundation for the hypothesis that stress may be able to regulate *Hnf4* expression in a way that reduces *Muc13* expression.

In order to investigate the ability of HNF4 to regulate *Muc13* expression, we first analyzed previously performed HNF4 and H3K27ac ChIP-seq on wildtype duodenal villus cells to examine binding at the *Muc1*3 locus (Chen et al., 2019). Results indicated that in wildtype mice, both HNF4 and H3K27ac, a marker of transcription, are enriched in the promoter region of *Muc13* (Fig. 3A). This suggests that HNF4 binds the *Muc13* promoter at a site that is marked for active transcription, supporting the idea that HNF4 can regulate *Muc13* expression. We next wanted to examine the impacts of HNF4 deletion on *Muc13* expression in the intestine. To do this, we utilized the previously described *Villin-Cre*^{ERT2}; *Hnf4a*$^{F/F}$; *Hnf4g* $^{Crispr/Crispr}$ double knockout line (*Hnf4* DKO) which lacks both HNF4 paralogs (Chen et al., 2019). Analyzing previously performed RNA Polymerase II (RNAP2) ChIP-seq on duodenal villus epithelial cells in wildtype controls and *Hnf4* DKO animals, we found that the RNAP2 signal at the *Muc13* promoter is markedly reduced in the *Hnf4* DKO animals compared to controls (Fig. 3B). To complement this approach, we further examined previously performed H3K4me3 chromosome conformation capture with chromatin immunoprecipitation (HiChIP) and RNA-seq on control and *Hnf4* DKO duodenal villus epithelial cells (Chen et al., 2021). Analysis revealed fewer H3K4me3 chromatin loops in the *Muc13* promoter region of *Hnf4* DKO animals than in control duodenal villus epithelial cells, suggesting fewer sites of active transcription (Fig. 3C). In addition, RNA sequencing results showed a significant reduction in *Muc13* expression in duodenal villus epithelial cells after the loss of *Hnf4* (Fig. 3D). *Hnf4* deletion did not reduce expression of any other detectable mucins by RNA-seq (Supplementary Fig. 3A–C). To validate these sequencing results, we next performed qPCR for mucin expression on all sections of the intestines from control and *Hnf4* DKO animals. We found that in addition to the successful deletion of the *Hnf4* paralogs (Fig. 3E–F), there was also a significant reduction in *Muc13* expression across the intestines, validating the RNA-seq data (Fig. 3G). Given the dramatic reduction in *Muc13* expression in *Hnf4* DKO animals, we again sought to examine mucin 13 protein levels. To do this, we employed a mucin enrichment strategy that takes advantage of an inactive protease selective for mucin domains; mucins from *Hnf4* DKO and control animal intestines were enriched and subjected to MS analysis (Malaker et al., 2019; Malaker et al., 2022). Confirming our RNA-seq and qPCR data, *Hnf4* DKO animals had significant reductions in MUC13 protein expression across all sections of the intestine (Fig. 3H). Lastly, we analyzed intestinal expression of *Hnf4* from mice exposed to 3 weeks of UCMRS (Fig. 1A). Our results indicated that *Hnf4* expression is significantly reduced in the intestines after stress exposure (Fig. 3I–J). In addition, leucine rich repeat containing G protein

coupled receptor 5 (Lgr5), which is known to be suppressed in *Hnf4* knockout animals, was also significantly reduced, demonstrating successful *Hnf4* deletion (Supplementary Fig. 3D) (Chen et al., 2020). Further supporting our data, germ-free mice that had been given fecal pellets from stressed or naïve mice showed no differences in *Hnf4* expression, suggesting that *Hnf4* expression changes are not driven by transferrable microbial products from stressed or naïve mice (Supplementary Fig. 3E–F).

To confirm our results *in vitro* and examine the impacts of HNF4 on *Muc13* expression more directly, we utilized HT-29 cells. HT-29 cells are a human colon cancer cell line that is known to express both mucins and *Hnf4* (Darsigny et al., 2010; Gupta et al., 2014). Cells were treated with an HNF4 antagonist (BI6015) or a DMSO control for 24 h (Kiselyuk et al., 2012; Lee et al., 2022). We then extracted the RNA from the collected cells and examined mucin expression as before. We found that treatment with the antagonist BI6015 showed a significant downregulation of *MUC13* expression (Supplementary Fig. 3G). In addition, *LGR5* showed decreased expression with BI6015, demonstrating successful antagonist activity on HNF4 (Supplementary Fig. 3H) (Gupta et al., 2014). These results further support the hypothesis that *MUC13* is regulated by HNF4.

Together, our data suggest that in the absence of HNF4, there is less active transcription at, and fewer transcripts of, the *Muc13* gene. In addition, loss of *Hnf4* significantly reduces MUC13 protein expression across the intestines. These data support the hypothesis that *Muc13* expression is regulated by HNF4. Our results also demonstrate that after UCMRS exposure, there is a significant reduction in *Hnf4* that occurs independently of transferrable microbial products, suggesting that stress can reduce *Hnf4 in vivo*. Finally, we show that direct modulation of HNF4 results in *Muc13* expression changes *in vitro,* validating our *in vivo* findings. Taken together, these results demonstrate that *Muc13* expression is modulated by HNF4 *in vitro*, *in vivo,* and after stress exposure.

3.5. Muc13 deletion induces baseline behavioral and microbiome changes and renders mice more susceptible to UCMRS

Given our data demonstrating that *Muc13* is specifically downregulated in stressed animals (Fig. 2B), we sought to examine if deleting *Muc13* impacted the microbiome and behavioral outputs in mice. Using the *i*-GONAD system, we created a *Muc13* knockout ($Muc13^{-/-}$) mouse line by deleting a 475 bp region of the *Muc13* gene containing the start codon (Fig. 4A) (Gurumurthy et al., 2019; Ohtsuka et al., 2018). Validation of the knockout line was performed using both qPCR (Fig. 4B–C) and immunofluorescence (Fig. 4D–E). Importantly, no changes were observed in *Muc2* at the transcript or protein levels, suggesting that *Muc2* expression was not changed with the loss of *Muc13* (Fig. 4C and F). To complement this approach, and given the dramatic reduction in mucin 13 transcript, we also examined detectable mucins at the protein level by mass spectrometry in $Muc13^{-/-}$ and control animals. We found a significant reduction in MUC13 protein abundance in all sections of the intestine (Fig. 4G). No other detectable mucin was statistically significantly changed (Fold Change > 5), suggesting that none of the other membrane mucins nor soluble mucins, compensate for the loss of MUC13. In addition, to confirm no changes in barrier integrity, we examined expression of tight junction proteins in our $Muc13^{-/-}$ animals. No changes in

tight junction RNA expression were observed (Supplementary Fig. 4A–B). Together, these data demonstrate a successful deletion of mucin 13 in our knockout line.

We next sought to understand the impacts of *Muc13* deletion on microbiome composition. We compared 16S sequencing results from fecal samples collected from adult wildtype and *Muc13*$^{-/-}$ animals that were separated by genotype at weaning. Interestingly, we found that *Muc13*$^{-/-}$ animals (light green) clustered distinctly from wildtype controls (light orange), suggesting that *Muc13* deletion significantly impacts the composition of the microbiome at baseline (Fig. 5B). In addition, to understand if *Muc13*$^{-/-}$ animals have stress-induced microbiome shifts, we used an abbreviated 1-week UCMRS protocol (Fig. 5A). In our hands, this abbreviated protocol allows for substantial microbial shifts, but does not yet yield all stress-induced anxiety-like and despair behaviors in wildtype animals (Fig. 5D–G, light orange to dark pink bars). This allowed us to examine if *Muc13*$^{-/-}$ mice are more susceptible to UCMRS-induced behavioral changes than their *Muc13* competent controls. As animals that are more susceptible to UCMRS-induced behavioral changes would be expected to show behavioral changes sooner than wildtype animals, our 1 week UCMRS protocol allowed us to examine behavior differences at an earlier timepoint. Our results show that while wildtype samples display a significant shift in microbial composition after 1 week of UCMRS (light orange to dark pink dots), *Muc13*$^{-/-}$ (light green to dark green dots) samples remained clustered together (Fig. 5B). This suggests that the microbiome of *Muc13*$^{-/-}$ animals is different from widltype animals at baseline and is less modified by 1-week of UCMRS exposure. In addition, samples from wildtype animals exposed to 1 week of UCMRS shifted towards both *Muc13*$^{-/-}$ groups (baseline and 1 week UCMRS, light and dark green dots), supporting the idea the *Muc13*$^{-/-}$ animals have baseline microbial signatures which resemble stress-induced microbiome changes (Fig. 5B). To further understand the similarities between the *Muc13*$^{-/-}$ microbiome and the UCMRS-exposed microbiome, we compared the significantly changed bacterial families between baseline wildtype and baseline *Muc13*$^{-/-}$ animals to the significantly changed bacterial families between baseline wildtype animals and wildtype animals exposed to 1 week of UCMRS. Of the bacterial families that had significant changes in either group, 69% of those changes overlapped (Fig. 5C). While we also examined overlapping changes at the genus and ASV levels, algorithm matching limitations hindered our ability to draw conclusions. While 58% of genera and 62% of ASV changes overlapped between groups, only ~45% of total reads could be matched to a known genus or ASV – making clear comparisons at these levels difficult (Extended Data Table 3). Nonetheless, data at the family level suggests significant overlap in changes between baseline control and baseline *Muc13*$^{-/-}$ animals when compared to baseline wildtype and UCMRS exposed wildtype animals. This suggests that the overlapping changes between baseline wildtype and UCMRS exposed wildtype animals and wildtype to *Muc13*$^{-/-}$ animals may be driven by reductions in *Muc13*. Taken together, these data support the hypothesis that reductions in *Muc13* drive microbiome changes.

Given the established connection between microbiome changes and mental health, we sought to examine if *Muc13* deletion impacted anxiety-like and despair behaviors in mice (Marin et al., 2017). Both *Muc13*$^{-/-}$ animals and wildtype controls were subjected to the open field, nestlet shred, tail suspension, and forced swim tests (Fig. 5A, D–G). Behavior

was collected at baseline and after 1 week of UCMRS for all animals. Interestingly, at baseline, we observed no differences in anxiety-like behaviors in the open field or nestlet shredding tests between *Muc13*$^{-/-}$ and wildtype controls (Fig. 5D–E, left columns). However, strong despair behaviors were observed in both the tail suspension and forced swim tests (Fig. 5F–G, left columns), suggesting *Muc13*$^{-/-}$ mice display innate despair, but not anxiety-like, behaviors. In addition, to gain a full picture of the impact of *Muc13* deletion on susceptibility to stress-induced despair and anxiety-like behaviors, we subjected wildtype and *Muc13*$^{-/-}$ mice to 1 week of UCMRS. As stated above, 1 week of UCMRS exposure represents a subclinical model of stress that does not induce all expected behavioral changes in wildtype animals (Peng et al., 2012; Pothion et al., 2004). Thus, we hypothesized that if *Muc13*$^{-/-}$ deletion rendered animals more susceptible to stress, they would exhibit despair and anxiety-like behaviors earlier than wildtype animals (Nollet et al., 2013). Supporting this hypothesis, following 1 week of UCMRS, *Muc13*$^{-/-}$ animals had significant reductions in the amount of time spent in the center of the open field test, as well as significant increases in the amount of nestlet removed in the nestlet shred test. Of note, no changes in distance traveled were observed between groups in the open field test at baseline or after 1 week of UCMRS (data not shown). These results indicate that 1 week of UCMRS is sufficient to increase anxiety-like phenotypes in *Muc13*$^{-/-}$ animals, but not their wildtype counterparts (Fig. 5D–E, green columns). Furthermore, in the tail suspension and forced swim tests, we saw no increase in time spent inactive as the *Muc13*$^{-/-}$ animals presented with despair behaviors at baseline and likely hit a ceiling effect (Fig. 5F–G, green columns). To complement these classical behavioral assays, we used unbiased artificial intelligence (DeepLabCut) to detect animal poses (Fig. 5H–J and Supplementary Fig. 5) (Mathis et al., 2018; Rivet-Noor et al., 2022). In this approach, 10-minute videos of mice exploring an open field box were broken down into 25 individual motifs (Fig. 5H). Each motif was characterized and grouped into a general behavioral classification (rearing/grooming, turning, etc.). Individual motifs represent a behavioral pattern based on mouse limb and tail position detected by DeepLabCut. For example, the general behavior classification “turning” included motifs such “head turning left”, “mid-point of right turn”, etc. As these motifs together make up a complete behavior, they were grouped in general behavioral classifications. Once grouped, changes in the percentage of time spent in each behavioral motif were quantified between *Muc13*$^{-/-}$ and wildtype animals (Fig. 5H–J). Baseline analysis revealed that of the 25 distinct motifs, 16% were significantly changed between groups (Supplementary Fig. 5A–B), suggesting that, like in classical behavioral assays, distinctions between *Muc13*$^{-/-}$ and wildtype animals are present at baseline. Similarly, the DeepLabCut software was able to detect significant differences between groups after 1 week of UCMRS exposure, with 40% of behavioral motifs being changed between *Muc13*$^{-/-}$ and wildtype controls (Fig. 5I–J).

Our results show that *Muc13* deletion can drive both microbiome shifts that mirror microbial changes induced by stress, and despair behaviors at baseline – highlighting the critical role of mucin 13 in maintaining microbial and behavioral homeostasis. In addition, deletion of *Muc13* increases stress-induced anxiety-like behaviors. Together, these results support the hypothesis that stress-induced *Muc13* reductions can drive microbial shifts that lead to behavioral changes in mice.

4. Discussion

Our work demonstrates that stress-induced microbiome and behavioral changes are accompanied by a reduction in expression of a key component of the glycocalyx, mucin 13. While more work is needed to fully understand the mechanisms behind this reduced expression, our data suggest that the intestinal transcription factor HNF4 is a key mediator. Furthermore, we demonstrate for the first time that deletion of a glycocalyx protein is sufficient to drive microbiome shifts and behavioral changes, suggesting that transmembrane mucins have a larger role in microbiome homeostasis than previously acknowledged. In addition, this work provides the foundation for understanding a mechanism by which stress can alter the microbiome, providing a new therapeutic target that avoids current microbiome treatment pitfalls.

Our results, while novel, are supported by concepts previously published in literature. For example, it is well known that there is a reciprocal relationship between the mucus layer and microbes (Hansson, 2020). Disruption of the intestinal mucus layer results in sweeping microbiome changes, heightened inflammation, and disease onset–supporting the idea that changes in mucus can impact other systems in the body (Bergstrom et al., 2010, 2020; Borisova et al., 2020; Hansson, 2020; Johansson et al., 2008, 2009; Van der Sluis et al., 2006; Velcich et al., 2002; Wu et al., 2018). We take this concept a step further and demonstrate that changes in a glycocalyx mucin can shift the composition of microbes. Additionally, stress has been shown to alter the glycosylation patterns of soluble mucins (Silva et al., 2014). As changes in glycosylation are also known to alter the microbiome, the connection between stress and mucin induced microbiome changes is well supported (Marczynski et al., 2021; Werlang et al., 2019). Finally, the connection between mucins and depression has also been suggested in the literature. Specifically, single nucleotide polymorphisms (SNPs) in *MUC13* have been identified in GWAS studies of depressed populations (Dunn et al., 2018; Rivet-Noor and Gaultier, 2020; Ware et al., 2015). In addition, SNPs in O-glycosylation have also been identified in populations with treatment resistant depression (McClain et al., 2020; Rivet-Noor and Gaultier, 2020). In aggregate, these published concepts support our rational for performing these experiments and suggest that mucin 13 is an important driver of microbiome shifts and despair behaviors in mice.

The quantification and detection of mucins and their glycan chains has long proven to be a challenge for glycobiologists (Atanasova and Reznikov, 2019; Carraway, 2000; Harrop et al., 2012; Kesimer and Sheehan, 2012). Recent advances, including utilization of inactive mucin-specific proteases for mass spectrometry, has allowed researchers to begin to interrogate many previously unanswered questions about these glycan rich proteins (Harrop et al., 2012; Kesimer and Sheehan, 2012; Malaker et al., 2019, 2022). However, even with these cutting edge techniques, limitations remain. While mass spectrometry is among the most successful methods of mucin detection, we were unable to capture subtle differences in mucin expression at the protein level. In addition, while able to detect several mucins in our samples, we remained unable to identify other members of the intestinal transmembrane mucin family, namely mucin 17. This is likely due to the heavy ratio of glycans. Immunofluorescent staining of mucins can be employed to great success when examining where specific mucins are located and their turnover times (Henwood, 2017;

Schneider et al., 2018). However, quantifying mucins, especially subtle changes, with this technique remains challenging as intestinal villi often shift in and out of imaging fields, making quantification along a villus or detection of changes in fluorescence across the intestine difficult to assess. Furthermore, preservation of mucus and mucins can be inconsistent across intestinal sections due to fecal accumulation and physical manipulation, even while using identical methods. This limitation precludes confident protein level quantification of identical areas across samples. Western blotting and ELISA detection of mucins can be utilized in some cases, however, the isolation of mucins remains a large technical hurdle (Atanasova and Reznikov, 2019). Together, these limitations explain why RNA quantification of mucins remains a reliable method for examining differences in mucin expression. Future studies with more sensitive and replicable methods for mucin quantification at the protein level will need to be performed to confirm our stress-induced mucin expression results.

Mechanistically, our results show that HNF4 can bind to the *Muc13* promoter, while the loss of *Hnf4* results in reduced transcription of *Muc13* in the intestines of mice. In addition, we have shown that chronic stress induces reductions in both *Muc13* and *Hnf4* expression. While more work is needed to understand how stress regulates *Hnf4* in our chronic stress model, literature suggests that this regulation could occur through the phosphorylation of extracellular signal-regulated kinase (ERK) 1/2. While there is no glucocorticoid response element (GRE) in the *Hnf4* gene, ERK 1/2 is known to be a potent inhibitor of *Hnf4* expression (Vető et al., 2017). Strikingly, stress hormones have repeatedly been demonstrated to enhance ERK 1/2 phosphorylation (Gourley et al., 2008; Yang et al., 2004; Yu et al., 2010). These works provide a mechanistic foundation for how stress could be reducing *Hnf4* expression in the intestines. While the basis for our hypothesis is well supported, no works have demonstrated how stress specifically regulates *Hnf4*, leaving a gap in knowledge to be filled by future studies.

By defining a novel mechanism through which stress alters the microbiome, our results have brought to light a key aspect in stress-induced behavioral changes. We have demonstrated that a transmembrane mucin is specifically and indirectly regulated by stress in a way that interferes with its homeostatic expression patterns, inducing microbiome composition changes and despair behaviors in mice. Mucin 13 is conserved between humans and mice, suggesting it could be a broadly applicable therapeutic target for patients with stress-induced depression who present with microbiome changes. Our results, while directly related to stress-induced depression, provide a basis for further research to target transmembrane mucins as intervention points for diseases that present with, or are driven by, pathogenic microbiome alterations, such as colitis or Parkinson’s Disease (Herath et al., 2020).

Extended Data

Extended Data Table 1

Table of naïve vs stress genus level Wilcox Rank Sum statistics (for Supplemental Fig. 1J).

Naïve vs Stress			
Genus	**p value**	**Bonferroni-adjusted p value**	**Star**
Clostridium sensu stricto 1	7.99E-09	4.87E-07	****
Romboutsia	1.47E-07	8.94E-06	****
[Eubacterium] ventriosum group	1.68E-07	1.02E-05	****
Lachnospiraceae UCG-001	9.83E-07	6.00E-05	****
Marvinbryantia	1.94E-06	0.000118164	****
Staphylococcus	3.79E-06	0.000231457	****
Lachnospiraceae FCS020 group	6.88E-06	0.000419638	***
Unidentified	1.57E-05	0.000956612	***
[Eubacterium] nodatum group	1.97E-05	0.00119998	**
Incertae Sedis	1.97E-05	0.00119998	**
[Eubacterium] siraeum group	3.60E-05	0.002198371	**
[Eubacterium] brachy group	4.23E-05	0.002577603	**
Lactobacillus	6.60E-05	0.004024766	**
Family XIII AD3011 group	6.66E-05	0.004060181	**
Anaeroplasma	7.81E-05	0.004765721	**
Tuzzerella	9.25E-05	0.005640638	**
Oscillospira	0.000339724	0.020723155	*
NK4A214 group	0.00037941	0.023144017	*
GCA-900066575	0.00039326	0.023988861	*
Anaerotruncus	0.000551996	0.03367175	*
Harryflintia	0.00367754	0.224329947	
ASF356	0.004282089	0.261207403	
Roseburia	0.004291511	0.261782185	
Tyzzerella	0.008777645	0.535436319	
Lachnospiraceae UCG-010	0.013523212	0.82491592	
[Eubacterium] oxidoreducens group	0.589533221	1	
[Eubacterium] xylanophilum group	0.147193088	1	
A2	0.130510373	1	
Acetatifactor	0.584766531	1	
Akkermansia	0.057741754	1	
Arsenicicoccus	0.3378947	1	
Bacillus	0.3378947	1	
Burkholderia-Caballeronia-Paraburkholderia	0.3378947	1	
Butyricicoccus	0.06679277	1	
Colidextribacter	0.147193088	1	

Naïve vs Stress			
Genus	**p value**	**Bonferroni-adjusted p value**	**Star**
Corynebacterium	0.3378947	1	
Curtobacterium	1	1	
Desulfovibrio	0.3378947	1	
Enterococcus	0.678841491	1	
Enterorhabdus	0.020288409	1	
Erysipelatoclostridium	0.072758087	1	
Exiguobacterium	0.3378947	1	
HT002	0.3378947	1	
Intestinimonas	0.017242287	1	
Lachnoclostridium	0.814269221	1	
Lachnospiraceae NC2004 group	0.3378947	1	
Lachnospiraceae NK4A136 group	0.351411522	1	
Lachnospiraceae NK4B4 group	0.133661781	1	
Lachnospiraceae UCG-004	0.147774975	1	
Lachnospiraceae UCG-006	0.630998004	1	
Monoglobus	0.630998004	1	
Nocardiopsis	0.161691678	1	
Ornithinimicrobium	0.3378947	1	
Oscillibacter	0.033682558	1	
Parvibacter	0.046071649	1	
Ralstonia	0.161691678	1	
Ruminococcus	0.395580536	1	
Sanguibacter-Flavimobilis	0.3378947	1	
Turicibacter	0.327313318	1	
UCG-005	0.017069953	1	
UCG-009	0.675265662	1	

Extended Data Table 2

Table of statistics for genus level changes between baseline control, baseline *Muc13*$^{-/-}$, 1wk UCMRS control, 1wk UCMRS *Muc13*$^{-/-}$ animals.

Baseline Control vs. Muc13 KO- 33.4% coverage			
Genus	**tstat**	**p_val**	**p_adj**
Alistipes	−5.906873503	0.000595337	0.012943066
Bacteroides	−5.607695288	0.000809375	0.012943066
Odoribacter	−5.588133367	0.000826153	0.012943066
Muribaculum	−4.763260118	0.002051689	0.022701292
Prevotellaceae UCG-001	−4.623889432	0.002415031	0.022701292

Baseline Control vs. Muc13 KO- 33.4% coverage			
Genus	**tstat**	**p_val**	**p_adj**
Intestinimonas	3.894457548	0.00300306	0.023523973
Bifidobacterium	−3.921415122	0.005738596	0.038530574
Oscillibacter	3.264826755	0.010629363	0.062447507
Lachnoclostridium	3.167010682	0.015031735	0.070649153
Ruminococcus	2.828785268	0.013738733	0.070649153
Ligilactobacillus	−3.132610491	0.016549203	0.070710232
Alloprevotella	−2.878795057	0.023692332	0.085656894
Roseburia	−2.890222916	0.023308834	0.085656894
A2	2.503323677	0.02838	0.095275714
Candidatus Saccharimonas	−2.69615309	0.030810076	0.096538238

Wildtype Baseline vs 1wk UCMRS- 26.4% coverage			
Genus	**tstat**	**p_val**	**p_adj**
Alistipes	−9.135862606	3.87E-05	0.000870574
Prevotellaceae UCG-001	−9.609585728	2.78E-05	0.000870574
Bacteroides	−6.418234757	0.000360945	0.005414182
Odoribacter	−6.116007048	0.000483403	0.005438285
Ruminococcus	3.89327961	0.002875679	0.025881113
Alloprevotella	−4.098199411	0.00458341	0.034375578
Lachnoclostridium	3.332877095	0.012541499	0.080623924
Muribaculum	−3.226870145	0.014514543	0.081644302
[Eubacterium] xylanophilum group	2.696965122	0.020343235	0.098082324
Ligilactobacillus	−2.937322606	0.021796072	0.098082324
Intestinimonas	2.466953441	0.027653502	0.113127965
Parabacteroides	−2.615690041	0.034625544	0.129845792

Extended Data Table 3

Table of statistics for ASV level changes between baseline control, baseline *Muc13*$^{-/-}$, 1wk UCMRS control, 1wk UCMRS *Muc13*$^{-/-}$ animals.

Baseline Control vs. Muc13 KO- 56.7% coverage			
ASV	**tstat**	**p_val**	**p_adj**
ASV261	13.55474313	4.38E-08	3.91E-05
ASV508	18.35322467	5.48E-08	3.91E-05
ASV309	20.8989131	1.44E-07	6.86E-05
ASV252	10.30073205	2.46E-07	8.76E-05
ASV579	18.14495266	3.82E-07	0.000108944
ASV658	8.886294194	6.87E-07	0.000163375
ASV209	10.56315343	2.92E-06	0.000462696

Baseline Control vs. Muc13 KO- 56.7% coverage			
ASV	**tstat**	**p_val**	**p_adj**
ASV221	12.23303713	2.43E-06	0.000462696
ASV375	8.709734713	2.74E-06	0.000462696
ASV157	11.86206446	4.02E-06	0.000573785
ASV139	−12.22784171	5.60E-06	0.000580085
ASV479	9.711390083	5.70E-06	0.000580085
ASV499	12.05471762	4.67E-06	0.000580085
ASV507	9.274542305	5.50E-06	0.000580085
ASV17	−11.80225232	7.11E-06	0.000626425
ASV259	−11.71552992	7.47E-06	0.000626425
ASV723	11.89549577	6.74E-06	0.000626425
ASV210	9.685252445	1.16E-05	0.000754124
ASV212	9.133909209	1.07E-05	0.000754124
ASV543	10.26401728	1.03E-05	0.000754124
ASV6	−10.9756093	1.15E-05	0.000754124
ASV810	9.969756019	1.07E-05	0.000754124
ASV170	10.54225436	1.51E-05	0.000935521
ASV540	9.790630844	1.64E-05	0.000976801
ASV537	10.16091857	1.85E-05	0.00105454
ASV703	10.12336975	1.97E-05	0.001082212
ASV240	−9.8230063	2.41E-05	0.001165969
ASV67	−9.745713299	2.53E-05	0.001165969
ASV690	9.663420615	2.28E-05	0.001165969
ASV799	9.766995866	2.50E-05	0.001165969
ASV809	8.070231752	2.37E-05	0.001165969
ASV149	9.139513451	2.78E-05	0.001219691
ASV450	8.939979187	2.83E-05	0.001219691
ASV581	8.569228461	2.91E-05	0.001219691
ASV16	−9.119727895	3.91E-05	0.001559557
ASV272	8.554968202	4.24E-05	0.001559557
ASV462	8.807212142	4.27E-05	0.001559557
ASV608	9.07368902	4.05E-05	0.001559557
ASV672	9.030297271	4.17E-05	0.001559557
ASV199	8.933250548	4.48E-05	0.001596125
ASV55	−8.898985274	4.59E-05	0.001596557
ASV568	8.231115378	5.12E-05	0.001739587
ASV12	−8.599851126	5.73E-05	0.001894653
ASV166	8.262399644	5.85E-05	0.001894653
ASV341	−8.514751246	6.11E-05	0.001935655

Baseline Control vs. Muc13 KO- 56.7% coverage			
ASV	**tstat**	**p_val**	**p_adj**
ASV233	−8.414312687	6.59E-05	0.002003358
ASV695	8.412500859	6.60E-05	0.002003358
ASV191	7.899890992	8.30E-05	0.002365922
ASV585	8.142565289	8.14E-05	0.002365922
ASV776	7.238906207	8.26E-05	0.002365922
ASV841	7.663499042	9.13E-05	0.002552304
ASV38	−7.920130544	9.72E-05	0.002623258
ASV381	−7.915999155	9.75E-05	0.002623258
ASV356	−7.882119892	0.000100199	0.002646003
ASV344	−7.781088935	0.000108769	0.002732749
ASV582	7.721589103	0.000108645	0.002732749
ASV766	6.967111759	0.000109233	0.002732749
ASV481	7.594850443	0.000126824	0.003106634
ASV525	7.526268861	0.000128535	0.003106634
ASV29	−7.525171194	0.000134431	0.003194968
ASV138	7.415407048	0.000139897	0.003217687
ASV574	6.852858701	0.000139899	0.003217687
ASV225	7.404122877	0.0001489	0.003370339
ASV625	6.840196243	0.000176735	0.0038959
ASV713	7.199177191	0.000177583	0.0038959
ASV607	7.014797005	0.000208794	0.00451121
ASV70	−6.969364349	0.000217403	0.004627117
ASV623	6.879783804	0.000235574	0.004940135
ASV19	−6.844143848	0.000243274	0.005027668
ASV239	−6.773745545	0.00025933	0.0052161
ASV440	−6.772147445	0.000259708	0.0052161
ASV411	−6.67747883	0.000283248	0.00560989
ASV306	−6.598698476	0.000304675	0.005871173
ASV314	−6.609031063	0.000301764	0.005871173
ASV59	−6.462062044	0.000346297	0.006584259
ASV198	6.305065991	0.000399351	0.007493078
ASV10	−6.282502554	0.000411037	0.007514601
ASV231	−6.293436992	0.000406728	0.007514601
ASV27	−6.180039262	0.000454004	0.008195066
ASV422	−6.045925544	0.000518049	0.009234218
ASV32	−6.0157506	0.000533816	0.00939779
ASV2	−5.904253527	0.000596913	0.010336786
ASV54	−5.8964196	0.00060165	0.010336786

Baseline Control vs. Muc13 KO- 56.7% coverage			
ASV	**tstat**	**p_val**	**p_adj**
ASV340	−5.855977118	0.000626787	0.010393011
ASV44	−5.863150546	0.000622244	0.010393011
ASV46	−5.860520556	0.000623906	0.010393011
ASV256	4.706161095	0.000643761	0.010510196
ASV78	−5.822333475	0.000648596	0.010510196
ASV195	−5.797324604	0.000665356	0.010660656
ASV122	−5.783395389	0.000674901	0.010693438
ASV706	−5.741046884	0.000704873	0.011045599
ASV470	−5.723702226	0.000717576	0.011122429
ASV388	−5.709909977	0.00072786	0.011160514
ASV285	−5.688736497	0.000743969	0.01116736
ASV638	−5.697656306	0.000737134	0.01116736
ASV460	−5.672022871	0.000756966	0.011244098
ASV899	5.550262883	0.000772846	0.011361631
ASV147	−5.548590603	0.000861192	0.012438068
ASV417	−5.546035035	0.000863512	0.012438068
ASV321	−5.531194688	0.000877129	0.012507853
ASV36	−5.505700205	0.000901083	0.012722215
ASV106	−5.472547064	0.000933331	0.012926397
ASV64	−5.472201334	0.000933674	0.012926397
ASV325	−5.453458473	0.000952481	0.013059979
ASV114	−5.414513776	0.000992925	0.013400381
ASV31	−5.411530033	0.000996101	0.013400381
ASV359	−5.374337342	0.001036664	0.013438931
ASV436	−5.375147019	0.001035761	0.013438931
ASV68	−5.389449182	0.001019965	0.013438931
ASV717	5.380382212	0.001029948	0.013438931
ASV150	−5.333446368	0.001083396	0.013918227
ASV200	4.673127059	0.001119223	0.014250112
ASV1	−5.245627724	0.0011919	0.015041144
ASV178	−5.218044609	0.001228435	0.015232598
ASV396	−5.22225532	0.001222778	0.015232598
ASV154	−5.157391332	0.001313236	0.015349796
ASV232	−5.162932727	0.001305225	0.015349796
ASV302	−5.17244321	0.001291601	0.015349796
ASV363	−5.191103378	0.001265327	0.015349796
ASV555	−5.168581322	0.001297114	0.015349796
ASV71	−5.197120666	0.001256982	0.015349796

Baseline Control vs. Muc13 KO- 56.7% coverage			
ASV	**tstat**	**p_val**	**p_adj**
ASV81	−5.185965215	0.001272502	0.015349796
ASV519	−5.132702465	0.001349602	0.015646606
ASV141	−5.116998394	0.001373315	0.015793125
ASV372	−5.089499325	0.001415962	0.016025096
ASV9	−5.090768816	0.001413961	0.016025096
ASV364	−5.053363941	0.001474256	0.016553459
ASV400	−5.037066344	0.001501416	0.016726709
ASV428	−5.018206139	0.001533541	0.016952169
ASV11	−5.007317612	0.001552435	0.01702902
ASV389	−4.992055048	0.001579355	0.017192067
ASV332	−4.968318	0.001622258	0.017433003
ASV99	−4.966313887	0.001625939	0.017433003
ASV216	4.382425608	0.001656223	0.017625176
ASV135	−4.923171485	0.001707471	0.01774414
ASV292	−4.916202075	0.001721062	0.01774414
ASV358	−4.936870775	0.001681101	0.01774414
ASV383	−4.912030292	0.001729255	0.01774414
ASV480	−4.905553364	0.001742061	0.01774414
ASV588	−4.909878173	0.001733499	0.01774414
ASV63	−4.887155805	0.001779014	0.017992009
ASV357	−4.880773027	0.001792036	0.017996078
ASV112	−4.874340887	0.001805266	0.018002161
ASV230	−4.773862224	0.00202663	0.02006927
ASV245	−4.749352576	0.002085081	0.020365243
ASV7	−4.750186661	0.002083062	0.020365243
ASV43	−4.737396892	0.002114268	0.020509837
ASV335	−4.671892061	0.002282421	0.021991438
ASV391	−4.658946344	0.002317374	0.022178357
ASV570	−4.61334642	0.002445283	0.023246491
ASV413	−4.603732473	0.002473234	0.023356506
ASV184	−4.587685821	0.002520677	0.023459504
ASV352	−4.587118877	0.002522372	0.023459504
ASV51	−4.58340777	0.002533495	0.023459504
ASV617	4.421729905	0.002704518	0.024881567
ASV224	−4.516131673	0.002744816	0.025049325
ASV339	−4.512160206	0.002757885	0.025049325
ASV392	−4.503812037	0.002785581	0.025140752
ASV387	−4.494826052	0.002815737	0.025253085

Baseline Control vs. Muc13 KO- 56.7% coverage			
ASV	**tstat**	**p_val**	**p_adj**
ASV119	−4.421749879	0.003074768	0.027233664
ASV23	−4.422637434	0.003071469	0.027233664
ASV524	−4.415501536	0.003098107	0.027270988
ASV18	−4.405577152	0.003135577	0.027311339
ASV678	−4.404152866	0.003140996	0.027311339
ASV710	−4.382968329	0.003222816	0.027852943
ASV274	−4.364232576	0.003297136	0.028323592
ASV72	−4.359295154	0.003317034	0.028323898
ASV554	−4.335383768	0.003415286	0.028989277
ASV266	−4.311928678	0.003514782	0.029310402
ASV629	−4.314230706	0.003504877	0.029310402
ASV675	−4.318031766	0.00348859	0.029310402
ASV265	−4.286937803	0.003624311	0.029532957
ASV277	−4.295623708	0.003585823	0.029532957
ASV49	−4.287621787	0.003621264	0.029532957
ASV754	−4.30023588	0.003565569	0.029532957
ASV709	4.143944085	0.003661733	0.029668359
ASV506	−4.25028742	0.003791785	0.030548503
ASV327	−4.240086758	0.003839896	0.030590454
ASV666	−4.242897269	0.003826573	0.030590454
ASV183	−4.228940349	0.003893235	0.030843072
ASV109	−4.182853446	0.004122572	0.031798536
ASV350	−4.190980286	0.004081077	0.031798536
ASV40	−4.183539375	0.004119052	0.031798536
ASV542	−4.195847865	0.004056444	0.031798536
ASV610	−4.177987971	0.004147635	0.031798536
ASV648	−4.178169722	0.004146696	0.031798536
ASV164	−4.161734436	0.004232581	0.032276263
ASV429	−4.134732242	0.004377951	0.033207227
ASV260	−4.108935107	0.004521958	0.033341898
ASV28	−4.111360309	0.004508202	0.033341898
ASV386	−4.113948765	0.004493569	0.033341898
ASV438	−4.118084875	0.004470296	0.033341898
ASV693	−4.106468955	0.004535995	0.033341898
ASV73	−4.117021684	0.004476266	0.033341898
ASV348	−4.099063145	0.004578433	0.033481256
ASV179	3.484278319	0.004720759	0.034179892
ASV530	−4.074571212	0.004721907	0.034179892

Baseline Control vs. Muc13 KO- 56.7% coverage			
ASV	**tstat**	**p_val**	**p_adj**
ASV92	−4.050792182	0.004865925	0.035044493
ASV172	−4.039444314	0.004936343	0.035110754
ASV257	4.033509542	0.004973613	0.035110754
ASV320	−4.03525974	0.00496259	0.035110754
ASV35	−4.038187587	0.004944209	0.035110754
ASV447	−4.021280039	0.005051389	0.035484143
ASV446	−4.013458278	0.00510183	0.035662792
ASV630	−3.999874445	0.005190743	0.036107314
ASV155	−3.986347836	0.005280967	0.03648656
ASV515	−3.984054005	0.005296436	0.03648656
ASV572	−3.969105277	0.005398469	0.037010661
ASV742	−3.957841901	0.005476766	0.037367794
ASV473	−3.942189097	0.005587643	0.037942756
ASV273	−3.922110902	0.005733469	0.038433322
ASV368	−3.928042643	0.00568996	0.038433322
ASV378	−3.921124175	0.005740742	0.038433322
ASV86	−3.907888171	0.005839278	0.038910332
ASV347	−3.896592845	0.005924828	0.039296764
ASV557	−3.869967503	0.006131942	0.040482172
ASV649	−3.861642477	0.006198311	0.040731755
ASV291	−3.850244223	0.006290452	0.041147637
ASV243	−3.836962774	0.006399704	0.041494753
ASV30	−3.836720643	0.006401715	0.041494753
ASV925	−3.822859703	0.006517982	0.042057203
ASV595	−3.817413261	0.006564294	0.042165242
ASV244	−3.808008399	0.006645112	0.042303259
ASV550	−3.808099022	0.006644328	0.042303259
ASV298	−3.790696288	0.006796725	0.04307613
ASV105	−3.77716107	0.006917882	0.043649999
ASV251	−3.770397314	0.006979305	0.043843562
ASV874	3.723564722	0.007202096	0.045044685
ASV107	−3.734455037	0.007315808	0.045556078
ASV431	−3.728660822	0.007371687	0.045704457
ASV211	−3.718158092	0.007474159	0.045803912
ASV270	−3.717148637	0.007484089	0.045803912
ASV674	3.72343236	0.007422507	0.045803912
ASV614	−3.709382314	0.007560969	0.046076675
ASV621	−3.701075311	0.007644151	0.046385361

Baseline Control vs. Muc13 KO- 56.7% coverage			
ASV	**tstat**	**p_val**	**p_adj**
ASV395	−3.690129883	0.007755274	0.046860255
ASV573	−3.678922369	0.007870876	0.047358097
ASV120	−3.673277073	0.007929812	0.047452552
ASV249	−3.671056354	0.007953128	0.047452552
ASV181	−3.638544959	0.008303111	0.049334316
ASV616	−3.631178233	0.008384711	0.049407432
ASV843	−3.633667994	0.008357036	0.049407432
ASV487	−3.627627368	0.008424354	0.049436745
ASV173	−3.618185394	0.008530758	0.049810399
ASV4	−3.615798391	0.008557888	0.049810399
ASV379	−3.610016827	0.008623986	0.049991076
Non-Signficiant Changes			
ASV34	−3.601177034	0.00872612	0.05037833
ASV146	−3.597558968	0.0087683	0.050417726
ASV3	−3.594407743	0.008805217	0.050426666
ASV8	−3.563597836	0.009175155	0.052335083
ASV708	−3.559517699	0.009225393	0.052411994
ASV50	−3.553765125	0.00929673	0.052607685
ASV313	−3.544226432	0.009416335	0.053073891
ASV115	−3.537147757	0.00950617	0.053369285
ASV113	−3.529604531	0.009602921	0.053701038
ASV222	3.526279815	0.009645901	0.053730684
ASV452	−3.500973462	0.009979944	0.055375099
ASV82	−3.496174074	0.010044694	0.055518347
ASV726	−3.487914376	0.010157192	0.055923381
ASV609	−3.482457626	0.010232259	0.056120004
ASV238	3.467334033	0.010443456	0.057058883
ASV180	−3.463959342	0.010491222	0.057101077
ASV56	−3.461096993	0.01053192	0.057104632
ASV483	−3.449105409	0.010704283	0.057819349
ASV129	−3.431400835	0.010964346	0.059000592
ASV289	−3.422581234	0.01109643	0.059264079
ASV456	−3.423261509	0.011086181	0.059264079
ASV380	−3.412392193	0.011251161	0.059341419
ASV657	−3.410681488	0.011277366	0.059341419
ASV69	−3.414987738	0.011211525	0.059341419
ASV795	−3.413934264	0.011227594	0.059341419
ASV218	−3.407584848	0.01132497	0.059372822

Baseline Control vs. Muc13 KO- 56.7% coverage			
ASV	**tstat**	**p_val**	**p_adj**
ASV94	−3.373131463	0.011869448	0.06199939
ASV423	−3.369708113	0.011925067	0.062062577
ASV126	2.978127459	0.012070957	0.06250167
ASV584	−3.359227302	0.012097097	0.06250167
ASV394	−3.32858135	0.012615596	0.064684915
ASV466	−3.323657476	0.012701105	0.064684915
ASV488	−3.323841815	0.012697893	0.064684915
ASV700	−3.329369895	0.012601959	0.064684915
ASV58	−3.315842533	0.012838102	0.065149943
ASV88	−3.312289376	0.012900913	0.065236534
ASV132	−3.30608338	0.013011413	0.065562807
ASV20	−3.289375573	0.013313977	0.066616602
ASV98	−3.29054263	0.0132926	0.066616602
ASV333	−3.260254885	0.013859512	0.068150565
ASV458	−3.266178887	0.013746623	0.068150565
ASV502	−3.269151391	0.01369035	0.068150565
ASV587	−3.263514593	0.013797272	0.068150565
ASV663	−3.262173546	0.013822841	0.068150565
ASV598	−3.254693229	0.0139664	0.068440158
ASV722	3.244710048	0.014160485	0.069153602
ASV207	−3.240641966	0.0142404	0.069306521
ASV513	−3.230932256	0.014433099	0.070005441
ASV128	−3.223096525	0.014590642	0.070291405
ASV503	−3.22320152	0.014588519	0.070291405
ASV627	−3.218770042	0.014678417	0.07047617
ASV415	−3.214480613	0.014765998	0.070658767
ASV103	−3.201713353	0.01503	0.070736575
ASV299	3.201699844	0.015030282	0.070736575
ASV414	−3.204807826	0.014965552	0.070736575
ASV553	−3.207168572	0.014916584	0.070736575
ASV873	3.210273329	0.014852444	0.070736575
ASV142	−3.193099591	0.015210964	0.071247552
ASV406	−3.191785201	0.015238782	0.071247552
ASV267	−3.186745718	0.015345943	0.07140339
ASV661	−3.185513924	0.015372259	0.07140339
ASV401	−3.179616806	0.015498911	0.071757946
ASV62	−3.17690216	0.015557588	0.071796507
ASV433	−3.170202438	0.01570342	0.072003462

Baseline Control vs. Muc13 KO- 56.7% coverage			
ASV	**tstat**	**p_val**	**p_adj**
ASV764	−3.170349661	0.0157002	0.072003462
ASV226	−3.157550828	0.015982801	0.072584311
ASV5	−3.158848864	0.015953894	0.072584311
ASV667	−3.158166535	0.015969082	0.072584311
ASV220	−3.15274912	0.01609022	0.07284017
ASV349	3.137589579	0.016302565	0.072868727
ASV366	3.14118793	0.016352028	0.072868727
ASV454	−3.144867646	0.01626821	0.072868727
ASV604	−3.142142361	0.016330244	0.072868727
ASV692	−3.148686032	0.016181717	0.072868727
ASV117	−3.127362417	0.016671093	0.073124649
ASV124	−3.126505125	0.016691095	0.073124649
ASV187	−3.12539063	0.016717136	0.073124649
ASV304	−3.130032782	0.016608953	0.073124649
ASV531	−3.126915408	0.016681519	0.073124649
ASV544	−3.129009651	0.016632732	0.073124649
ASV322	−3.100153659	0.017318558	0.075523741
ASV311	−3.092502203	0.01750542	0.076105883
ASV186	−3.081595109	0.017775511	0.077045224
ASV131	−3.053012611	0.018504545	0.079253998
ASV246	−3.052902257	0.01850742	0.079253998
ASV25	−3.057864315	0.018378589	0.079253998
ASV475	3.034446429	0.018486529	0.079253998
ASV65	−3.049916849	0.018585393	0.079349613
ASV121	−3.037012276	0.018926473	0.080324852
ASV175	−3.037615776	0.018910375	0.080324852
ASV590	−3.034404725	0.018996197	0.080381533
ASV516	−3.025067354	0.019248117	0.081206552
ASV370	−3.021328282	0.019349988	0.081395527
ASV815	−3.013161049	0.019574501	0.082097761
ASV174	−2.995718759	0.020063286	0.082928248
ASV202	−2.99779726	0.020004367	0.082928248
ASV296	−2.999852286	0.019946294	0.082928248
ASV494	−2.996571342	0.020039096	0.082928248
ASV599	−2.996717502	0.020034952	0.082928248
ASV201	−2.991379394	0.020186887	0.082956685
ASV307	2.991107239	0.020194666	0.082956685
ASV430	−2.989359766	0.020244689	0.082956685

Baseline Control vs. Muc13 KO- 56.7% coverage			
ASV	**tstat**	**p_val**	**p_adj**
ASV449	−2.983829605	0.020403861	0.083369358
ASV560	−2.976819522	0.020607538	0.083721791
ASV601	−2.978018114	0.020572561	0.083721791
ASV426	2.951222545	0.020709011	0.083895029
ASV206	−2.959839271	0.021109874	0.085035819
ASV583	−2.96124796	0.021067711	0.085035819
ASV84	−2.944856831	0.021563875	0.086619961
ASV215	−2.938866231	0.021748285	0.086874056
ASV606	−2.938843914	0.021748975	0.086874056
ASV419	−2.93278823	0.02193709	0.087380698
ASV45	−2.929750258	0.022032109	0.087514729
ASV89	−2.926310352	0.022140225	0.087699893
ASV324	2.921299841	0.02229871	0.088082993
ASV39	−2.918711017	0.022381065	0.088164084
ASV342	2.903622271	0.022867501	0.089095781
ASV37	−2.908309103	0.022715221	0.089095781
ASV626	−2.905073272	0.022820241	0.089095781
ASV74	−2.904365109	0.022843293	0.089095781
ASV227	−2.901099784	0.022949905	0.089173199
ASV492	2.894921593	0.023153059	0.089718104
ASV143	−2.891225735	0.023275495	0.089948118
ASV24	−2.883715243	0.02352641	0.090427657
ASV628	−2.885041787	0.023481885	0.090427657
ASV229	−2.87759026	0.023733149	0.090977072
ASV158	−2.86775999	0.024068969	0.092017022
ASV407	−2.865741094	0.024138555	0.09203631
ASV893	2.863428779	0.024218516	0.092094945
ASV248	−2.842184848	0.024966333	0.094686144
ASV491	−2.834568775	0.025240316	0.095393184
ASV562	−2.833292099	0.025286552	0.095393184
ASV660	−2.826232553	0.025543836	0.096109526
ASV159	−2.81740173	0.025869555	0.09707891
ASV14	−2.811307125	0.026096896	0.097674995
ASV845	−2.80890315	0.026187145	0.097756201
ASV527	−2.798887979	0.026566675	0.097891677
ASV611	−2.800700444	0.026497565	0.097891677
ASV669	−2.799727913	0.026534625	0.097891677
ASV757	−2.800180646	0.026517366	0.097891677

Baseline Control vs. Muc13 KO- 56.7% coverage			
ASV	**tstat**	**p_val**	**p_adj**
ASV862	−2.805357922	0.026320838	0.097891677
ASV500	−2.794918166	0.026718709	0.097945703
ASV509	−2.795261814	0.026705512	0.097945703
ASV161	−2.791086362	0.026866323	0.097983061
ASV444	−2.791865977	0.02683622	0.097983061
ASV312	2.784969229	0.027103753	0.098390891
ASV443	2.582747593	0.027185141	0.098390891
ASV850	−2.784390763	0.02712632	0.098390891
ASV404	2.747455283	0.028005575	0.101021909
ASV489	−2.761043258	0.02805377	0.101021909
ASV338	2.694742572	0.028276874	0.101313623
ASV354	2.733390548	0.028272773	0.101313623
ASV208	−2.746445315	0.028650494	0.101630856
ASV361	2.749843495	0.028510408	0.101630856
ASV376	2.747594362	0.028603045	0.101630856
ASV486	−2.750772361	0.028472242	0.101630856
ASV546	−2.740147069	0.028912041	0.102304144
ASV780	−2.737029092	0.029042445	0.102511203
ASV770	2.733081264	0.029208439	0.102842555
ASV288	2.731007866	0.029296017	0.102896849
ASV177	−2.72009884	0.029761349	0.104274407
ASV337	−2.70107847	0.030591252	0.106919426
ASV253	−2.694368981	0.030889743	0.107024652
ASV408	−2.695757418	0.030827725	0.107024652
ASV631	−2.696290942	0.030803929	0.107024652
ASV846	−2.693657594	0.030921568	0.107024652
ASV679	−2.68566425	0.031281536	0.108008401
ASV412	−2.681856116	0.031454564	0.1083435
ASV504	−2.674275071	0.031802001	0.109276274
ASV676	−2.665379502	0.032214792	0.11042859
ASV755	2.445772066	0.032311966	0.110496077
ASV355	2.65009225	0.032937281	0.112364983
ASV116	−2.640653829	0.033391759	0.113643552
ASV410	2.637705806	0.033535046	0.113859466
ASV167	−2.630229796	0.03390129	0.114829547
ASV858	−2.610670092	0.034879318	0.117862341
ASV751	2.603801104	0.035229702	0.118764906
ASV250	−2.59871995	0.03549124	0.119209068

Baseline Control vs. Muc13 KO- 56.7% coverage			
ASV	**tstat**	**p_val**	**p_adj**
ASV323	−2.597274058	0.035566032	0.119209068
ASV849	−2.596382199	0.035612246	0.119209068
ASV597	−2.584755749	0.036220442	0.120961007
ASV645	2.493652881	0.036520692	0.121678756
ASV538	−2.576172096	0.036676373	0.121912605
ASV310	−2.572367486	0.036880359	0.122305561
ASV792	−2.567315603	0.037153037	0.122923968
ASV247	−2.548126616	0.038207951	0.125026375
ASV377	−2.55009735	0.038098195	0.125026375
ASV497	2.547787718	0.038226858	0.125026375
ASV83	−2.551016578	0.03803184	0.125026375
ASV911	2.547742334	0.038146892	0.125026375
ASV228	−2.543195197	0.038484032	0.125579472
ASV397	−2.53880138	0.038731754	0.125812031
ASV76	2.345171478	0.038677007	0.125812031
ASV326	−2.528081102	0.039343106	0.126947107
ASV343	−2.529114138	0.039283762	0.126947107
ASV586	−2.52799142	0.039348262	0.126947107
ASV301	2.296119746	0.039698782	0.127670254
ASV752	−2.521015805	0.039751468	0.127670254
ASV980	−2.516228171	0.040030672	0.128278063
ASV145	−2.512550284	0.040246533	0.128680619
ASV33	−2.508559396	0.040482125	0.129144317
ASV163	−2.505438085	0.040667375	0.129157409
ASV57	2.432215271	0.04059114	0.129157409
ASV176	−2.502304769	0.040854218	0.12917542
ASV566	−2.50296207	0.040814949	0.12917542
ASV962	2.46788553	0.041236393	0.130095344
ASV716	2.478475647	0.042304457	0.133170322
ASV498	−2.470044375	0.042830201	0.134251181
ASV728	−2.469950278	0.042836106	0.134251181
ASV591	−2.466842802	0.043031597	0.134568109
ASV165	−2.463958384	0.043213878	0.134842428
ASV461	−2.460865674	0.043410204	0.135159281
ASV485	−2.456312021	0.043700943	0.13576807
ASV22	−2.44961867	0.044131935	0.136038452
ASV360	−2.452663328	0.043935347	0.136038452
ASV496	2.451297843	0.044023402	0.136038452

Baseline Control vs. Muc13 KO- 56.7% coverage			
ASV	**tstat**	**p_val**	**p_adj**
ASV851	2.449037432	0.044169567	0.136038452
ASV547	−2.444219354	0.044482786	0.136707873
ASV620	−2.438858513	0.044833973	0.13749085
ASV529	−2.431411336	0.045326567	0.138425559
ASV859	−2.431315911	0.045332915	0.138425559
ASV827	−2.425508571	0.045720951	0.139312127
ASV300	−2.415712831	0.046383224	0.140800962
ASV316	2.373964534	0.046407049	0.140800962
ASV293	−2.412126766	0.046628125	0.141171351
ASV926	−2.407068187	0.046975843	0.14192278
ASV577	−2.395909726	0.047752281	0.143889205
ASV600	−2.394823966	0.04782853	0.143889205
ASV144	−2.392240461	0.04801046	0.143981708
ASV785	−2.3915215	0.048061215	0.143981708
ASV459	−2.38866843	0.048263171	0.144087449
ASV523	−2.388169197	0.048298598	0.144087449
ASV643	−2.384651023	0.048549017	0.144532145
ASV605	−2.380429732	0.048851236	0.14512888
ASV763	−2.375549429	0.049203035	0.145870121
ASV659	−2.37160887	0.049488982	0.146413461

Wildtype Baseline vs 1wk UCMRS- 57.6%			
ASV	**tstat**	**p_val**	**p_adj**
ASV309	18.96281637	9.76E-09	1.28E-05
ASV261	14.52511376	2.17E-07	0.000103094
ASV508	19.47036634	2.35E-07	0.000103094
ASV579	18.14495266	3.82E-07	0.000125579
ASV221	11.36785902	7.84E-07	0.000181346
ASV56	−16.21015026	8.27E-07	0.000181346
ASV45	−15.30504959	1.22E-06	0.000201359
ASV460	−15.49670293	1.13E-06	0.000201359
ASV658	10.71910331	1.84E-06	0.000221892
ASV71	−14.3988046	1.86E-06	0.000221892
ASV723	7.916415472	1.57E-06	0.000221892
ASV454	−13.69089501	2.61E-06	0.000277689
ASV543	8.962604291	2.75E-06	0.000277689
ASV209	10.72388476	3.03E-06	0.000284738
ASV112	−13.18653777	3.37E-06	0.000295357
ASV252	12.97062416	3.77E-06	0.000309565

Wildtype Baseline vs 1wk UCMRS- 57.6%			
ASV	**tstat**	**p_val**	**p_adj**
ASV124	−12.47118258	4.91E-06	0.000358564
ASV30	−12.56554363	4.67E-06	0.000358564
ASV499	12.35019578	5.24E-06	0.000362723
ASV157	12.25478151	5.52E-06	0.000363036
ASV507	9.180206003	6.55E-06	0.000403014
ASV74	−11.81692606	7.05E-06	0.000403014
ASV810	9.45603514	6.85E-06	0.000403014
ASV170	9.530982984	9.63E-06	0.000507105
ASV210	9.349997669	1.07E-05	0.000507105
ASV212	9.313092514	1.01E-05	0.000507105
ASV375	10.43884125	1.02E-05	0.000507105
ASV81	−11.08651102	1.08E-05	0.000507105
ASV479	10.34020121	1.16E-05	0.000526182
ASV323	−10.79522357	1.29E-05	0.000530939
ASV537	9.310908218	1.33E-05	0.000530939
ASV703	9.329078834	1.30E-05	0.000530939
ASV799	8.946772762	1.27E-05	0.000530939
ASV149	8.405887581	1.74E-05	0.000592744
ASV180	−10.50637887	1.54E-05	0.000592744
ASV231	−10.30186542	1.76E-05	0.000592744
ASV372	−10.44638349	1.60E-05	0.000592744
ASV581	7.786667174	1.67E-05	0.000592744
ASV809	6.584532678	1.71E-05	0.000592744
ASV540	10.2075465	1.87E-05	0.000599178
ASV9	−10.21562437	1.86E-05	0.000599178
ASV450	8.781299037	2.06E-05	0.000644618
ASV68	−9.966699106	2.19E-05	0.000668808
ASV690	9.834667108	2.39E-05	0.000713598
ASV306	−9.769792597	2.49E-05	0.000728782
ASV39	−9.483476803	3.03E-05	0.000866606
ASV199	8.500711067	3.55E-05	0.00097234
ASV348	−9.228360068	3.62E-05	0.00097234
ASV49	−9.234626938	3.61E-05	0.00097234
ASV462	8.291734357	3.78E-05	0.000993624
ASV230	−9.058580151	4.09E-05	0.000997584
ASV608	9.07368902	4.05E-05	0.000997584
ASV67	−9.074588031	4.04E-05	0.000997584
ASV672	8.716493198	4.10E-05	0.000997584
ASV16	−8.989773258	4.30E-05	0.00102746

Wildtype Baseline vs 1wk UCMRS- 57.6%			
ASV	**tstat**	**p_val**	**p_adj**
ASV695	7.295874148	4.46E-05	0.001046246
ASV119	−8.842006159	4.79E-05	0.00108506
ASV272	8.852774111	4.75E-05	0.00108506
ASV321	−8.782944237	5.00E-05	0.001114049
ASV38	−8.73941212	5.16E-05	0.001117545
ASV51	−8.73364314	5.18E-05	0.001117545
ASV1	−8.662575599	5.47E-05	0.001121609
ASV102	−8.623102144	5.63E-05	0.001121609
ASV109	−8.632463289	5.59E-05	0.001121609
ASV585	5.833275265	5.57E-05	0.001121609
ASV84	−8.654892298	5.50E-05	0.001121609
ASV568	8.570170277	5.86E-05	0.001132799
ASV59	−8.578579255	5.82E-05	0.001132799
ASV183	−8.523094333	6.07E-05	0.001156788
ASV166	8.299868012	6.40E-05	0.001163752
ASV191	7.241510588	6.55E-05	0.001163752
ASV2	−8.427486424	6.53E-05	0.001163752
ASV4	−8.446414166	6.43E-05	0.001163752
ASV73	−8.449915035	6.42E-05	0.001163752
ASV569	−8.392309742	6.71E-05	0.001175763
ASV480	−8.347097049	6.94E-05	0.001201327
ASV19	−8.3065331	7.16E-05	0.001207759
ASV335	−8.315272538	7.12E-05	0.001207759
ASV239	−8.217847398	7.67E-05	0.001261577
ASV63	−8.233255933	7.58E-05	0.001261577
ASV106	−8.158930916	8.04E-05	0.00130482
ASV841	7.962420407	9.18E-05	0.001472938
ASV485	−7.972478112	9.32E-05	0.001476231
ASV776	7.955040868	9.45E-05	0.001479177
ASV220	−7.926000207	9.67E-05	0.001496267
ASV7	−7.906611136	9.82E-05	0.001502135
ASV582	7.643741584	0.000106408	0.001608347
ASV12	−7.747848221	0.000111767	0.001650698
ASV357	−7.740796839	0.000112415	0.001650698
ASV86	−7.734729403	0.000112976	0.001650698
ASV20	−7.71905301	0.000114439	0.001653712
ASV138	7.027367946	0.00011579	0.001655035
ASV225	6.801290729	0.000118612	0.001677149
ASV766	7.506544905	0.000123532	0.001728139

Wildtype Baseline vs 1wk UCMRS- 57.6%			
ASV	**tstat**	**p_val**	**p_adj**
ASV481	7.266382748	0.000129877	0.00179683
ASV625	6.332315332	0.000131175	0.00179683
ASV320	−7.494106128	0.000137987	0.001870643
ASV452	−7.426008343	0.000146159	0.001961212
ASV525	6.51038827	0.000152333	0.002023413
ASV574	7.042071223	0.000155434	0.002043951
ASV64	−7.253117696	0.000169473	0.002184866
ASV65	−7.261919293	0.000168189	0.002184866
ASV14	−7.216251412	0.000174969	0.002191868
ASV31	−7.234606661	0.000172208	0.002191868
ASV46	−7.21594438	0.000175016	0.002191868
ASV36	−7.188926972	0.000179173	0.002208827
ASV457	−7.185364962	0.00017973	0.002208827
ASV713	7.100619729	0.000183015	0.002228381
ASV121	−7.139118012	0.000187132	0.002257606
ASV152	−7.097226035	0.000194135	0.002279358
ASV206	−7.109009846	0.000192136	0.002279358
ASV44	−7.104419469	0.000192912	0.002279358
ASV34	−7.072938589	0.00019833	0.002308005
ASV113	−7.02254128	0.000207365	0.002366929
ASV322	−7.030600882	0.000205889	0.002366929
ASV607	7.014797005	0.000208794	0.002366929
ASV3	−7.001554003	0.000211263	0.002374451
ASV164	−6.928318708	0.000225526	0.002513275
ASV380	−6.851073544	0.000241755	0.002671497
ASV623	6.343252022	0.000249752	0.00273687
ASV18	−6.7911897	0.000255243	0.002756912
ASV37	−6.788903934	0.000255774	0.002756912
ASV172	−6.76104858	0.00026235	0.002759926
ASV35	−6.7616925	0.000262196	0.002759926
ASV54	−6.764438477	0.00026154	0.002759926
ASV438	−6.739891773	0.000267472	0.002791475
ASV455	−6.698802744	0.000277744	0.002875849
ASV32	−6.649081998	0.00029077	0.00298721
ASV43	−6.625291191	0.000297245	0.003030058
ASV449	−6.610481258	0.000301358	0.003034017
ASV95	−6.607304332	0.000302248	0.003034017
ASV423	−6.580985303	0.00030974	0.003085667
ASV326	−6.551090433	0.000318504	0.003149116

Wildtype Baseline vs 1wk UCMRS- 57.6%			
ASV	**tstat**	**p_val**	**p_adj**
ASV314	−6.535855996	0.000323077	0.003149323
ASV408	−6.527194523	0.000325709	0.003149323
ASV459	−6.530145264	0.00032481	0.003149323
ASV99	−6.500656307	0.000333927	0.003205214
ASV395	−6.488214658	0.00033786	0.003219461
ASV277	−6.474355336	0.000342302	0.003238324
ASV406	−6.461702131	0.000346415	0.003253824
ASV285	−6.429079151	0.000357277	0.003332049
ASV340	−6.393479956	0.000369568	0.003422409
ASV588	−6.3783825	0.000374924	0.003447723
ASV11	−6.326400466	0.00039404	0.003549057
ASV150	−6.326732812	0.000393914	0.003549057
ASV514	−6.338391839	0.000389535	0.003549057
ASV10	−6.288141483	0.000408808	0.003560152
ASV110	−6.308028924	0.000401055	0.003560152
ASV198	6.173009931	0.000408365	0.003560152
ASV298	−6.300301405	0.000404048	0.003560152
ASV92	−6.301766007	0.000403479	0.003560152
ASV359	−6.266537514	0.000417421	0.003611245
ASV147	−6.217313288	0.000437817	0.00371438
ASV389	−6.225692992	0.000434267	0.00371438
ASV78	−6.218424414	0.000437344	0.00371438
ASV302	−6.198017941	0.000446114	0.003760513
ASV332	−6.168656149	0.000459081	0.003845168
ASV473	−6.141466222	0.000471466	0.00392391
ASV347	−6.086033272	0.000497893	0.004117794
ASV141	−6.066710858	0.000507491	0.004170946
ASV400	−6.057741059	0.000512018	0.004182007
ASV50	−6.018893799	0.000532148	0.004319599
ASV90	−6.010570043	0.000536576	0.00432882
ASV397	−5.968848156	0.0005594	0.004485437
ASV232	−5.925671096	0.000584171	0.00465567
ASV396	−5.908860996	0.000594146	0.004706635
ASV107	−5.897889681	0.000600758	0.004730519
ASV72	−5.856997739	0.000626139	0.004901027
ASV291	−5.850044731	0.000630573	0.004906526
ASV200	5.498458195	0.00064646	0.004971315
ASV6	−5.829257489	0.000644039	0.004971315
ASV188	−5.815013941	0.000653452	0.004995867

Wildtype Baseline vs 1wk UCMRS- 57.6%			
ASV	**tstat**	**p_val**	**p_adj**
ASV304	−5.795746341	0.00066643	0.005065641
ASV115	−5.771820349	0.00068295	0.005161373
ASV169	−5.746806388	0.000700711	0.005228506
ASV350	−5.742582716	0.000703761	0.005228506
ASV351	−5.751987945	0.00069699	0.005228506
ASV40	−5.726951005	0.000715177	0.005283474
ASV387	−5.704829258	0.000731689	0.005375259
ASV417	−5.695565181	0.00073873	0.005396834
ASV616	−5.68168043	0.000749425	0.005444718
ASV139	−5.648050601	0.000776053	0.005576555
ASV899	5.485040863	0.000774036	0.005576555
ASV487	−5.635692285	0.000786102	0.005618067
ASV98	−5.607522746	0.000809556	0.005754411
ASV27	−5.587120245	0.000827031	0.005847019
ASV422	−5.57038574	0.000841678	0.005918755
ASV386	−5.561036395	0.000849988	0.005945393
ASV433	−5.532610969	0.000875819	0.006061588
ASV66	−5.533219339	0.000875257	0.006061588
ASV137	−5.516504898	0.000890843	0.006098068
ASV23	−5.518069927	0.00088937	0.006098068
ASV627	−5.512100045	0.000895002	0.006098068
ASV413	−5.506468665	0.00090035	0.006102888
ASV378	−5.497264953	0.000909168	0.006131056
ASV442	−5.4814207	0.000924575	0.006203144
ASV524	−5.474184132	0.000931709	0.006219273
ASV22	−5.465413216	0.000940437	0.006245831
ASV352	−5.437991569	0.000968319	0.006398692
ASV101	−5.417145541	0.000990132	0.006492397
ASV425	−5.415032035	0.000992374	0.006492397
ASV260	−5.401566854	0.001006791	0.006554109
ASV388	−5.394173242	0.001014806	0.006573745
ASV17	−5.385097684	0.001024742	0.00660557
ASV33	−5.365129823	0.001046987	0.006688442
ASV504	−5.364434919	0.001047771	0.006688442
ASV297	−5.340231124	0.001075483	0.006826036
ASV407	−5.332164757	0.001084899	0.006826036
ASV458	−5.336425619	0.001079913	0.006826036
ASV28	−5.32374304	0.001094827	0.006855704
ASV165	−5.312582761	0.001108141	0.006906187

Wildtype Baseline vs 1wk UCMRS- 57.6%			
ASV	**tstat**	**p_val**	**p_adj**
ASV440	−5.287633512	0.001138561	0.0070623
ASV185	−5.280022501	0.001148025	0.007087572
ASV58	−5.241172847	0.001197718	0.007325577
ASV717	5.151952783	0.001194328	0.007325577
ASV300	−5.225675179	0.001218205	0.007388952
ASV679	−5.22484197	0.001219318	0.007388952
ASV24	−5.191773495	0.001264394	0.007626966
ASV29	−5.180557718	0.001280102	0.007686454
ASV363	−5.173573918	0.001289992	0.00770283
ASV464	−5.170379161	0.001294544	0.00770283
ASV333	−5.162018156	0.001306543	0.007737774
ASV392	−5.158116247	0.001312185	0.007737774
ASV752	−5.153498689	0.001318897	0.007742632
ASV292	−5.133252585	0.00134878	0.007882868
ASV177	−5.122777906	0.001364535	0.00793617
ASV70	−5.119195378	0.00136997	0.00793617
ASV42	−5.10968943	0.001384509	0.007985219
ASV62	−5.095649357	0.001406298	0.008075468
ASV419	−5.076238017	0.001437053	0.008216193
ASV240	−5.060407826	0.001462687	0.008326551
ASV61	−5.049333847	0.001480921	0.008394014
ASV429	−4.992401255	0.001578739	0.008910051
ASV270	−4.979256292	0.00160233	0.009004544
ASV619	−4.926532885	0.001700958	0.009518128
ASV135	−4.907592714	0.001738018	0.009684295
ASV245	−4.893592827	0.001765987	0.009798618
ASV193	−4.881513717	0.001790519	0.009849607
ASV466	−4.881463208	0.001790623	0.009849607
ASV494	−4.87803865	0.001797647	0.009849607
ASV412	−4.87103263	0.001812113	0.009887668
ASV572	−4.850175694	0.001855946	0.010084996
ASV341	−4.827101214	0.001905814	0.010264057
ASV519	−4.824142385	0.001912315	0.010264057
ASV638	−4.829798413	0.001899909	0.010264057
ASV646	−4.819221263	0.001923182	0.010280424
ASV55	−4.788355035	0.001992922	0.010544386
ASV649	−4.78744628	0.001995018	0.010544386
ASV97	−4.786753088	0.001996618	0.010544386
ASV500	−4.75890209	0.002062088	0.010846585

Wildtype Baseline vs 1wk UCMRS- 57.6%			
ASV	**tstat**	**p_val**	**p_adj**
ASV391	−4.742199064	0.002102491	0.010976639
ASV41	−4.741783013	0.002103508	0.010976639
ASV243	−4.733526771	0.002123812	0.011038788
ASV483	−4.728308336	0.002136758	0.011062348
ASV431	−4.721502624	0.002153772	0.011106707
ASV617	4.645935153	0.0023531	0.012087214
ASV83	−4.638188846	0.002368349	0.012118206
ASV130	−4.612371246	0.002448102	0.012429554
ASV356	−4.613029192	0.0024462	0.012429554
ASV379	−4.604664638	0.002470509	0.012495074
ASV343	−4.586997962	0.002522733	0.012710324
ASV174	−4.574810863	0.00255947	0.012846194
ASV383	−4.567460318	0.002581912	0.012909562
ASV118	−4.539022299	0.002670807	0.013253249
ASV530	−4.541950815	0.002661498	0.013253249
ASV436	−4.527558389	0.002707593	0.013385279
ASV145	−4.508869361	0.002768766	0.013607112
ASV709	4.507544494	0.002773161	0.013607112
ASV675	−4.470469933	0.002899297	0.014173144
ASV87	−4.454635803	0.002955085	0.014392358
ASV461	−4.445577367	0.002987531	0.014496692
ASV163	−4.400270055	0.003155819	0.015256994
ASV757	−4.386416461	0.00320934	0.015458909
ASV520	−4.355999417	0.00333039	0.01598344
ASV313	−4.327090781	0.003450106	0.016413751
ASV394	−4.329621212	0.003439441	0.016413751
ASV8	−4.325342374	0.003457497	0.016413751
ASV242	3.608995893	0.00356349	0.016856077
ASV662	−4.291351572	0.003604697	0.016989879
ASV93	−4.284370231	0.003635775	0.017075157
ASV53	−4.281334728	0.003649379	0.017078056
ASV360	−4.250410507	0.003791208	0.017660811
ASV491	−4.248372057	0.003800768	0.017660811
ASV772	−4.237021932	0.003854481	0.017847335
ASV656	−4.227835494	0.003898566	0.017988121
ASV648	−4.223574092	0.003919204	0.018020115
ASV256	3.436485834	0.004011011	0.018377978
ASV146	−4.201138943	0.004029852	0.018400192
ASV103	−4.185458592	0.00410922	0.018633187

Wildtype Baseline vs 1wk UCMRS- 57.6%			
ASV	**tstat**	**p_val**	**p_adj**
ASV503	−4.186022452	0.004106336	0.018633187
ASV131	−4.178986511	0.004142478	0.018719444
ASV681	−4.167608896	0.004201661	0.018875974
ASV842	3.46338912	0.004205825	0.018875974
ASV325	−4.136725832	0.004367034	0.019532821
ASV444	−4.128353595	0.004413085	0.019671888
ASV726	−4.061115336	0.004802821	0.021336855
ASV132	−4.04950938	0.00487383	0.021435073
ASV5	−4.052100186	0.00485788	0.021435073
ASV631	−4.051354327	0.004862466	0.021435073
ASV257	4.033509542	0.004973613	0.021801004
ASV612	−4.025217125	0.005026206	0.021958343
ASV108	−4.010204353	0.005122976	0.022306998
ASV233	−4.001006545	0.005183268	0.022495043
ASV663	−3.99558228	0.005219188	0.022576423
ASV134	−3.946060732	0.005559992	0.023971769
ASV202	−3.942327485	0.005586652	0.024007998
ASV91	−3.932392822	0.00565828	0.024236607
ASV583	−3.928017798	0.005690141	0.024293946
ASV207	−3.91404633	0.005793206	0.024653934
ASV411	−3.901912747	0.005884366	0.024961103
ASV552	−3.890716963	0.005969871	0.025242379
ASV527	−3.885507235	0.006010119	0.025250181
ASV596	−3.887052541	0.00599815	0.025250181
ASV874	3.878955426	0.006061157	0.025383508
ASV368	−3.85784107	0.006228876	0.025920797
ASV584	−3.8600078	0.006211434	0.025920797
ASV244	−3.835863105	0.006408842	0.026501974
ASV598	−3.837320505	0.006396735	0.026501974
ASV69	−3.800057124	0.006714284	0.027678005
ASV661	−3.782536713	0.006869484	0.028229287
ASV267	−3.776712228	0.00692194	0.02830057
ASV401	−3.77583547	0.006929874	0.02830057
ASV659	−3.772197627	0.006962898	0.028347403
ASV674	3.72343236	0.007422507	0.0301253
ASV179	3.147106743	0.007449502	0.030141832
ASV89	−3.691913261	0.007737049	0.031209263
ASV538	−3.682646199	0.00783226	0.031496701
ASV428	−3.680288982	0.00785668	0.03149858

Wildtype Baseline vs 1wk UCMRS- 57.6%			
ASV	**tstat**	**p_val**	**p_adj**
ASV529	−3.674275089	0.007919358	0.031653363
ASV498	−3.664183872	0.008025754	0.031884792
ASV563	−3.664214935	0.008025424	0.031884792
ASV667	−3.659563622	0.008074983	0.031983744
ASV13	−3.644426394	0.00823858	0.032533733
ASV217	−3.633752741	0.008356095	0.032898999
ASV562	−3.622162046	0.008485768	0.033309805
ASV167	−3.613099478	0.008588675	0.033613415
ASV125	−3.609880832	0.008625548	0.033657553
ASV587	−3.607232183	0.00865602	0.033676526
ASV192	−3.577122671	0.00901073	0.034910441
ASV611	−3.575832765	0.009026274	0.034910441
ASV467	−3.565763051	0.009148615	0.03527985
ASV578	−3.553982052	0.009294029	0.035735813
ASV222	3.526279815	0.009645901	0.036980642
ASV921	−3.503973298	0.009939702	0.037996243
ASV111	−3.482138782	0.010236664	0.039018007
ASV238	3.467334033	0.010443456	0.03969117
ASV676	−3.463203173	0.010501957	0.039798482
ASV456	−3.44628494	0.010745264	0.040538176
ASV555	−3.445355809	0.010758801	0.040538176
ASV506	−3.414242983	0.011222883	0.042165974
ASV187	−3.397825397	0.01147642	0.042995705
ASV669	−3.385129384	0.011676711	0.043621804
ASV259	−3.373783185	0.011858892	0.043804614
ASV344	−3.377272478	0.011802542	0.043804614
ASV521	−3.375310404	0.011834193	0.043804614
ASV993	−3.37693532	0.011807975	0.043804614
ASV862	−3.370234863	0.011916491	0.043894078
ASV689	−3.348179654	0.012281324	0.045111565
ASV434	−3.340598277	0.012409491	0.045455376
ASV246	−3.337828207	0.012456678	0.045501476
ASV547	−3.284778343	0.013398547	0.048806341
ASV21	−3.271441429	0.013647165	0.049349573
ASV577	−3.274684978	0.01358625	0.049349573
ASV715	−3.268757631	0.01369779	0.049349573
ASV755	3.241772295	0.013690065	0.049349573
Non-Signficant Changes			
ASV722	3.244710048	0.014160485	0.050877153

Wildtype Baseline vs 1wk UCMRS- 57.6%			
ASV	**tstat**	**p_val**	**p_adj**
ASV778	−3.179942778	0.015491881	0.055509057
ASV586	−3.135495789	0.016482596	0.058898406
ASV398	−3.126500013	0.016691214	0.05948224
ASV161	−3.121539117	0.016807463	0.059574323
ASV301	2.986473036	0.016852964	0.059574323
ASV694	−3.120229343	0.016838299	0.059574323
ASV116	−3.112329113	0.017025577	0.060023146
ASV553	−3.098533894	0.017357937	0.061031251
ASV486	−3.095614296	0.01742916	0.061118253
ASV443	2.974903876	0.017791662	0.062223499
ASV353	3.062288628	0.018264524	0.063379871
ASV544	−3.065787996	0.018174838	0.063379871
ASV94	−3.06219623	0.018266898	0.063379871
ASV381	−3.055209016	0.01844741	0.063837749
ASV556	−3.039857645	0.0188507	0.065062127
ASV534	−3.012596035	0.019590135	0.067437245
ASV548	−2.99837502	0.019988022	0.068627281
ASV725	−2.986588532	0.020324287	0.069600097
ASV697	−2.962640253	0.021026126	0.071816508
ASV307	2.94760685	0.021397609	0.072895999
ASV216	2.591093085	0.021514369	0.07310438
ASV712	−2.942254537	0.021643778	0.073354557
ASV654	−2.933244633	0.021922852	0.074109385
ASV566	−2.927373975	0.022106736	0.074539379
ASV253	−2.925302274	0.022172015	0.074568287
ASV336	−2.903052632	0.022886082	0.076773464
ASV492	2.894921593	0.023153059	0.077471432
ASV60	−2.889032475	0.023348475	0.077927018
ASV158	−2.882784496	0.023557703	0.078426278
ASV488	−2.879085828	0.023682493	0.07864262
ASV120	−2.865196093	0.024157377	0.079816458
ASV144	−2.865724742	0.02413912	0.079816458
ASV590	−2.857918294	0.024410199	0.080248529
ASV613	−2.858031357	0.02440625	0.080248529
ASV510	−2.850935521	0.024655393	0.080651348
ASV628	−2.851391357	0.024639308	0.080651348
ASV489	−2.829612084	0.025420328	0.082947224
ASV805	−2.823793134	0.025633379	0.08343538
ASV846	−2.820871423	0.02574106	0.083578998

Wildtype Baseline vs 1wk UCMRS- 57.6%			
ASV	**tstat**	**p_val**	**p_adj**
ASV143	−2.815931781	0.025924196	0.0839663
ASV416	−2.812818257	0.026040332	0.084135226
ASV76	2.685297937	0.026928761	0.086792453
ASV117	−2.764858356	0.027899976	0.089484069
ASV589	−2.765321757	0.027881356	0.089484069
ASV361	2.749843495	0.028510408	0.091219433
ASV376	2.747594362	0.028603045	0.091293701
ASV816	−2.73135543	0.029281318	0.093232282
ASV128	−2.725786971	0.029517761	0.093758105
ASV962	2.71103903	0.029634204	0.093901153
ASV136	−2.716064398	0.029935393	0.094627505
ASV346	−2.690023441	0.031084687	0.098024854
ASV502	−2.680871394	0.031499469	0.09909522
ASV865	−2.679172046	0.031577119	0.099102415
ASV184	−2.669977037	0.032000755	0.100192839
ASV355	2.65009225	0.032937281	0.102880106
ASV175	−2.643887131	0.033235338	0.103565095
ASV893	2.588625478	0.033404204	0.103845219
ASV156	2.5559634	0.033991536	0.105421863
ASV364	−2.622546612	0.034282021	0.106072605
ASV178	−2.613830047	0.034719348	0.107173575
ASV155	−2.590108822	0.035939087	0.110678922
ASV229	−2.569918931	0.037012261	0.113629486
ASV463	−2.568273775	0.037101159	0.113629486
ASV516	−2.567253348	0.03715641	0.113629486
ASV334	−2.563599779	0.037354933	0.113971547
ASV248	−2.555434422	0.037802594	0.115070397
ASV318	2.502130656	0.03830609	0.116333737
ASV518	−2.540380882	0.038642513	0.117085033
ASV415	−2.538783609	0.03873276	0.117088687
ASV470	−2.532623905	0.039082831	0.117875971
ASV237	−2.530014065	0.039232141	0.118055526
ASV176	−2.527160617	0.039396061	0.11827813
ASV186	−2.523583322	0.039602565	0.118357667
ASV827	−2.524689323	0.039538601	0.118357667
ASV153	−2.521645571	0.039714891	0.118424222
ASV219	−2.491441174	0.041508911	0.123493706
ASV114	−2.488359699	0.041696578	0.12377201
ASV173	−2.484547749	0.041929944	0.124184405

Wildtype Baseline vs 1wk UCMRS- 57.6%			
ASV	**tstat**	**p_val**	**p_adj**
ASV716	2.478475647	0.042304457	0.125012047
ASV25	−2.459717496	0.043483324	0.127705917
ASV385	−2.462253996	0.043321959	0.127705917
ASV657	−2.459339632	0.043507415	0.127705917
ASV203	−2.453670087	0.04387054	0.12848499
ASV201	−2.434999465	0.04508854	0.131758733
ASV279	−2.432047744	0.045284255	0.132037241
ASV926	−2.430429463	0.045391926	0.132058369
ASV370	−2.420404617	0.046064801	0.133720118
ASV641	−2.406273774	0.04703069	0.136223255
ASV511	2.402927272	0.047262459	0.136593702
ASV122	−2.399195146	0.047522316	0.137043521
ASV597	−2.396851284	0.04768626	0.137215386
ASV714	−2.386519778	0.048415836	0.139010534
ASV159	−2.380546089	0.04884288	0.139931126

Extended Data Table 4

Table of statistics for all data in manuscript.

Figure	Panel	Test	P-value(s)	Error Bars	Sample Numbers	Replicate Numbers	Samples Taken from
1	B	1WANOVA with Tukey's Multiple Comparison Test	**Nestlet Shred** ANOVA p-value: 0.0005 (***) Baseline to Naïve: 0.9998 (n.s) Basline to Stress: 0.0006 (***) Naïve to Stress: 0.0050 (**)	Standard Error Mean	11 naïve animals 12 stressed animals	Representative of 2 independent experiments	- Baseline samples from distinct animals - Naïve and stressed animals were re-sampled after 3 weeks stress
1	B	Un-paired t-test, two-tailed	**Elevated Plus Maze** Naïve to Stress: 0.0449 (*)	Standard Error Mean	11 naïve animals 12 stressed animals	Representative of 2 independent experiments	Samples collected from distinct animals
1	B	1WANOVA with Tukey's Multiple Comparison Test	**Tail Suspension Test** ANOVA p-value: <0.0001 (****) Baseline to Naïve: 0.9471 (n.s) Basline to Stress: <0.0001 (****) Naïve to Stress: 0.0001 (***)	Standard Error Mean	11 naïve animals 12 stressed animals	Representative of 2 independent experiments	- Baseline samples from distinct animals - Naïve and stressed animals were re-sampled

Figure	Panel	Test	P-value(s)	Error Bars	Sample Numbers	Replicate Numbers	Samples Taken from
							after 3 weeks stress
1	B	1WANOVA with Tukey's Multiple Comparison Test	**Forced Swim Test** ANOVA p-value: 0.0023 (**) Baseline to Naïve: 0.9100 (n.s) Basline to Stress: 0.0022 (**) Naïve to Stress: 0.0205 (*)	Standard Error Mean	11 naïve animals 12 stressed animals	Representative of 2 independent experiments	- Baseline samples from distinct animals - Naïve and stressed animals were re-sampled after 3 weeks stress
1	B	1WANOVA with Tukey's Multiple Comparison Test	**Sucrose Preference Test** ANOVA p-value: 0.0002 (***) Baseline to Naïve: 0.0343 (*) Basline to Stress: 0.0355 (*) Naïve to Stress: 0.0001 (***)	Standard Error Mean	11 naïve animals 12 stressed animals	Representative of 2 independent experiments	- Baseline samples from distinct animals - Naïve and stressed animals were re-sampled after 3 weeks stress
1	C	Un-paired t-test, two-tailed	**Cortisol** Naïve to Stress: 0.0081 (**)	Standard Error Mean	11 naïve animals 12 stressed animals	Representative of 1 experiment	Samples collected from distinct animals
1	C	Un-paired t-test, two-tailed	**Serotonin** Naïve to Stress: <0.0001 (****)	Standard Error Mean	11 naïve animals 12 stressed animals	Representative of 1 experiment	Samples collected from distinct animals
1	C	Un-paired t-test, two-tailed	**Glutamine** Naïve to Stress: 0.0440 (*)	Standard Error Mean	11 naïve animals 12 stressed animals	Representative of 1 experiment	Samples collected from distinct animals
1	D	Wilcoxon Rank Sum test	**Alpha Diversity** Baseline to Stress: 0.28	center line, median; box limits, 75% and 25% percentiles; whiskers, 1.5x interquartile range; points, outliers	24 basline samples 24 stressed samples	Representative of 1 experiment	Samples collected from same animals before and after stress exposure
1	E	PERMANOVA	**Beta Diversity** Baseline to Stress: 0.001 (***)	N/A	24 basline samples 24 stressed samples	Representative of 1 experiment	Samples collected from same animals before

Figure	Panel	Test	P-value(s)	Error Bars	Sample Numbers	Replicate Numbers	Samples Taken from
							and after stress exposure
1	F	Wilcox Rank Sum Test with Bonferroni correction	**Order Composition** Baseline to Stress Acholeplasmatales: 0.0006 (***) Baseline to Stress Bacteriodales: 4.31E-05 (****) Baseline to Stress Clostridiales: 6.39E-08 (****) Baseline to Stress Erysipelotichales: 1 (n.s) Baseline to Stress Lachnospirales: 1 (n.s) Baseline to Stress Lactobacillales: 0.0002 (***) Baseline to Stress Oscillospirales: 1 (n.s) Baseline to Stress Peptostreptococcales-Tissierellales: 6.02E-07 (****)	center line, median; box limits, 75% and 25% percentiles; whiskers, 1.5x interquartile range; points, outliers	24 basline samples 24 stressed samples	Representative of 1 experiment	Samples collected from same animals before and after stress exposure
2	B	Unpaired t-tests, two-tailed	***Muc13*** Duodenum Naïve to Stress: 0.0004 (***) Jejunum Naïve to Stress: 0.0059 (**) Ileum Naïve to Stress: 0.01 (*) Colon Naïve to Stress: 0.02 (*)	Standard Error Mean	11 naïve animals 12 stressed animals	Representative of 2 independent experiments	Samples collected from distinct animals
2	C	Unpaired t-tests, two-tailed	***Muc2*** Duodenum Naïve to Stress: 0.2019 Jejunum Naïve to Stress: 0.6569 Ileum Naïve to Stress: 0.3130	Standard Error Mean	11 naïve animals 12 stressed animals	Representative of 2 independent experiments	Samples collected from distinct animals
2	E	Unpaired t-tests, two-tailed	***Muc13*** Duodenum Naïve to Stress: 0.4595 Jejunum Naïve to Stress: 0.7147 Ileum Naïve to Stress: 0.5270 Colon Naïve to Stress: 0.5636	Standard Error Mean	12 animals per group	Representative of 1 independent experiments	Samples collected from distinct animals
2	F	Unpaired t-tests, two-tailed	***Muc2*** Duodenum Naïve to Stress: 0.2837 Jejunum Naïve to Stress: 0.7825 Ileum Naïve to Stress: 0.2700	Standard Error Mean	12 animals per group	Representative of 1 independent experiments	Samples collected from distinct animals
2	G	Unpaired t-tests, two-tailed	***Muc13*** Duodenum Naïve to Stress: 0.6552 Jejunum Naïve to Stress: 0.9773 Ileum Naïve to	Standard Error Mean	7 animals per group	Representative of 1 independent experiments	Samples collected from distinct animals

Figure	Panel	Test	P-value(s)	Error Bars	Sample Numbers	Replicate Numbers	Samples Taken from
			Stress: 0.1015 Colon Naïve to Stress: 0.5430				
2	H	Unpaired t-tests, two-tailed	***Muc2*** Duodenum Naïve to Stress: 0.2369 Jejunum Naïve to Stress: 0.0289 (*) Ileum Naïve to Stress: 0.0537	Standard Error Mean	7 animals per group	Representative of 1 independent experiments	Samples collected from distinct animals
3	B	N/A	**POL LL ChIP-Seq Muc13 Counts:** Control: 4684, 4353, 6391 HNF4 DKO: 1018, 1322, 2117	N/A	3 animals per group	Representative of 1 independent experiments	Samples collected from distinct animals
3	D	Unpaired t-tests, two-tailed	**Muc13 RNA-Seq:** 0.0113 (*)	Standard Error Mean	3 animals per group	Representative of 1 independent experiments	Samples collected from distinct animals
3	E	2WANOVA with Sidak's multiple comparisons test OR T-test comparing intra-section results	***Hnf4a*:** ANOVA Results: Interaction: 0.4805 Section: 0.4861 Group: <0.0001 (****) **Multiple Comparisons:** Duodenum Naïve to Stress: 0.7301 Jejunum Naïve to Stress: 0.0083 (**) Ileum Naïve to Stress: 0.1330 Colon Naïve to stress: 0.1120 **Intrasection T-tests:** Duodenum Naïve to Stress: 0.0507 Jejunum Naïve to Stress: 0.0781 Ileum Naïve to Stress: 0.0484 (*) Colon Naïve to Stress: 0.0002 (***)	Standard Error Mean	5 animals per group	Representative of 1 independent experiments	Samples collected from distinct animals
3	F	2WANOVA with Sidak's multiple comparisons test OR T-test comparing intra-section results	***Hnf4g*:** ANOVA Results: Interaction: 0.1579 Section: 0.0024 (**) Group: 0.0010 (**) **Multiple Comparisons:** Duodenum Naïve to Stress: 0.6756 Jejunum Naïve to Stress: 0.0303 (*) Ileum Naïve to Stress: 0.0202 (*) Colon Naïve to stress: 0.9996 **Intrasection T-tests:**	Standard Error Mean	5 animals per group	Representative of 1 independent experiments	Samples collected from distinct animals

Figure	Panel	Test	P-value(s)	Error Bars	Sample Numbers	Replicate Numbers	Samples Taken from
			Duodenum Naïve to Stress: 0.0528 Jejunum Naïve to Stress: 0.0605 Ileum Naïve to Stress: 0.0676 Colon Naïve to Stress: 0.0092 (**)				
3	G	2WANOVA with Sidak's multiple comparisons test OR T-test comparing intra-section results	***Muc13*:** ANOVA Results: Interaction: 0.4789 Section: 0.1639 Group: 0.0003 (***) **Multiple Comparisons:** Duodenum Naïve to Stress: 0.7356 Jejunum Naïve to Stress: 0.2258 Ileum Naïve to Stress: 0.0097 (**) Colon Naïve to stress: 0.2679 **Intrasection T-tests:** Duodenum Naïve to Stress: 0.0770 Jejunum Naïve to Stress: 0.0709 Ileum Naïve to Stress: 0.0592 Colon Naïve to Stress: 0.0533	Standard Error Mean	5 animals per group	Representative of 1 independent experiments	Samples collected from distinct animals
3	H	Perseus Software	Muc13: -Log(p-value) = 6.7390 Muc18: = 3.1777 Muc2: = 0.3269	N/A	3 animals per group	Representative of 1 independent experiments	Samples collected from distinct animals
3	I	2WANOVA with Sidak's multiple comparisons test OR T-test comparing intra-section results	**HNF4a:** Stress V Naive: 0.0020 (**) Multiple Comparisons (Stress to KO): Duodenum: 0.8896 Jejunum: 0.1468 Ileum: 0.4461 Colon: 0.1808 **Intrasection T-tests:** Duodenum Naïve to Stress: 0.0090 (**) Jejunum Naïve to Stress: 0.0285 (*) Ileum Naïve to Stress: 0.3432 Colon Naïve to Stress: 0.0267 (*)	Standard Error Mean	11 naïve animals 12 stressed animals	Representative of 1 independent experiment	Samples collected from distinct animals
3	J	2WANOVA with Sidak's multiple comparisons test	**HNF4g:** Stress V Naive: 0.0208 (*) Multiple	Standard Error Mean	11 naïve animals 12 stressed animals	Representative of 1 independent experiment	Samples collected from distinct animals

Figure	Panel	Test	P-value(s)	Error Bars	Sample Numbers	Replicate Numbers	Samples Taken from
		OR T-test comparing intra-section results	Comparisons (Stress to KO): Duodenum: 0.2800 Jejunum: 0.0814 Ileum: 0.9859 Colon: >0.9999 **Intrasection T-tests:** Duodenum Naïve to Stress: 0.0173 (*) Jejunum Naïve to Stress: 0.0304 (*) Ileum Naïve to Stress: 0.7766 Colon Naïve to Stress: 0.6020				
4	B	Unpaired t-tests, two-tailed	***Muc13*** Duodenum Wildtype to Muc13−/−: <0.0001 (****) Jejunum Wildtype to Muc13−/−: 0.0007 (***) Ileum Wildtype to Muc13−/−: <0.0001 (****) Colon Wildtype to Muc13−/−: <0.0001 (****)	Standard Error Mean	2–3 animals per group	Representative of 1 independent experiments	Samples collected from distinct animals
4	C	Unpaired t-tests, two-tailed	***Muc2*** Duodenum Wildtype to Muc13−/−: 0.0763 Jejunum Wildtype to Muc13−/−: 0.6885 Ileum Wildtype to Muc13−/−: 0.2886 Colon Wildtype to Muc13−/−: 0.3858	Standard Error Mean	2–3 animals per group	Representative of 1 independent experiments	Samples collected from distinct animals
4	E	Unpaired t-tests, two-tailed	***Muc13*** Duodenum Wildtype to Muc13−/−: 0.0002 (***)	Standard Error Mean	4–6 animals per group	Representative of 2 independent experiments	Samples collected from distinct animals
4	E	Unpaired t-tests, two-tailed	***Muc13*** Colon Wildtype to Muc13−/−: 0.0089 (**)	Standard Error Mean	4–6 animals per group	Representative of 2 independent experiments	Samples collected from distinct animals
4	F	Unpaired t-tests, two-tailed	***Muc2*** Duodenum Wildtype to Muc13−/−: 0.1353	Standard Error Mean	4–6 animals per group	Representative of 2 independent experiments	Samples collected from distinct animals
4	F	Unpaired t-tests, two-tailed	***Muc2*** Colon Wildtype to Muc13−/−: 0.9461	Standard Error Mean	4–6 animals per group	Representative of 2 independent experiments	Samples collected from distinct animals
4	G	Perseus Software	Muc13: -Log(p-value) = 17.8270 Muc18: = 0.4110 Muc2: = 0.7614 Muc1: = 1.4100	N/A	3 animals per group	Representative of 1 independent experiments	Samples collected from distinct animals

Figure	Panel	Test	P-value(s)	Error Bars	Sample Numbers	Replicate Numbers	Samples Taken from
5	D	2WANOVA, repeated measures with Sidak's multiple comparisons test	**Open Field** Baseline to 1wk-Wildtype: 0.0825 Baseline to 1wk-Muc13−/−: 0.0014 (**) Wildtype to Muc13−/− Baseline: 0.1164 Wildtype to Muc13−/− 1wk stress: 0.7982	Standard Error Mean	12–13 animals per group	Representative of 2 independent experiments	Data collected from distinct animals, repeated measures from baseline to 1 wk
5	E	2WANOVA, repeated measures with Sidak's multiple comparisons test	**Nestlet Shred** Baseline to 1wk-Wildtype: 0.1129 Baseline to 1wk-Muc13−/−: 0.0009 (***) Wildtype to Muc13−/− Baseline: 0.0588 Wildtype to Muc13−/− 1wk stress: 0.0483 (*)	Standard Error Mean	12–13 animals per group	Representative of 2 independent experiments	Data collected from distinct animals, repeated measures from baseline to 1 wk
5	F	2WANOVA, repeated measures with Sidak's multiple comparisons test	**Tail Suspension** Baseline to 1wk-Wildtype: 0.7624 Baseline to 1wk-Muc13−/−: 0.4045 Wildtype to Muc13−/− Baseline: 0.0089 (**) Wildtype to Muc13−/− 1wk stress: 0.0026 (**)	Standard Error Mean	12–13 animals per group	Representative of 2 independent experiments	Data collected from distinct animals, repeated measures from baseline to 1 wk
5	G	2WANOVA, repeated measures with Sidak's multiple comparisons test	**Forced Swim Test** Baseline to 1wk-Wildtype: <0.0001 (****) Baseline to 1wk-Muc13−/−: 0.8711 Wildtype to Muc13−/− Baseline: <0.0001 (****) Wildtype to Muc13−/− 1wk stress: 0.8728	Standard Error Mean	12–13 animals per group	Representative of 2 independent experiments	Data collected from distinct animals, repeated measures from baseline to 1 wk
5	J	Unpaired t-tests, two-tailed	**DeepLabCut Motif Analysis** Wildtype to Muc13−/− Rearing/Grooming 1: 0.4417 Wildtype to Muc13−/− Rearing/Grooming 2: 0.0036 (**) Wildtype to Muc13−/− Rearing/Grooming 3: 0.0693 Wildtype to Muc13−/− Rearing/Grooming 4: 0.4396 Wildtype to Muc13−/− Rearing/Grooming 5: 0.8772 Wildtype to Muc13−/− Rearing/Grooming 6: 0.1651 Wildtype to Muc13−/− Rearing/Grooming 7: 0.7005 Wildtype to Muc13−/− Sitting/Sniffing 1:	Standard Error Mean	12–13 animals per group	Representative of 2 independent experiments	Data collected from distinct animals, repeated measures from baseline to 1 wk

Figure	Panel	Test	P-value(s)	Error Bars	Sample Numbers	Replicate Numbers	Samples Taken from
			0.0395 (*) Wildtype to Muc13−/− Sitting/Sniffing 2: 7.85E-04 (***) Wildtype to Muc13−/− Sitting/Sniffing 3: 0.0948 Wildtype to Muc13−/− Sitting/Sniffing 4: 0.9309 Wildtype to Muc13−/− Sitting/Sniffing 5: 1.70E-04 (***) Wildtype to Muc13−/− Turning 1: 0.0202 (*) Wildtype to Muc13−/− Turning 2: 0.9412 Wildtype to Muc13−/− Turning 3: 0.0041 (**) Wildtype to Muc13−/− Turning 4: 0.1687 Wildtype to Muc13−/− Turning 5: 0.0057 (**) Wildtype to Muc13−/− Turning 6: 6.47E-06 (****) Wildtype to Muc13−/− Turning 7: 8.26E-04 (***) Wildtype to Muc13−/− Turning 8: 0.0476 (*) Wildtype to Muc13−/− Turning 9: 0.3798 Wildtype to Muc13−/− Walking 1: 0.1251 Wildtype to Muc13−/− Walking 2: 0.9924 Wildtype to Muc13−/− Walking 3: 0.7105 Wildtype to Muc13−/− Walking 4: 0.6467				
Extended Data 1	A	Un-paired t-test, two-tailed	**Corticosterone** Naïve to Stress: 0.40	Standard Error Mean	11 naïve animals 12 stressed animals	Representative of 1 experiment	Samples collected from distinct animals
Extended Data 1	B	Un-paired t-test, two-tailed	**Tryptophan** Naïve to Stress: 0.55	Standard Error Mean	11 naïve animals 12 stressed animals	Representative of 1 experiment	Samples collected from distinct animals
Extended Data 1	C	Un-paired t-test, two-tailed	**Kynurenine** Naïve to Stress: 0.36	Standard Error Mean	11 naïve animals 12 stressed animals	Representative of 1 experiment	Samples collected from distinct animals
Extended Data 1	D	Un-paired t-test, two-tailed	**Kynurenic Acid** Naïve to Stress: 0.16	Standard Error Mean	11 naïve animals 12 stressed animals	Representative of 1 experiment	Samples collected from distinct animals
Extended Data 1	E	Un-paired t-test, two-tailed	**Dopamine** Naïve to Stress: 0.19	Standard Error Mean	11 naïve animals 12	Representative of 1 experiment	Samples collected from

Figure	Panel	Test	P-value(s)	Error Bars	Sample Numbers	Replicate Numbers	Samples Taken from
					stressed animals		distinct animals
Extended Data 1	F	Un-paired t-test, two-tailed	**Thyroxine** Naïve to Stress: 0.18	Standard Error Mean	11 naïve animals 12 stressed animals	Representative of 1 experiment	Samples collected from distinct animals
Extended Data 1	G	Un-paired t-test, two-tailed	**Aldosterone** Naïve to Stress: 0.06	Standard Error Mean	11 naïve animals 12 stressed animals	Representative of 1 experiment	Samples collected from distinct animals
Extended Data 1	H	Wilcoxon Rank Sum test.	**Species Evenness** Baseline to Stress: 0.27	center line, median; box limits, 75% and 25% percentiles; whiskers, 1.5x interquartile range; points, outliers	24 basline samples 24 stressed samples	Representative of 1 experiment	Samples collected from same animals before and after stress exposure
Extended Data 1	J	Wilcoxon Rank Sum test.	Individual Comparisons can be Found in Tab 1	center line, median; box limits, 75% and 25% percentiles; whiskers, 1.5x interquartile range; points, outliers	24 basline samples 24 stressed samples	Representative of 1 experiment	Samples collected from same animals before and after stress exposure
Extended Data 2	A	Unpaired t-tests, two-tailed	***Muc1*** Colon Naïve to Stress: 0.9184	Standard Error Mean	11 naïve animals 12 stressed animals	Representative of 1 experiment	Samples collected from distinct animals
Extended Data 2	B	2WANOVA with Sidak's multiple comparisons test	***Muc4*** Duodenum Naïve to Stress: >0.9999 Jejunum Naïve to Stress: >0.9999 Ileum Naïve to Stress: >0.9999 Colon Naïve to Stress: >0.9999	Standard Error Mean	11 naïve animals 12 stressed animals	Representative of 1 experiment	Samples collected from distinct animals
Extended Data 2	C	2WANOVA with Sidak's multiple comparisons test	***Muc17*** Duodenum Naïve to Stress: 0.9943 Jejunum Naïve to Stress: 0.9995 Ileum Naïve to Stress: 0.8353 Colon Naïve to Stress: >0.9999	Standard Error Mean	11 naïve animals 12 stressed animals	Representative of 1 experiment	Samples collected from distinct animals
Extended Data 2	D	Unpaired t-tests, two-tailed	***Muc13- Balb/cJ*** Duodenum Naïve to Stress: 0.0027 (**) Jejunum Naïve to Stress: 0.0993 Ileum Naïve to	Standard Error Mean	5 naïve animals 5 stressed animals	Representative of 1 experiment	Samples collected from distinct animals

Figure	Panel	Test	P-value(s)	Error Bars	Sample Numbers	Replicate Numbers	Samples Taken from
			Stress: 0.0463 (*) Colon Naïve to Stress: 0.3892				
Extended Data 2	E	Unpaired t-tests, two-tailed	***Muc2- Balb/cJ*** Duodenum Naïve to Stress: 0.5833 Jejunum Naïve to Stress: 0.3738 Ileum Naïve to Stress: 0.2412	Standard Error Mean	5 naïve animals 5 stressed animals	Representative of 1 experiment	Samples collected from distinct animals
Extended Data 2	H	Unpaired t-tests, two-tailed	**Muc1:** Naïve to Stress: 0.2862	Standard Error Mean	12 animals per group	Representative of 1 experiment	Samples collected from distinct animals
Extended Data 2	I	2WANOVA with Sidak's multiple comparisons test	**Muc4:** ANOVA Results: Interaction: 0.5997 Section: 0.2204 Group: 0.6271 **Multiple Comparisons:** Duodenum Naïve to Stress: 0.9739 Jejunum Naïve to Stress: 0.8886 Ileum Naïve to Stress: 0.8050 Colon Naïve to stress: 0.9920	Standard Error Mean	12 animals per group	Representative of 1 experiment	Samples collected from distinct animals
Extended Data 2	J	2WANOVA with Sidak's multiple comparisons test	**Muc17:** ANOVA Results: Interaction: 0.9122 Section: 0.6856 Group: 0.2386 **Multiple Comparisons:** Duodenum Naïve to Stress: 0.03533 (*) Jejunum Naïve to Stress: 0.1008 Ileum Naïve to Stress: 0.2617 Colon Naïve to stress: 0.2726	Standard Error Mean	12 animals per group	Representative of 1 experiment	Samples collected from distinct animals
Extended Data 2	K	Unpaired t-tests, two-tailed	**Muc1:** Naïve Feces to Stress Feces: 0.2072	Standard Error Mean	7 animals per group	Representative of 1 experiment	Samples collected from distinct animals
Extended Data 2	L	2WANOVA with Sidak's multiple comparisons test	**Muc4:** ANOVA Results: Interaction: 0.9676 Section: <0.0001 (****) Group: 0.9757 **Multiple Comparisons:** Duodenum Naïve Feces to Stress Feces: 0.9998 Jejunum Naïve Feces to Stress Feces: 0.9971	Standard Error Mean	7 animals per group	Representative of 1 experiment	Samples collected from distinct animals

Figure	Panel	Test	P-value(s)	Error Bars	Sample Numbers	Replicate Numbers	Samples Taken from
			Ileum Naïve Feces to Stress Feces: >0.9999 Colon Naïve Feces to Stress Feces: 0.9924				
Extended Data 2	M	2WANOVA with Sidak's multiple comparisons test	**Muc17:** ANOVA Results: Interaction: 0.7158 Section: 0.3010 Group: 0.2726 **Multiple Comparisons:** Duodenum Naïve Feces to Stress Feces: 0.9879 Jejunum Naïve Feces to Stress Feces: 0.8759 Ileum Naïve Feces to Stress Feces: 0.9096 Colon Naïve Feces to Stress Feces: 0.7535	Standard Error Mean	7 animals per group	Representative of 1 experiment	Samples collected from distinct animals
Extended Data 3	A	Unpaired t-tests, two-tailed	**Muc2 RNA-Seq:** 0.8589	Standard Error Mean	3 animals per group	Representative of 1 independent experiments	Samples collected from distinct animals
Extended Data 3	B	Unpaired t-tests, two-tailed	**Muc4 RNA-Seq:** 0.0603	Standard Error Mean	3 animals per group	Representative of 1 independent experiments	Samples collected from distinct animals
Extended Data 3	C	Unpaired t-tests, two-tailed	**Muc6 RNA-Seq:** 0.4540	Standard Error Mean	3 animals per group	Representative of 1 independent experiments	Samples collected from distinct animals
Extended Data 3	D	2WANOVA with Sidak's multiple comparisons test	***Lgr5:*** ANOVA Results: Interaction: 0.1172 Section: <0.0001 (****) Group: 0.0005 (***) **Multiple Comparisons:** Duodenum Naïve to Stress: 0.8914 Jejunum Naïve to Stress: 0.9385 Ileum Naïve to Stress: 0.0010 Colon Naïve to Stress: 0.1623	Standard Error Mean	5 animals per group	Representative of 1 independent experiments	Samples collected from distinct animals
Extended Data 3	E	2WANOVA with Sidak's multiple comparisons test	***Hnf4a:*** ANOVA Results: Interaction: 0.8681 Section: 0.2734 Group: 0.0913 **Multiple Comparisons:** Duodenum Naïve Feces to Stress Feces: 0.9095 Jejunum Naïve Feces	Standard Error Mean	7 animals per group	Representative of 1 experiment	Samples collected from distinct animals

Figure	Panel	Test	P-value(s)	Error Bars	Sample Numbers	Replicate Numbers	Samples Taken from
			to Stress Feces: 0.9932 Ileum Naïve Feces to Stress Feces: 0.9011 Colon Naïve Feces to Stress Feces: 0.4283				
Extended Data 3	F	2WANOVA with Sidak's multiple comparisons test	***Hnf4g*:** ANOVA Results: Interaction: 0.6030 Section: <0.0001 (****) Group: 0.4134 **Multiple Comparisons:** Duodenum Naïve Feces to Stress Feces: 0.8864 Jejunum Naïve Feces to Stress Feces: 0.5946 Ileum Naïve Feces to Stress Feces: 0.9951 Colon Naïve Feces to Stress Feces: 0.9997	Standard Error Mean	7 animals per group	Representative of 1 experiment	Samples collected from distinct animals
Extended Data 3	G	Unpaired t-tests, two-tailed	***MUC13:*** Control to BI6015: <0.0001 (****)	Standard Error Mean	11 wells per group	3 Independent Experiments Combined	Samples collected from distinct wells
Extended Data 3	H	Unpaired t-tests, two-tailed	***LGR5:*** Control to BI6015: <0.0001 (****)	Standard Error Mean	11 wells per group	3 Independent Experiments Combined	Samples collected from distinct wells
Extended Data 4	A	Unpaired t-tests, two-tailed	***Tjp1:*** ANOVA Results: Interaction: 0.3821 Section: <0.0001 (****) Group: 0.0250 (*) **Multiple Comparisons:** Duodenum Muc13−/− to WT: 0.9963 Jejunum Muc13−/− to WT: 0.9973 Ileum Muc13−/− to WT: 0.0901 Colon Muc13−/− to WT: 0.3144	Standard Error Mean	12 animals per group	Representative of 1 independent experiments	Samples collected from distinct animals
Extended Data 4	B	Unpaired t-tests, two-tailed	***Ocln:*** ANOVA Results: Interaction: 0.3718 Section: <0.0001 (****) Group: 0.3844 **Multiple Comparisons:** Duodenum Muc13−/− to WT: 0.8950 Jejunum Muc13−/− to WTs: 0.8668 Ileum Muc13−/− to WT: 0.7340	Standard Error Mean	12 animals per group	Representative of 1 independent experiments	Samples collected from distinct animals

Figure	Panel	Test	P-value(s)	Error Bars	Sample Numbers	Replicate Numbers	Samples Taken from
			Colon Muc13−/− to WT: 0.6644				
Extended Data 4	B	Unpaired t-tests, two-tailed	**DeepLabCut Motif Analysis** Wildtype to Muc13−/− Rearing/Grooming 1: 0.9060 Wildtype to Muc13−/− Rearing/Grooming 2: 0.3644 Wildtype to Muc13−/− Rearing/Grooming 3: 0.8186 Wildtype to Muc13−/− Rearing/Grooming 4: 0.4812 Wildtype to Muc13−/− Rearing/Grooming 5: 0.2569 Wildtype to Muc13−/− Rearing/Grooming 6: 0.006 (**) Wildtype to Muc13−/− Rearing/Grooming 7: 0.0850 Wildtype to Muc13−/− Sitting/Sniffing 1: 0.3279 Wildtype to Muc13−/− Sitting/Sniffing 2: 0.8804 Wildtype to Muc13−/− Sitting/Sniffing 3: 0.4656 Wildtype to Muc13−/− Sitting/Sniffing 4: 0.1149 Wildtype to Muc13−/− Sitting/Sniffing 5: 0.0038 (**) Wildtype to Muc13−/− Turning 1: 0.1492 Wildtype to Muc13−/− Turning 2: 0.2971 Wildtype to Muc13−/− Turning 3: 0.0018 (**) Wildtype to Muc13−/− Turning 4: 0.0313 (*) Wildtype to Muc13−/− Turning 5: 0.6256 Wildtype to Muc13−/− Turning 6: 0.0652 Wildtype to Muc13−/− Turning 7: 0.6078 Wildtype to Muc13−/− Turning 8: 0.2135 Wildtype to Muc13−/− Turning 9: 0.2463 Wildtype to Muc13−/− Walking 1: 0.6618 Wildtype to Muc13−/− Walking 2: 0.4751 Wildtype to Muc13−/− Walking 3: 0.4861 Wildtype to Muc13−/− Walking 4: 0.8117	Standard Error Mean	12–13 animals per group	Representative of 3 independent experiments	Data collected from distinct animals, repeated measures from baseline to 1 wk

Extended Data Table 5

Table of qPCR probes used in manuscript.

Target	Probe Product/Sequence Information	Purchased From:
Gapdh	Taqman- Mm99999915_g1	ThermoFisher
Actin	Taqman- Mm02619580_g1	ThermoFisher
Muc1	Taqman- Mm00449604_m1	ThermoFisher
Muc2	Taqman- Mm01276696_m1	ThermoFisher
Muc3	Taqman- Mm01207064_m1	ThermoFisher
Muc4	Taqman- Mm00466866_m1	ThermoFisher
Muc13	Taqman- Mm00495397_m1	ThermoFisher
MUC2	F: 5’ CTGCTATGTCGAGGACACCC 3’	IDT
	R: 5’ GAGTTGGTACACACGCAGGA 3’	IDT
MUC4	F: 5’ CTTTTGTCCTCTTCCCAGGTTCC 3’	IDT
	R: 5’ CAGTGTGAGGAGCAGACGTGA 3’	IDT
MUC13	F: 5’ GGGAACTGCCAAAAGTGTGC 3’	IDT
	R: 5’ CTGAGAATGACAATGCCAGCG 3’	IDT
MUC17	F: 5’ GTTTCAACACCACTGGCACC 3’	IDT
	R: 5’ CTGGTCCCGGTACTCCACTA 3’	IDT
Tjp1	F: 5’ CCACCTCTGTCCAGCTCTTC 3’	IDT
	R: 5’ CACCGGAGTGATGGTTTTCT 3’	IDT
Ocln	F: 5’ CCTCCAATGGCAAAGTGAAT 3’	IDT
	R: 5’ CTCCCCACCTGTCGTGTAGT 3’	IDT

Extended Data Table 6

Table of mass over charge number (m/z) for analytes examined between naïve and stressed animals.

Analyte	Precursor m/z	Product m/z	RT
01_Dopamine	154.086	137.059	2.88
02_Norepinephrine	170.081	152.07	1.6
03_Serotonin	177.102	160.073	4.09
04_Kynurenic acid	190.05	162.055	8.05
05_Tryptophan	205.097	188.07	6.52
06_Kynurenin	209.092	94.065	4.73
07_Corticosterone	347.222	329.21	11.06
08_Aldosterone	361.201	343.189	10.8
09_Cortisol	363.217	327.194	10.93
10_Thyroxine	777.694	731.684	10.91
11_Glutamine	147.076	84.044	1.46

Supplementary Material

Refer to Web version on PubMed Central for supplementary material.

Acknowledgements

The mass spectrometry experiments in Fig. 1 were performed in the UVA Biomolecular Research Facility Core. The W.M. Keck Biomedical Mass Spectrometry Laboratory is funded by a grant from the University of Virginia's School of Medicine. Alexandria Battison provided additional technical assistance in intestinal tissue mass spectrometry experiments. The authors are supported by grants from the UVA Trans University Microbiome Initiative pilot grant, the Miller family, and the Owens Family Foundation. C.R.N is supported by the UVA Presidential Fellowship in Neuroscience. A.R.M. is supported by the NINDS T32 NS115657 and F31 AI174782. N.M.G is supported by the NIGMS T32 GM139787. Work from the R.O., K.V., and L.C. from the lab of M.V. was supported by NIH grants R01DK121915 and R01DK126446. A.D.S. is supported by the National Institutes of Health Chemical Biology Training Grant (T32 GM067543). K.E.M. is supported by the Yale Endowed Postdoctoral Fellowship in the Biological Sciences.

Data availability

The datasets supporting the conclusions of this article are available in the NCBI Gene Expression Omnibus repository accession number GSE112946 (RNA-seq and ChIP-seq) and GSE148691 (HiChIP-seq). 16S Raw sequencing reads can be found in the NCBI Sequence Read Archive (SRA) database under PRJNA867333. Mass spectrometry data is located at: https://www.metabolomicsworkbench.org under study ID: ST002345.

References

Atanasova KR, Reznikov LR, 2019. Strategies for measuring airway mucus and mucins. Respir. Res. 20 (1), 261. 10.1186/s12931-019-1239-z. [PubMed: 31752894]

Babeu JP, Boudreau F, 2014. Hepatocyte nuclear factor 4-alpha involvement in liver and intestinal inflammatory networks. World J. Gastroenterol. 20 (1), 22–30. 10.3748/wjg.v20.i1.22. Epub 2014/01/15. PubMed PMID: 24415854; PubMed Central PMCID: PMCPMC3886012. [PubMed: 24415854]

Baek JH, Jung S, Son H, Kang JS, Kim HJ, 2020. Glutamine supplementation prevents chronic stress-induced mild cognitive impairment. Nutrients 12 (4). 10.3390/nu12040910. Epub 20200326. PubMed PMID: 32224923; PubMed Central PMCID: PMCPMC7230523.

Bailey MT, Dowd SE, Galley JD, Hufnagle AR, Allen RG, Lyte M, 2011. Exposure to a social stressor alters the structure of the intestinal microbiota: implications for stressor-induced immunomodulation. Brain Behav. Immun. 25 (3), 397–407. 10.1016/j.bbi.2010.10.023. Epub 2010/11/03. PubMed PMID: 21040780; PubMed Central PMCID: PMC3039072. [PubMed: 21040780]

Bastiaanssen TFS, Cussotto S, Claesson MJ, Clarke G, Dinan TG, Cryan JF, 2020. Gutted! Unraveling the Role of the Microbiome in Major Depressive disorder. Harv. Rev. Psychiatry 28 (1), 26–39. 10.1097/HRP.0000000000000243. PubMed PMID: 31913980. [PubMed: 31913980]

Berding K, Cryan JF, 2022. Microbiota-targeted interventions for mental health. Curr Opin Psychiatry. 35 (1) 10.1097/yco.0000000000000758. Epub 2021/11/10. PubMed PMID: 34750307; PubMed Central PMCID: PMCPMC8654258 Neuropharmex, Yakult, and Alkermes, has been a consultant for Nestle, and has received research funding from Mead Johnson, Cremo, Nutricia, and DuPont. K.B. has been an invited speaker at a meeting organized by Yakult.

Bergstrom KS, Kissoon-Singh V, Gibson DL, Ma C, Montero M, Sham HP, et al. , 2010. Muc2 protects against lethal infectious colitis by disassociating pathogenic and commensal bacteria from the colonic mucosa. PLoS pathogens 6 (5), e1000902. 10.1371/journal.ppat.1000902. Epub 2010/05/21. PubMed PMID: 20485566; PubMed Central PMCID: PMCPMC2869315.

Bergstrom K, Shan X, Casero D, Batushansky A, Lagishetty V, Jacobs JP, et al. , 2020. Proximal colon–derived O-glycosylated mucus encapsulates and modulates the microbiota. Science (New York, N.Y.) 370 (6515), 467–472. 10.1126/science.aay7367. [PubMed: 33093110]

Biol-N'garagba M-C, Niepceron E, Mathian B, Louisot P, 2003. Glucocorticoid-induced maturation of glycoprotein galactosylation and fucosylation processes in the rat small intestine. J. Steroid Biochem. Mol. Biol. 84 (4), 411–422. 10.1016/S0960-0760(03)00062-1. [PubMed: 12732286]

Borisova MA, Achasova KM, Morozova KN, Andreyeva EN, Litvinova EA, Ogienko AA, et al. , 2020. Mucin-2 knockout is a model of intercellular junction defects, mitochondrial damage and ATP depletion in the intestinal epithelium. Sci. Rep. 10 (1), 21135. 10.1038/s41598-020-78141-4. Epub 2020/12/05. PubMed PMID: 33273633; PubMed Central PMCID: PMCPMC7713437. [PubMed: 33273633]

Cairns MT, Gupta A, Naughton JA, Kane M, Clyne M, Joshi L, 2017. Glycosylation-related gene expression in HT29-MTX-E12 cells upon infection by Helicobacter pylori. World J. Gastroenterol. 23 (37), 6817–6832. 10.3748/wjg.v23.i37.6817. PubMed PMID: 29085225. [PubMed: 29085225]

Callahan BJ, McMurdie PJ, Rosen MJ, Han AW, Johnson AJ, Holmes SP, 2016. DADA2: High-resolution sample inference from Illumina amplicon data. Nat. Methods 13 (7), 581–583. 10.1038/nmeth.3869. Epub 2016/05/24. PubMed PMID: 27214047; PubMed Central PMCID: PMCPMC4927377. [PubMed: 27214047]

Carraway KL, 2000. Preparation of membrane mucin. In: Corfield AP (Ed.), Glycoprotein Methods and Protocols: the Mucins. Humana Press, Totowa, NJ, pp. 15–26.

Chahar S, Gandhi V, Yu S, Desai K, Cowper-Sal-lari R, Kim Y, et al. , 2014. Chromatin profiling reveals regulatory network shifts and a protective role for hepatocyte nuclear factor 4α during colitis. Mol. Cell Biol. 34 (17), 3291–3304. 10.1128/mcb.00349-14. Epub 2014/07/02. PubMed PMID: 24980432; PubMed Central PMCID: PMCPMC4135557. [PubMed: 24980432]

Chen L, Toke NH, Luo S, Vasoya RP, Fullem RL, Parthasarathy A, et al. , 2019. A reinforcing HNF4-SMAD4 feed-forward module stabilizes enterocyte identity. Nat. Genet. 51 (5), 777–785. 10.1038/s41588-019-0384-0. Epub 2019/04/17. PubMed PMID: 30988513; PubMed Central PMCID: PMCPMC6650150. [PubMed: 30988513]

Chen L, Vasoya RP, Toke NH, Parthasarathy A, Luo S, Chiles E, et al. , 2020. HNF4 regulates fatty acid oxidation and is required for renewal of intestinal stem cells in mice. Gastroenterology 158 (4), 985–999.e9. 10.1053/j.gastro.2019.11.031. Epub 2019/11/25. PubMed PMID: 31759926; PubMed Central PMCID: PMCPMC7062567. [PubMed: 31759926]

Chen L, Luo S, Dupre A, Vasoya RP, Parthasarathy A, Aita R, et al. , 2021. The nuclear receptor HNF4 drives a brush border gene program conserved across murine intestine, kidney, and embryonic yolk sac. Nat. Commun. 12 (1), 2886. 10.1038/s41467-021-22761-5. [PubMed: 34001900]

Chen L, Cao W, Aita R, Aldea D, Flores J, Gao N, et al. , 2021. Three-dimensional interactions between enhancers and promoters during intestinal differentiation depend upon HNF4. Cell Rep. 34 (4) 10.1016/j.celrep.2020.108679.

Concordet J-P, Haeussler M, 2018. CRISPOR: intuitive guide selection for CRISPR/Cas9 genome editing experiments and screens. Nucleic Acids Res. 46 (W1), W242–W245. 10.1093/nar/gky354. [PubMed: 29762716]

Darsigny M, Babeu J-P, Seidman EG, Gendron F-P, Levy E, Carrier J, et al. , 2010. Hepatocyte nuclear factor-4α promotes gut neoplasia in mice and protects against the production of reactive oxygen species. Cancer Res. 70 (22), 9423–9433. 10.1158/0008-5472.Can-10-1697. [PubMed: 21062980]

Dodiya HB, Forsyth CB, Voigt RM, Engen PA, Patel J, Shaikh M, et al. , 2020. Chronic stress-induced gut dysfunction exacerbates Parkinson's disease phenotype and pathology in a rotenone-induced mouse model of Parkinson's disease. Neurobiol. Dis. 135 10.1016/j.nbd.2018.12.012. Epub 2018/12/24. PubMed PMID: 30579705.

Duncan K, Carey-Ewend K, Vaishnava S, 2021. Spatial analysis of gut microbiome reveals a distinct ecological niche associated with the mucus layer. Gut Microbes 1–21. 10.1080/19490976.2021.1874815. Epub 2021/02/12. PubMed PMID: 33567985.

Dunn EC, Sofer T, Wang M-J, Soare TW, Gallo LC, Gogarten SM, et al. , 2018. Genome-wide association study of depressive symptoms in the Hispanic Community Health Study/Study of Latinos. J. Psychiatric Res. 99, 167–176. 10.1016/j.jpsychires.2017.12.010. Epub 2017/12/16. PubMed PMID: 29505938.

Fava M, 2003. Diagnosis and definition of treatment-resistant depression. Biol. Psychiatry 53 (8), 649–659. 10.1016/S0006-3223(03)00231-2. [PubMed: 12706951]

Foster JA, McVey Neufeld KA, 2013. Gut-brain axis: how the microbiome influences anxiety and depression. Trends Neurosci. 36 (5), 305–312. 10.1016/j.tins.2013.01.005. Epub 2013/02/07. PubMed PMID: 23384445. [PubMed: 23384445]

Fu J, Wei B, Wen T, Johansson ME, Liu X, Bradford E, et al. , 2011. Loss of intestinal core 1-derived O-glycans causes spontaneous colitis in mice. J. Clin. Invest. 121 (4), 1657–1666. 10.1172/jci45538. Epub 2011/03/09. PubMed PMID: 21383503; PubMed Central PMCID: PMCPMC3069788. [PubMed: 21383503]

Gamage HKAH, Chong RWW, Bucio-Noble D, Kautto L, Hardikar AA, Ball MS, et al. , 2020. Changes in dietary fiber intake in mice reveal associations between colonic mucin O-glycosylation and specific gut bacteria. Gut Microbes 12 (1), 1802209. 10.1080/19490976.2020.1802209.

Gao X, Cao Q, Cheng Y, Zhao D, Wang Z, Yang H, et al. , 2018. Chronic stress promotes colitis by disturbing the gut microbiota and triggering immune system response. Proc. Natl. Acad. Sci. 115 (13), E2960–E2969. 10.1073/pnas.1720696115. [PubMed: 29531080]

Gong S, Miao Y-L, Jiao G-Z, Sun M-J, Li H, Lin J, et al. , 2015. Dynamics and correlation of serum cortisol and corticosterone under different physiological or stressful conditions in mice. PLoS One 10 (2), e0117503-e. 10.1371/journal.pone.0117503.PubMed PMID: 25699675.

Gourley SL, Wu FJ, Taylor JR, 2008. Corticosterone regulates pERK1/2 map kinase in a chronic depression model. Ann. N. Y. Acad. Sci. 1148 (1), 509–514. 10.1196/annals.1410.076. [PubMed: 19120149]

Gupta BK, Maher DM, Ebeling MC, Stephenson PD, Puumala SE, Koch MR, et al. , 2014. Functions and regulation of MUC13 mucin in colon cancer cells. J. Gastroenterol. 49 (10), 1378. 10.1007/s00535-013-0885-z. Epub 2013/10/07. PubMed PMID: 24097071. [PubMed: 24097071]

Gurumurthy CB, Sato M, Nakamura A, Inui M, Kawano N, Islam MA, et al. , 2019. Creation of CRISPR-based germline-genome-engineered mice without ex vivo handling of zygotes by i-GONAD. Nat. Protoc. 14 (8), 2452–2482. 10.1038/s41596-019-0187-x. [PubMed: 31341289]

Hadley Wickham MA, Bryan J, Cheng W, D'Agostino L, François R, Grolemund G, Hayes A, Henry L, Kuhn M, Lin Pedersen T, 2019. Welcome to the Tidyverse. J. Open Source Softw. 4(43), 1686. doi: 10.21105/joss.01686.

Hansson GC, 2020. Mucins and the microbiome. Annu. Rev. Biochem 89 (1), 769–793. 10.1146/annurev-biochem-011520-105053. PubMed PMID: 32243763. [PubMed: 32243763]

Harrop CA, Thornton DJ, McGuckin MA, 2012. Detecting, visualising, and quantifying mucins. In: McGuckin MA, Thornton DJ (Eds.), Mucins: Methods and Protocols. Humana Press, Totowa, NJ, pp. 49–66.

He R, Zheng R, Zheng J, Li M, Wang T, Zhao Z, et al. , 2023. Causal association between obesity, circulating glutamine levels, and depression: a Mendelian randomization study. J. Clin. Endocrinol. Metab. 108 (6), 1432–1441. 10.1210/clinem/dgac707. PubMed PMID: 36510667; PubMed Central PMCID: PMCPMC10188313. [PubMed: 36510667]

Heim C, Binder EB, 2012. Current research trends in early life stress and depression: review of human studies on sensitive periods, gene–environment interactions, and epigenetics. Exp. Neurol. 233 (1), 102–111. 10.1016/j.expneurol.2011.10.032. [PubMed: 22101006]

Henwood AF, 2017. Hematoxylin and eosin staining of mucins of the gastrointestinal tract. J. Histotechnol. 40 (1), 21–24. 10.1080/01478885.2017.1264556.

Herath M, Hosie S, Bornstein JC, Franks AE, Hill-Yardin EL, 2020. The role of the gastrointestinal mucus system in intestinal homeostasis: implications for neurological disorders. Front. Cell. Infect. Microbiol. 10 (248) 10.3389/fcimb.2020.00248.

Israelyan N, Del Colle A, Li Z, Park Y, Xing A, Jacobsen JPR, et al. , 2019. Effects of serotonin and slow-release 5-HTP on gastrointestinal motility in a mouse model of depression. Gastroenterology. 10.1053/j.gastro.2019.04.022. Epub 2019/05/10. PubMed PMID: 31071306.

Jari Oksanen FGB, Friendly M, Kindt R, Legendre P, McGlinn D, Peter R, Minchin RBOH, Simpson GL, Solymos P, Stevens MHH, Szoecs E, Wagner H, 2020. vegan: Community Ecology Package. R package version 2.5–7. https://CRAN.R-project.org/package=vegan.

Johansson ME, Jakobsson HE, Holmén-Larsson J, Schütte A, Ermund A, Rodríguez-Piñeiro AM, et al. , 2015. Normalization of host intestinal mucus layers requires long-term microbial colonization. Cell Host Microbe. 18 (5), 582–592. 10.1016/j.chom.2015.10.007. Epub 2015/11/04. PubMed PMID: 26526499; PubMed Central PMCID: PMCPMC4648652. [PubMed: 26526499]

Johansson MEV, Phillipson M, Petersson J, Velcich A, Holm L, Hansson GC, 2008. The inner of the two Muc2 mucin-dependent mucus layers in colon is devoid of bacteria. Proc. Natl. Acad. Sci. 105 (39), 15064–15069. 10.1073/pnas.0803124105. [PubMed: 18806221]

Johansson MEV, Ambort D, Pelaseyed T, Schütte A, Gustafsson JK, Ermund A, et al. , 2011. Composition and functional role of the mucus layers in the intestine. Cell. Mol. Life Sci. 68 (22), 3635. 10.1007/s00018-011-0822-3. [PubMed: 21947475]

Johansson ME, Thomsson KA, Hansson GC, 2009. Proteomic analyses of the two mucus layers of the colon barrier reveal that their main component, the Muc2 mucin, is strongly bound to the Fcgbp protein. J. Proteome Res. 8 (7), 3549–3557. 10.1021/pr9002504. Epub 2009/05/13. PubMed PMID: 19432394. [PubMed: 19432394]

Johansson MEVaH GC The Mucins 2016.

Karl JP, Margolis LM, Madslien EH, Murphy NE, Castellani JW, Gundersen Y, et al. , 2017. Changes in intestinal microbiota composition and metabolism coincide with increased intestinal permeability in young adults under prolonged physiological stress. Am. J. Physiol. Gastrointestinal Liver Physiol. 312 (6), G559–G571. 10.1152/ajpgi.00066.2017. Epub 2017/03/25. PubMed PMID: 28336545.

Kent WJ, Sugnet CW, Furey TS, Roskin KM, Pringle TH, Zahler AM, et al. , 2002. The human genome browser at UCSC. Genome Res. 12 (6), 996–1006. 10.1101/gr.229102. Epub 2002/06/05. PubMed PMID: 12045153; PubMed Central PMCID: PMCPMC186604. [PubMed: 12045153]

Kesimer M, Sheehan JK, 2012. Mass spectrometric analysis of mucin core proteins. Methods Mol. Biol. 842, 67–79. 10.1007/978-1-61779-513-8_4. PubMed PMID: 22259130; PubMed Central PMCID: PMCPMC5151179.

Kiselyuk A, Lee SH, Farber-Katz S, Zhang M, Athavankar S, Cohen T, et al. , 2012. HNF4α antagonists discovered by a high-throughput screen for modulators of the human insulin promoter. Chem. Biol. 19 (7), 806–818. 10.1016/j.chembiol.2012.05.014. Epub 2012/07/31. PubMed PMID: 22840769; PubMed Central PMCID: PMCPMC3447631. [PubMed: 22840769]

Kozich JJ, Westcott SL, Baxter NT, Highlander SK, Schloss PD, 2013. Development of a dual-index sequencing strategy and curation pipeline for analyzing amplicon sequence data on the MiSeq Illumina sequencing platform. Appl. Environ. Microbiol. 79 (17), 5112–5120. 10.1128/aem.01043-13. Epub 2013/06/25. PubMed PMID: 23793624; PubMed Central PMCID: PMCPMC3753973. [PubMed: 23793624]

Kudelka MR, Stowell SR, Cummings RD, Neish AS, 2020. Intestinal epithelial glycosylation in homeostasis and gut microbiota interactions in IBD. Nat. Rev. Gastroenterol. Hepatol. 17 (10), 597–617. 10.1038/s41575-020-0331-7. Epub 2020/07/28. PubMed PMID: 32710014. [PubMed: 32710014]

Kuhn M, 2021 caret: Classification and Regression Training. R package version 60–90.

Lach G, Schellekens H, Dinan TG, Cryan JF, 2018. Anxiety, Depression, and the microbiome: a role for gut peptides. Neurotherapeutics: J. Am. Soc. Exp. NeuroTherapeutics 15 (1), 36–59. 10.1007/s13311-017-0585-0. Epub 2017/11/15. PubMed PMID: 29134359; PubMed Central PMCID: PMCPMC5794698.

Lee SH, Veeriah V, Levine F, 2022. A potent HNF4α agonist reveals that HNF4α controls genes important in inflammatory bowel disease and Paneth cells. PloS One 17 (4), e0266066. 10.1371/journal.pone.0266066. Epub 2022/04/07. PubMed PMID: 35385524; PubMed Central PMCID: PMCPMC8985954 following competing interests: FL holds equity in Brightseed.

Leo Lahti FGME, Shetty S, Borman T, Braccia DJ, Huang R, Bravo HC Microbiome R package. http://microbiome.github.io.

Li N, Wang Q, Wang Y, Sun A, Lin Y, Jin Y, et al. , 2019. Fecal microbiota transplantation from chronic unpredictable mild stress mice donors affects anxiety-like and depression-like behavior in recipient mice via the gut microbiota-inflammation-brain axis. Stress 22 (5), 592–602. 10.1080/10253890.2019.1617267. Epub 2019/05/28. PubMed PMID: 31124390. [PubMed: 31124390]

Liaw AWM Classification and regression by randomForest R news 22002.

Lickwar CR, Davison JM, Kelly C, Mercado GP, Wen J, Davis BR, et al. , 2022. Transcriptional integration of distinct microbial and nutritional signals by the small intestinal epithelium. Cell. Mol. Gastroenterol. Hepatol. 14 (2), 465–493. 10.1016/j.jcmgh.2022.04.013. [PubMed: 35533983]

Lu H, Lei X, Winkler R, John S, Kumar D, Li W, et al. , 2022. Crosstalk of hepatocyte nuclear factor 4a and glucocorticoid receptor in the regulation of lipid metabolism in mice fed a high-fat-high-sugar diet. Lipids Health Dis. 21 (1), 46. 10.1186/s12944-022-01654-6. [PubMed: 35614477]

Luo Y, Zeng B, Zeng L, Du X, Li B, Huo R, et al. , 2018. Gut microbiota regulates mouse behaviors through glucocorticoid receptor pathway genes in the hippocampus. Transl. Psychiatry. 8 (1), 187. 10.1038/s41398-018-0240-5. Epub 2018/09/09. PubMed PMID: 30194287; PubMed Central PMCID: PMCPMC6128920. [PubMed: 30194287]

Luxem K, Fuhrmann F, Kürsch J, Remy S, Bauer P, 2020. Identifying Behavioral Structure from Deep Variational Embeddings of Animal Motion. bioRxiv. 2020: 2020.05.14.095430. doi: 10.1101/2020.05.14.095430.

Malaker SA, Pedram K, Ferracane MJ, Bensing BA, Krishnan V, Pett C, et al. , 2019. The mucin-selective protease StcE enables molecular and functional analysis of human cancer-associated mucins. Proc. Natl. Acad. Sci. 116 (15), 7278–7287. 10.1073/pnas.1813020116. [PubMed: 30910957]

Malaker SA, Riley NM, Shon DJ, Pedram K, Krishnan V, Dorigo O, et al. , 2022. Revealing the human mucinome. Nat. Commun. 13 (1), 3542. 10.1038/s41467-022-31062-4. [PubMed: 35725833]

Marczynski M, Jiang K, Blakeley M, Srivastava V, Vilaplana F, Crouzier T, et al. , 2021. Structural alterations of mucins are associated with losses in functionality. Biomacromolecules. 10.1021/acs.biomac.1c00073. Epub 2021/03/ 23. PubMed PMID: 33749252.

Marin IA, Goertz JE, Ren T, Rich SS, Onengut-Gumuscu S, Farber E, et al. , 2017. Microbiota alteration is associated with the development of stress-induced despair behavior. Sci. Rep. 7, 43859 10.1038/srep43859. PubMed PMID: 28266612. [PubMed: 28266612]

Mathis A, Mamidanna P, Cury KM, Abe T, Murthy VN, Mathis MW, et al. , 2018. DeepLabCut: markerless pose estimation of user-defined body parts with deep learning. Nat. Neurosci. 21 (9), 1281–1289. 10.1038/s41593-018-0209-y. [PubMed: 30127430]

McClain LL, Shaw P, Sabol R, Chedia AM, Segretti AM, Rengasamy M, et al. , 2020. Rare variants and biological pathways identified in treatment-refractory depression. J. Neurosci. Res. 98 (7), 1322–1334. 10.1002/jnr.24609. Epub 2020/03/05. PubMed PMID: 32128872. [PubMed: 32128872]

McGonagle KA, Kessler RC, 1990. Chronic stress, acute stress, and depressive symptoms. Am. J. Commun. Psychol. 18 (5), 681–706. 10.1007/BF00931237.

McMurdie PJ, Holmes S, 2013. phyloseq: an R package for reproducible Interactive analysis and graphics of microbiome census data. PLoS One 8 (4), e61217. 10.1371/journal.pone.0061217.

Merchak AR, Wachamo S, Brown LC, Thakur A, Moreau B, Brown RM, et al. , 2024. Lactobacillus from the altered schaedler Flora maintain IFNγ homeostasis to promote behavioral stress resilience. Brain Behav. Immun. 115, 458–469. 10.1016/j.bbi.2023.11.001. [PubMed: 37924959]

Mineur YS, Belzung C, Crusio WE, 2006. Effects of unpredictable chronic mild stress on anxiety and depression-like behavior in mice. Behav. Brain Res. 175 (1), 43–50. 10.1016/j.bbr.2006.07.029. Epub 2006/10/07. PubMed PMID: 17023061. [PubMed: 17023061]

Moncrieff J, Cooper RE, Stockmann T, Amendola S, Hengartner MP, Horowitz MA, 2023. The serotonin theory of depression: a systematic umbrella review of the evidence. Mol. Psychiatry 28 (8), 3243–3256. 10.1038/s41380-022-01661-0. [PubMed: 35854107]

Nollet M, Guisquet A-M-L, Belzung C, 2013. Models of depression: unpredictable chronic mild stress in mice, 5.65.1–5.17 Curr. Protocols Pharmacol. 61 (1). 10.1002/0471141755.ph0565s61.

Ohtsuka M, Sato M, Miura H, Takabayashi S, Matsuyama M, Koyano T, et al. , 2018. i-GONAD: a robust method for in situ germline genome engineering using CRISPR nucleases. Genome Biol. 19 (1), 25. 10.1186/s13059-018-1400-x. [PubMed: 29482575]

Park S-Y, Rao C, Coyte KZ, Kuziel GA, Zhang Y, Huang W, et al. , 2022. Strain-level fitness in the gut microbiome is an emergent property of glycans and a single metabolite. Cell 185 (3), 513–529.e21. 10.1016/j.cell.2022.01.002. [PubMed: 35120663]

Pelaseyed T, Hansson GC, 2020. Membrane mucins of the intestine at a glance. J. Cell Sci. 10.1242/jcs.240929.

Peng Y-L, Liu Y-N, Liu L, Wang X, Jiang C-L, Wang Y-X, 2012. Inducible nitric oxide synthase is involved in the modulation of depressive behaviors induced by unpredictable chronic mild stress. J. Neuroinflammation 9 (1), 75. 10.1186/1742-2094-9-75. [PubMed: 22531370]

Pfleiderer B, Michael N, Erfurth A, Ohrmann P, Hohmann U, Wolgast M, et al. , 2003. Effective electroconvulsive therapy reverses glutamate/glutamine deficit in the left anterior cingulum of unipolar depressed patients. Psychiatry Res. Neuroimaging 122 (3), 185–192. 10.1016/S0925-4927(03)00003-9.

Pothion S, Bizot J-C, Trovero F, Belzung C, 2004. Strain differences in sucrose preference and in the consequences of unpredictable chronic mild stress. Behav. Brain Res. 155 (1), 135–146. 10.1016/j.bbr.2004.04.008. [PubMed: 15325787]

Quast C, Pruesse E, Yilmaz P, Gerken J, Schweer T, Yarza P, et al. , 2013. The SILVA ribosomal RNA gene database project: improved data processing and web-based tools. Nucleic Acids Res. 41 (Database issue), D590–D596. 10.1093/nar/gks1219. PubMed PMID: 23193283; PubMed Central PMCID: PMCPMC3531112. [PubMed: 23193283]

Rivet-Noor C, Gaultier A, 2020. The role of gut mucins in the etiology of depression. Front. Behav. Neurosci. 14, 592388 10.3389/fnbeh.2020.592388. Epub 2020/12/01. PubMed PMID: ; PubMed Central PMCID: PMCPMC7674283. [PubMed: 33250724]

Rivet-Noor CR, Merchak AR, Li S, Beiter RM, Lee S, Thomas JA, et al. , 2022. Stress-induced despair behavior develops independently of the Ahr-RORγt axis in CD4 + cells. Sci. Rep. 12 (1), 8594. 10.1038/s41598-022-12464-2. [PubMed: 35597802]

Robin X, Turck N, Hainard A, Tiberti N, Lisacek F, Sanchez J-C, et al. , 2011. pROC: an open-source package for R and S+ to analyze and compare ROC curves. BMC Bioinf. 12 (1), 77. 10.1186/1471-2105-12-77.

Santomauro DF, Mantilla Herrera AM, Shadid J, Zheng P, Ashbaugh C, Pigott DM, et al. , 2021. Global prevalence and burden of depressive and anxiety disorders in 204 countries and territories in 2020 due to the COVID-19 pandemic. Lancet 398 (10312), 1700–1712. 10.1016/S0140-6736(21)02143-7. [PubMed: 34634250]

Schneider H, Pelaseyed T, Svensson F, Johansson MEV, 2018. Study of mucin turnover in the small intestine by in vivo labeling. Sci. Rep. 8 (1), 5760. 10.1038/s41598-018-24148-x. [PubMed: 29636525]

Sheng YH, Triyana S, Wang R, Das I, Gerloff K, Florin TH, et al. , 2013. MUC1 and MUC13 differentially regulate epithelial inflammation in response to inflammatory and infectious stimuli. Mucosal Immunol. 6 (3), 557–568. 10.1038/mi.2012.98. [PubMed: 23149663]

Shurer CR, Kuo J-C-H, Roberts LM, Gandhi JG, Colville MJ, Enoki TA, et al. , 2019. Physical principles of membrane shape regulation by the glycocalyx. Cell 177 (7), 1757–1770.e21. 10.1016/j.cell.2019.04.017. [PubMed: 31056282]

Sicard J-F, Le Bihan G, Vogeleer P, Jacques M, Harel J, 2017. Interactions of intestinal bacteria with components of the intestinal mucus. Front. Cell. Infect. Microbiol. 7, 387 10.3389/fcimb.2017.00387. PubMed PMID: 28929087. [PubMed: 28929087]

Silva SD, Robbe-Masselot C, Ait-Belgnaoui A, Mancuso A, Mercade-Loubière M, Salvador-Cartier C, et al. , 2014. Stress disrupts intestinal mucus barrier in rats via mucin O-glycosylation shift: prevention by a probiotic treatment. Am. J. Physiol.-Gastrointestinal Liver Physiol. 307 (4), G420–G429. 10.1152/ajpgi.00290.2013. PubMed PMID: 24970779.

Sommer F, Adam N, Johansson MEV, Xia L, Hansson GC, Backhed F, 2014. ¨ Altered mucus glycosylation in Core 1 O-glycan-deficient mice affects microbiota composition and intestinal architecture. PLoS One 9 (1), e85254. 10.1371/journal.pone.0085254.

Suez J, Zmora N, Zilberman-Schapira G, Mor U, Dori-Bachash M, Bashiardes S, et al. , 2018. Post-antibiotic gut mucosal microbiome reconstitution is impaired by probiotics and improved by autologous FMT. Cell 174 (6), 1406–1423.e16. 10.1016/j.cell.2018.08.047. PubMed PMID: 30193113. [PubMed: 30193113]

Team RC, 2021. R: A language and environment for statistical computing. R Foundation for Statistical Computing. https://www.R-project.org/.

Tian P, Chen Y, Zhu H, Wang L, Qian X, Zou R, et al. , 2022. Bifidobacterium breve CCFM1025 attenuates major depression disorder via regulating gut microbiome and tryptophan metabolism: a randomized clinical trial. Brain Behav. Immun. 100, 233–241. 10.1016/j.bbi.2021.11.023. [PubMed: 34875345]

Tian E, Syed ZA, Edin ML, Zeldin DC, Ten Hagen KG, 2023. Dynamic expression of mucins and the genes controlling mucin-type O-glycosylation within the mouse respiratory system. Glycobiology 33 (6), 476–489. 10.1093/glycob/cwad031. [PubMed: 37115803]

Tyanova S, Temu T, Cox J, 2016. The MaxQuant computational platform for mass spectrometry-based shotgun proteomics. Nat. Protoc. 11 (12), 2301–2319. 10.1038/nprot.2016.136. [PubMed: 27809316]

Vahid-Ansari F, Albert PR, 2021. Rewiring of the serotonin system in major depression. Front. Psychiatry 12, 802581. 10.3389/fpsyt.2021.802581. Epub 20211216. PubMed PMID: 34975594; PubMed Central PMCID: PMCPMC8716791.

Valles-Colomer M, Falony G, Darzi Y, Tigchelaar EF, Wang J, Tito RY, et al. , 2019. The neuroactive potential of the human gut microbiota in quality of life and depression. Nat. Microbiol. 4 (4), 623–632. 10.1038/s41564-018-0337-x. [PubMed: 30718848]

Van der Sluis M, De Koning BAE, De Bruijn ACJM, Velcich A, Meijerink JPP, Van Goudoever JB, et al. , 2006. Muc2-deficient mice spontaneously develop colitis, indicating that MUC2 is critical for colonic protection. Gastroenterology 131 (1), 117–129. 10.1053/j.gastro.2006.04.020. [PubMed: 16831596]

Van Herreweghen F, De Paepe K, Marzorati M, Van de Wiele T, 2020. Mucin as a functional niche is a more important driver of in vitro gut microbiota composition and functionality than supplementation of akkermansia muciniphila. Appl. Environ. Microbiol. 87 (4) 10.1128/aem.02647. Epub 2020/12/06. PubMed PMID: 33277271; PubMed Central PMCID: PMCPMC7851700.

van Putten JPM, Strijbis K, 2017. transmembrane mucins: signaling receptors at the intersection of inflammation and cancer. J. Innate Immun. 9 (3), 281–299. 10.1159/000453594. Epub 2017/01/05. PubMed PMID: 28052300; PubMed Central PMCID: PMCPMC5516414. [PubMed: 28052300]

Velcich A, Yang W, Heyer J, Fragale A, Nicholas C, Viani S, et al. , 2002. Colorectal cancer in mice genetically deficient in the mucin Muc2. Science. 295 (5560), 1726–1729. 10.1126/science.1069094. Epub 2002/03/02. PubMed PMID: 11872843. [PubMed: 11872843]

Vető B, Bojcsuk D, Bacquet C, Kiss J, Sipeki S, Martin L, et al. , 2017. The transcriptional activity of hepatocyte nuclear factor 4 alpha is inhibited via phosphorylation by ERK1/2. PLoS One 12 (2), e0172020. 10.1371/journal.pone.0172020.

Ware EB, Mukherjee B, Sun YV, Diez-Roux AV, Kardia SLR, Smith JA, 2015. Comparative genome-wide association studies of a depressive symptom phenotype in a repeated measures setting by race/ethnicity in the multi-ethnic study of atherosclerosis. BMC Genet. 16 (1), 118. 10.1186/s12863-015-0274-0. [PubMed: 26459564]

Werlang C, Cárcarmo-Oyarce G, Ribbeck K, 2019. Engineering mucus to study and influence the microbiome. Nat. Rev. Mater. 4 (2), 134–145. 10.1038/s41578-018-0079-7.

Wheeler KM, Carcamo-Oyarce G, Turner BS, Dellos-Nolan S, Co JY, Lehoux S, et al. , 2019. Mucin glycans attenuate the virulence of Pseudomonas aeruginosa in infection. Nat. Microbiol. 10.1038/s41564-019-0581-8. Epub 2019/10/16. PubMed PMID: 31611643.

Wickham H, 2016. ggplot2: Elegant Graphics for Data Analysis. Springer-Verlag, New York.

Wu M, Wu Y, Li J, Bao Y, Guo Y, Yang W, 2018. The dynamic changes of gut microbiota in Muc2 deficient mice. Int. J. Mol. Sci. 19 (9) 10.3390/ijms19092809. Epub 2018/09/21. PubMed PMID: 30231491; PubMed Central PMCID: PMCPMC6164417.

Xu S, Liu Y, Pu J, Gui S, Zhong X, Tian L, et al. , 2020. Chronic stress in a rat model of depression disturbs the glutamine-glutamate-GABA cycle in the striatum, hippocampus, and cerebellum. Neuropsychiatr Dis Treat. 16, 557–570. 10.2147/ndt.S245282. Epub 20200224. PubMed PMID: 32158215; PubMed Central PMCID: PMCPMC7047974. [PubMed: 32158215]

Yang C-H, Huang C-C, Hsu K-S, 2004. Behavioral stress modifies hippocampal synaptic plasticity through corticosterone-induced sustained extracellular signal-regulated kinase/mitogen-activated

protein kinase activation. J. Neurosci. 24 (49), 11029–11034. 10.1523/jneurosci.3968-04.2004. [PubMed: 15590919]

Yu J, Yin P, Yin J, Liu F, Zhu X, Cheng G, et al. , 2010. Involvement of ERK1/2 signalling and growth-related molecules' expression in response to heat stress-induced damage in rat jejunum and IEC-6 cells. Int. J. Hyperth. 26 (6), 538–555. 10.3109/02656736.2010.481276.

Zmora N, Zilberman-Schapira G, Suez J, Mor U, Dori-Bachash M, Bashiardes S, et al. , 2018. Personalized gut mucosal colonization resistance to empiric probiotics is associated with unique host and microbiome features. Cell 174 (6), 1388–1405.e21. 10.1016/j.cell.2018.08.041. [PubMed: 30193112]

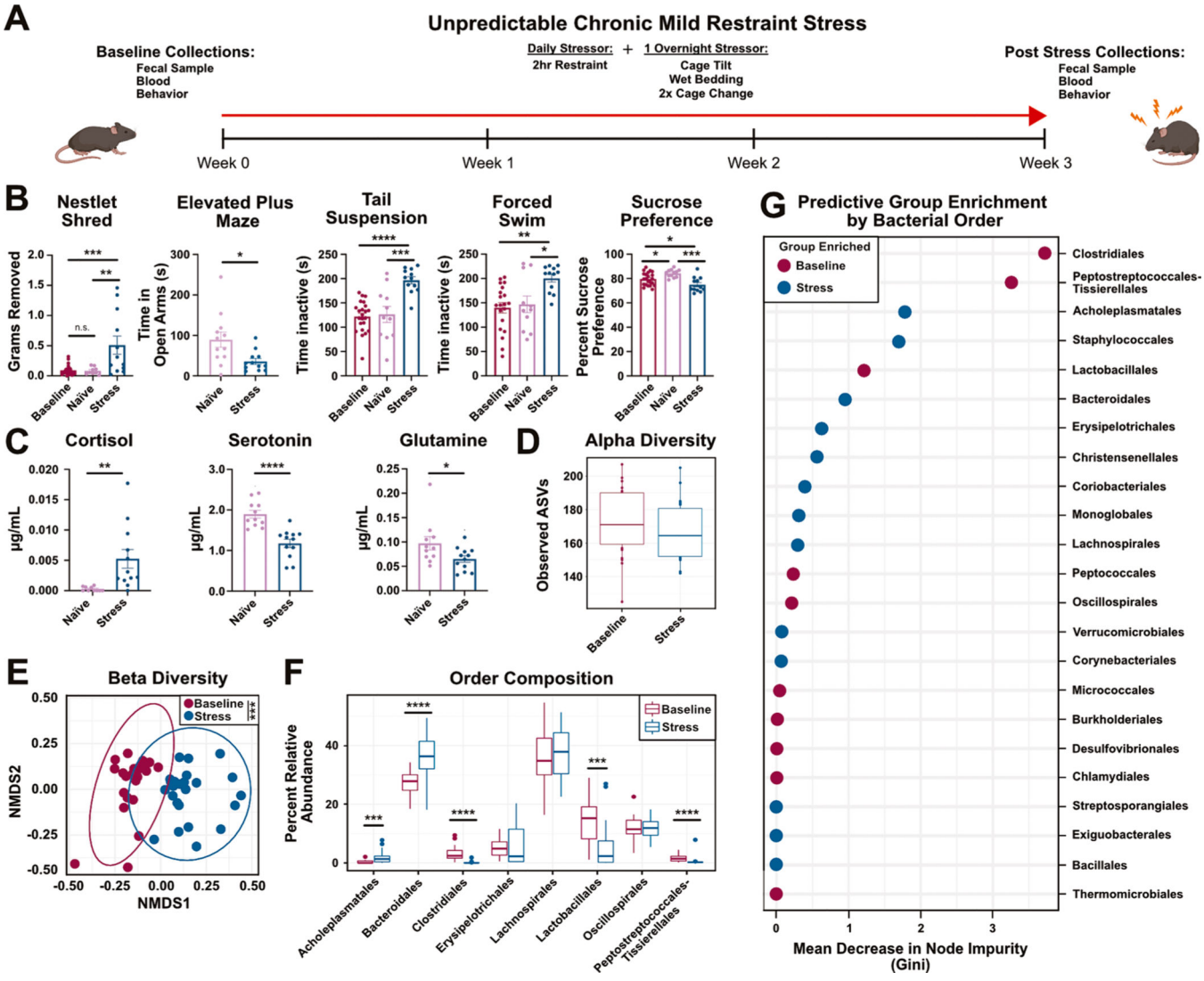

Fig. 1.

Unpredictable chronic mild restraint stress induces despair and anxiety-like behaviors and microbiome dysbiosis: (A) Experimental design. (B) Nestlet shred (One-way ANOVA), elevated plus maze (*t*-test), tail suspension (One-way ANOVA), forced swim (One-way ANOVA), and sucrose preference (One-way ANOVA) tests between baseline, naïve controls, and stress animals. Male mice, n = 11/12 per group, representative of N = 2. (C) Targeted mass spectrometry from serum of naïve or stress animals (t-tests, n = 11/12 per group). (D) Alpha diversity plot showing microbial richness (observed ASVs) between baseline and stress mice (Wilcoxon Rank Sum test). (E) NMDS plot of Bray-Curtis dissimilarity between baseline and stress fecal microbiome samples (PERMANOVA). (F) Relative abundances of bacterial orders > 1 % (Wilcoxon Rank Sum test with Bonferroni correction). (G) Importance plot from a random forest model predicting bacterial orders that discriminate between baseline and stress groups. Importance is based on the Gini index where larger values are more important to model. Male mice, n = 24/group, N = 1.

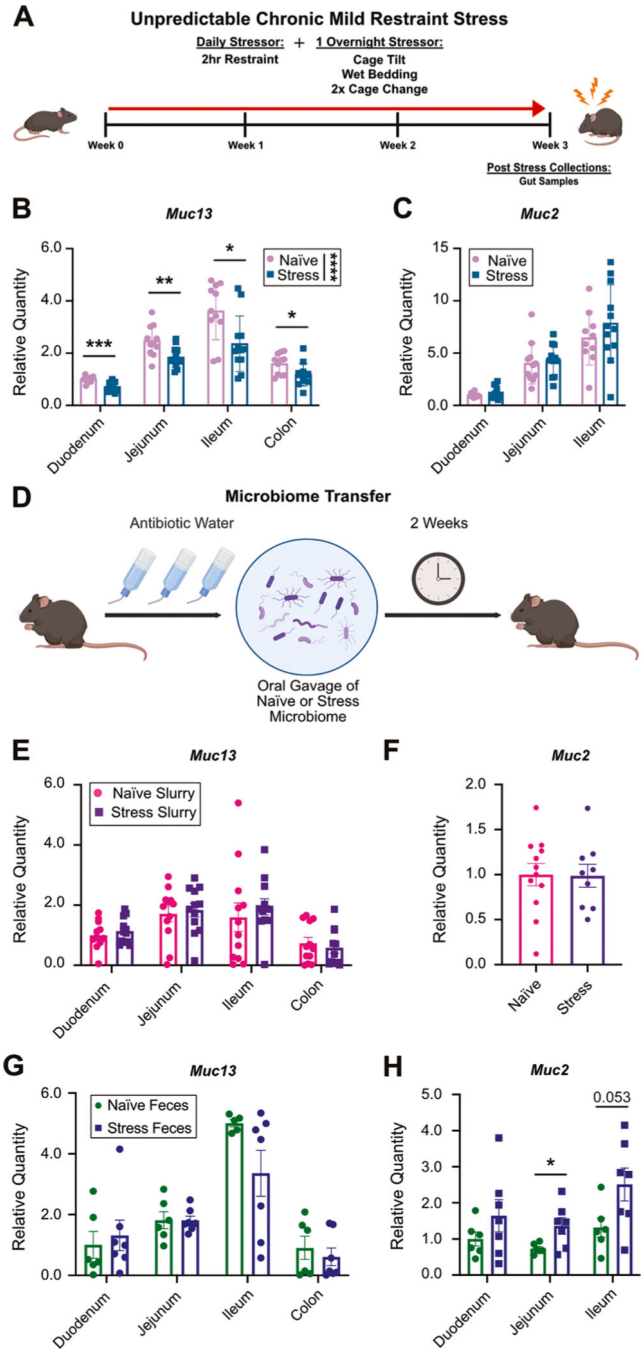

Fig. 2.

Stress drives *Muc13* reductions independently of transferrable microbial products: (A) Experimental design. Relative quantity of (B) *Muc13* and (C) *Muc2* transcripts by qPCR in individual sections of the intestine in naïve and stress animals. *Muc2* expression in the colon was higher than housekeeping genes preventing quantification by qPCR. Unpaired two-tailed, t-tests. Male mice, n = 11/12 per group, N = 2. (D) Experimental design for panels E and F. Relative quantity of (E) *Muc13* and (F) *Muc2* transcripts in the intestines of animals receiving a naïve or stress fecal microbiome slurry after antibiotic treatment via

gavage. Male mice, n = 12 per group. T-tests, two-tailed. Relative quantity of (G) *Muc13* and (H) *Muc2* in the intestines of germ-free mice given naïve or stress fecal pellets. Male mice, n = 7 per group. T-tests, two-tailed.

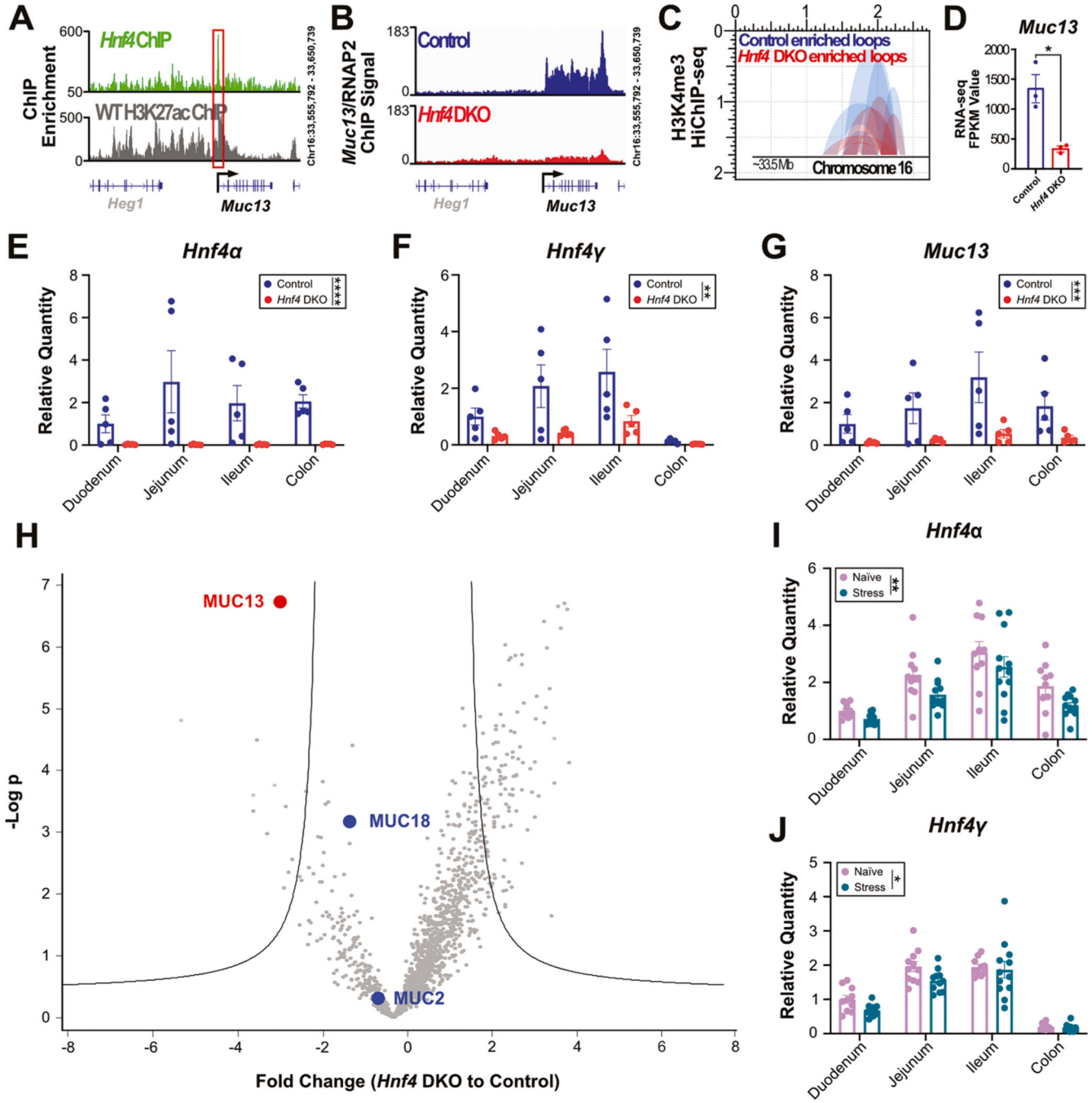

Fig. 3.

HNF4 regulates expression of *Muc13*: (A) HNF4 and H3K27ac ChIP-Seq of wildtype duodenal tissue at the *Muc13* promoter. (B) RNA Polymerase II ChIP-Seq in duodenal villus tissue in control and *Hnf4* DKO animals at the *Muc13* promoter. (C) H3K4me3 HiChIP-Seq examining chromatin loops in control and *Hnf4* DKO duodenal villus tissue at the *Muc13* promoter. (D) *Muc13* RNA-Seq fragments per kilobase per million in control and *Hnf4* DKO duodenal tissue (two-tailed unpaired *t*- test). All sequencing experiments performed on 3 mice/group. Male and female mice. Relative quantity of (E) *Hnf4α*, (F) *Hnf4γ*, and (G)

Muc13, across the intestines in control and *Hnf4* DKO animals. Female mice, 5 mice/group. Two-way ANOVA. (H) Fold changes of mucins in the intestines of *Hnf4* DKO and control animals by mass spectrometry. All sections of the intestines are pooled for a total of 12 samples from 3 mice per group. Female mice. Relative quantities of (I) *Hnf4α* and (J) *Hnf4γ* across the intestines in naïve and stress animals. Male mice, 11–12 mice per group; Two-way ANOVA.

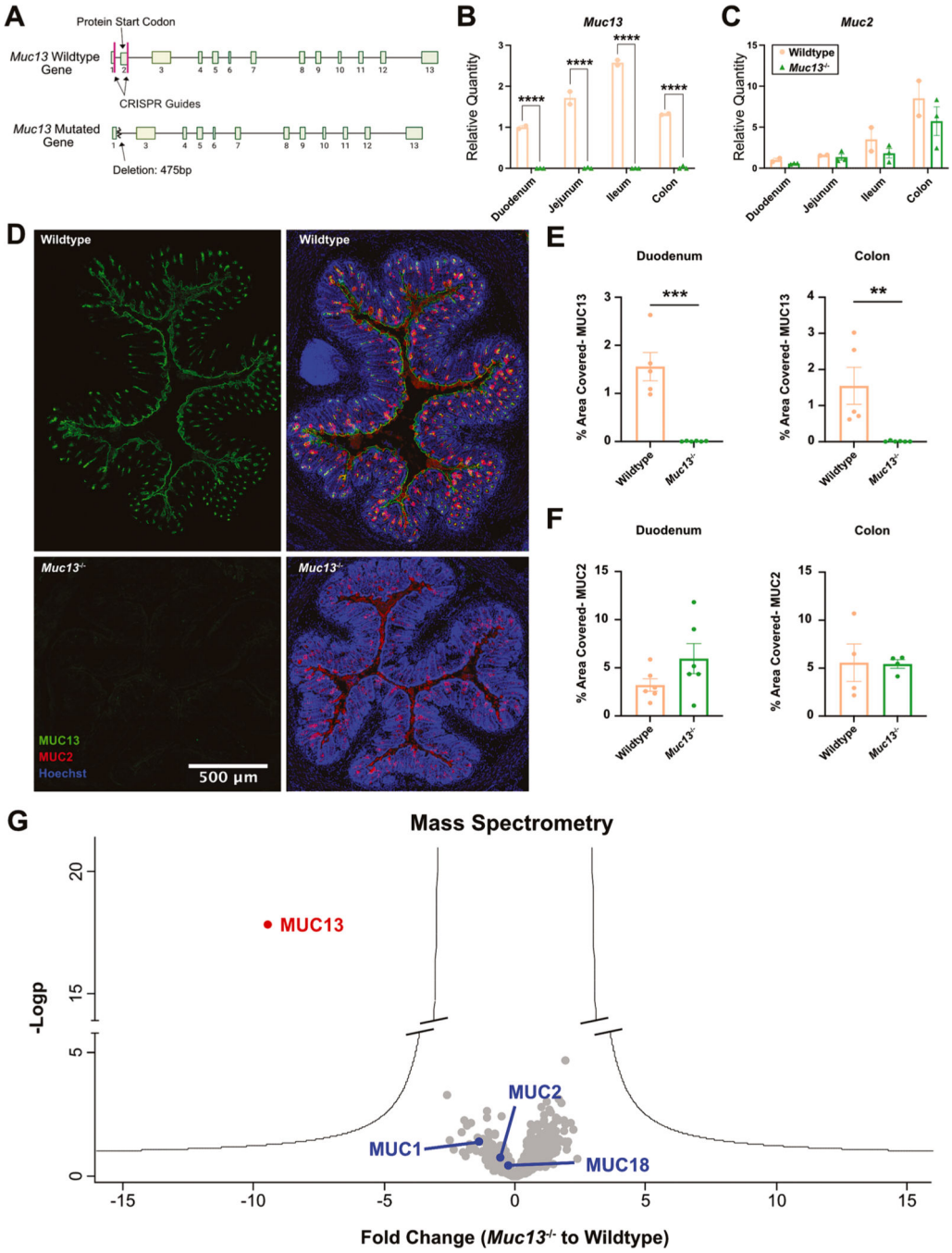

Fig. 4.

Muc13 deletion validation: (A) *Muc13* deletion schematic. Relative quantities of (B) *Muc13* and (C) *Muc2* in wildtype and *Muc13*$^{-/-}$ mice. Male mice, n = 2–3 per group, N = 1. T-tests, two-tailed. (D) Representative images of immunofluorescence (IF) staining of MUC13, MUC2 and Hoechst in the colon of wildtype and *Muc13*$^{-/-}$ animals. Quantification of IF of (E) MUC13 and (F) MUC2 in the duodenum and colon of wildtype and *Muc13*$^{-/-}$ mice. Male mice. T-tests, n = 4–6 per group, N = 2. (G) Fold change of mucins in the intestines of

Muc13$^{-/-}$ compared to wildtype controls by mass spectrometry. All sections of the intestines are pooled for a total of 12 samples from 3 mice per group. Male mice.

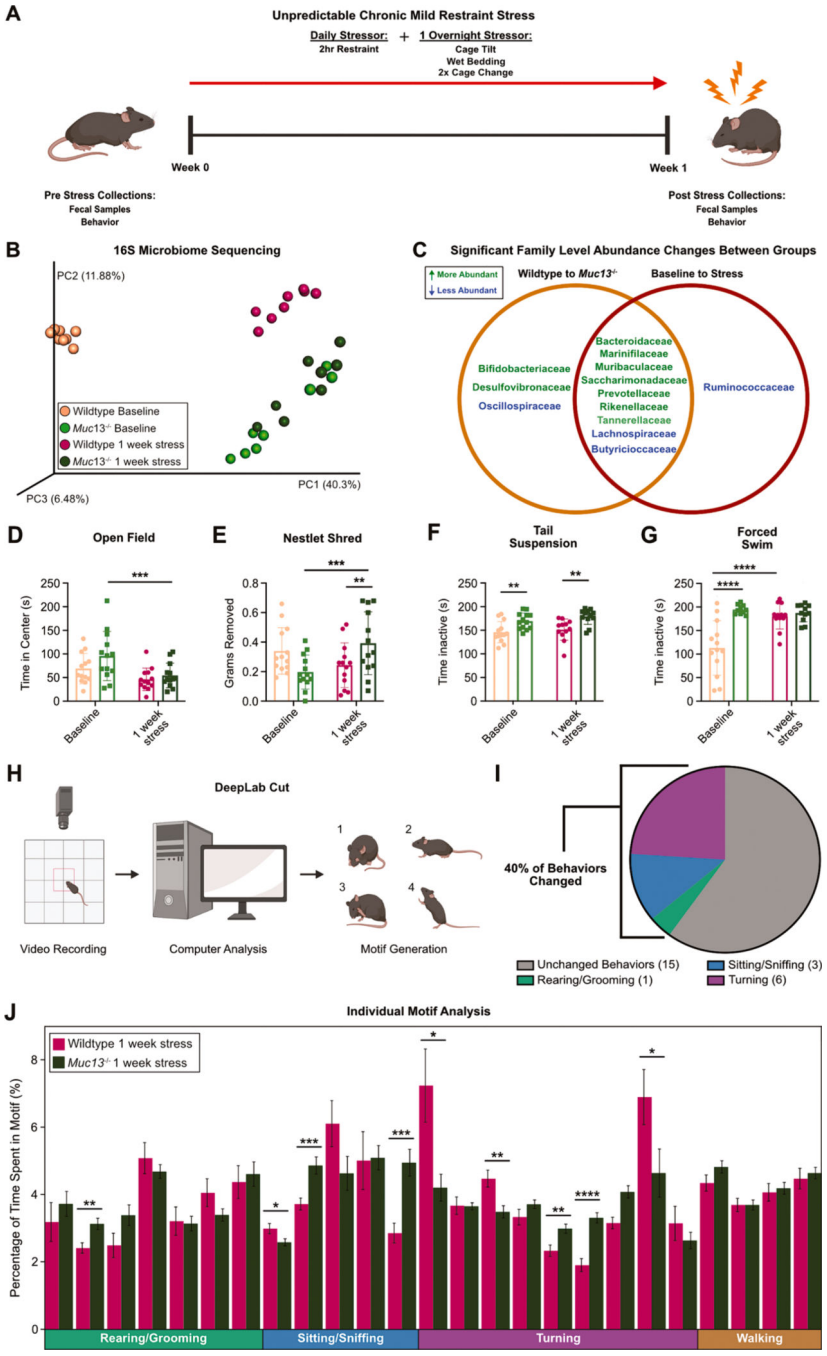

Fig. 5.

Microbiome and behavioral changes in *Muc13*$^{-/-}$ mice at baseline and after stress exposure: (A) Experimental design. (B) PCoA plot of 16S fecal microbial sequencing in wildtype and *Muc13*$^{-/-}$ animals at baseline and after 1 week of stress exposure. Male mice, n = 8 per group, N = 1. (C) Venn diagram comparing significantly changed families from 16S fecal microbiome sequencing between wildtype and *Muc13*$^{-/-}$ animals to families changed between wildtype baseline and stress exposed animals. (D) Open field and (E) nestlet shredding tests comparing anxiety-like behaviors between wildtype and *Muc13*$^{-/-}$ animals at

baseline and after 1 week of stress exposure. (F) Tail suspension and (G) forced swim tests between wildtype and *Muc13*$^{-/-}$ animals at baseline and after 1 week of stress exposure. Male mice, Two-way ANOVA, n = 13 per group, N = 2. (H) DeepLabCut experimental design. (I) Pie chart of quantified behavioral motifs changed between wildtype and *Muc13*$^{-/-}$ animals. (J) Individual motif analysis after 1 week of stress exposure between wildtype and *Muc13*$^{-/-}$ animals. Two-tailed T-tests, male and female mice, n = 13–24 per group, N = 3.